Allosteric Modulation and Structural Determination of G-Protein Coupled Receptors

by

James Geiger

A Dissertation Presented in Partial Fulfillment
of the Requirements for the Degree
Doctor of Philosophy

Approved November 2020 by the
Graduate Supervisory Committee:

Wei Liu , Chair
Jeremy Mills
Po-Lin Chiu

ARIZONA STATE UNIVERSITY

December 2020

ABSTRACT

G protein-coupled receptors (GPCRs) are known to be modulated by membrane cholesterol levels, but whether or not the effects are caused by specific receptor-cholesterol interactions or cholesterol's general effects on the membrane is not well-understood. Results from coarse-grained molecular dynamics (CGMD) simulations coupled and structural bioinformatics offer new insights into how cholesterol modulates GPCR function by showing cholesterol interactions with the β_2AR that agree with previously published data; additionally, differential and specific cholesterol binding in the cholecystokinin (CCK) receptor subfamily was observed while revealing a previously unreported Cholesterol Recognition Amino-acid Consensus (CRAC) sequence that is also conserved across 38% of class A GPCRs. Mutation of this conserved CRAC sequence of the β_2AR affects cholesterol stabilization of the receptor in a lipid bilayer. Serial femtosecond crystallography (SFX) with X-ray free electron lasers (XFELs) has proven highly successful for structure determination of challenging membrane proteins crystallized in lipidic cubic phase, however, as most techniques, it has limitations. Using an optimized SFX experimental setup in a helium atmosphere we determined the room temperature structure of the adenosine A_{2A} receptor (A_{2A}AR) at 2.0 Å resolution and compared it with previous A_{2A}AR structures determined in vacuum and/or at cryogenic temperatures. Specifically, we demonstrated the capability of utilizing high XFEL beam transmissions, in conjunction with a high dynamic range detector, to collect high-resolution SFX data while reducing crystalline material consumption and shortening the collection time required for a complete data set. The results of these studies provide a better understanding of receptor-cholesterol interactions that can contribute to novel and

improved therapeutics for a variety of diseases. Furthermore, the experimental setups presented herein can be applied to future molecular dynamics and SFX applications for protein nanocrystal samples to aid in structure-based discovery efforts of therapeutic targets that are difficult to crystallize.

DEDICATION

To my parents. My dad, who to this day is probably the hardest working and one of the smartest men that I have ever met. My mom, who started my entire education journey at home.

ACKNOWLEDGMENTS

I would like to first thank my PhD advisor Dr. Wei Liu, for his example and leadership throughout my graduate career. I remember working in PSC as an undergraduate researcher and listening to him tell me why joining his lab could be a better option than going to Stanford. Thank you for the invite! Wei is a renowned researcher and just being able to see how he works has taught me a lot about science and how to be successful in my field.

To the other members of the Liu lab. Thank you for your help and support on various projects.

Liang and Lan, thank you for the endless supply of biomass from the cell culture room. Lan, your insights helped me learn about LCP and protein expression before I even joined the lab. I remember you teaching me to “feel” when LCP was formed way back in the day. Thank you for all the work you have done supporting the Liu lab and allowing us to perform our research.

Thanks to Dr. Eugene Chun and Dr. Ming-Yue Lee. I learned much from both of you. Eugene, thanks for the fusion toolbox figures that we all stole from your paper for years! Ming, I learned a lot from our long conversations about all things science. You were my go-to for any questions, issues, random theories that I had. This work would not be possible without you!

A special shoutout to Zina, the lab partner extraordinaire! We worked incredibly closely now for years and it has definitely been a ride. From FRAP to FLOP and the Empty Western Gang, it has been a pleasure working with you the past almost 5 years. I

wouldn’t have thought that we’d be working this close when we first met so many years ago in undergrad! I’m proud of what we did in the lab and what you will continue to do!

Shout out to the Fromme lab FRAT boys.

To my mom and dad, there is really nothing else to say except thank you for everything. I love you both and very thankful for the insane work that you both put in to give your kids better opportunities than you had growing up. You inspire me to work hard every day!

Lastly, and probably most importantly, thank you to my wife, Abby. This PhD has been full of ups and downs and you have been supportive through it all. I often say that I am not the same fun person that I was when you married me at the beginning of this journey. But thank you for your love and support. I’m excited to see where life takes us next. Love you.

TABLE OF CONTENTS

Page

CHAPTER Page

LIST OF TABLES

LIST OF FIGURES

Figure Page

CHAPTER 1

INTRODUCTION

GPCRs: Why We Care and What They Do

G-Protein Coupled Receptors (GPCRs) facilitate downstream effects for most extra-cellular signals in eukaryotic cells. Various signals are received by this diverse family, including light, taste, hormones, and odors. In all, there are over 800 GPCRs encoded in the human genome [1]. The family is divided into five distinct subfamilies: Class A (Rhodopsin, 719 receptors), Class B (Secretin, 15), Class C (Glutamate, 22), Adhesion (33), and Frizzled (11) [1]. GPCRs are integral membrane proteins characterized by numerous conserved features including, a seven-transmembrane (TM) α-helical bundle, and an extracellular N-terminus, and an intracellular C-terminus. In class A GPCRs, ligands bind either near the extracellular end or inside the TM bundle and facilitate the activation of the receptor. Upon activation, conformational changes in the TM bundle (e.g., the outward movement of TM6) allow for the binding of a heterotrimeric G-protein [2, 3]. G-proteins are composed of three subunits (Gα, Gβ, & Gγ). In the inactive state, the G-protein complex contains a guanosine diphosphate (GDP) bound Gα along with Gβ and Gγ-subunits. Upon receptor activation, the GDP is hydrolyzed, which allows the Gα to bind the receptor. Next, the binding of guanosine triphosphate (GTP) [1] to Gα destabilizes interactions with the receptor and the Gβγ complex. The GTP-bound Gα, as well as the Gβγ complex, can then freely interact with downstream proteins and begin the signaling cascade [4]. After the signal is received by the receptor and sent through the G-proteins, the signal must be terminated. To facilitate this, a GPCR Kinase (GRK) phosphorylates the intracellular side of the activated

receptor. This leads to the binding of a different protein, an arrestin, that has a high affinity for the phosphorylated receptor. The binding of the arrestin blocks the binding of other G-proteins, thus desensitizing the receptor. Arrestin-bound receptors are then taken through endocytosis, recycled, re-sensitized, and shipped back to the membrane [5-7].

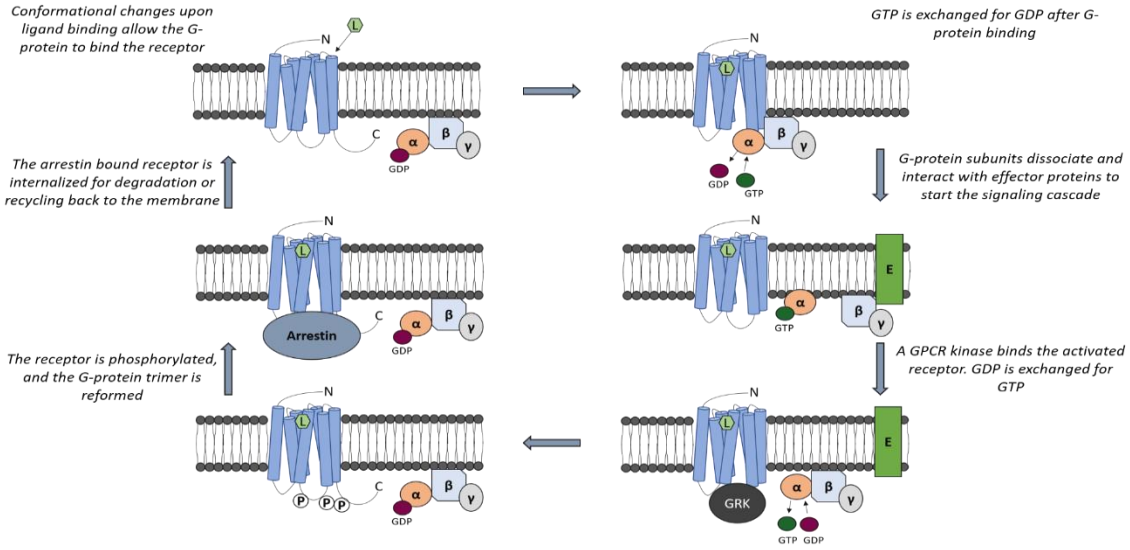

Figure1. 1 *Typical GCPR signaling. Conformational changes upon ligand binding allow for the G-protein to bind the activated receptor. After binding, GDP bound to the Gα is exchanged for GTP. The G-protein dissociates, and the subunits interact with effector proteins to start the signaling cascade. A GPCR kinase phosphorylates the activated receptor and GTP is re-exchanged for GDP in the Gα subunit. The G-protein trimer is reformed and an arrestin protein binds the phosphorylated receptor. The arrestin—receptor complex is internalized for either degradation or recycling back to the membrane.*

Over 20 Gα proteins are encoded in mammalian genomes [8]. These proteins are divided into four distinct subtypes: $G_{\alpha s}$, $G_{\alpha i}$, $G_{\alpha q}$, $G_{\alpha 12}$ [9]. Many GPCRs are capable of selectively binding multiple Gα subfamilies [10], which can lead to numerous signaling cascades originating from the same receptor. With over 800 receptors and the possibility of a variety of signaling cascades originating from the same receptor, it is easy to see the significance of this family in human physiology. Furthermore, GPCRs are widely recognized as potent drug targets. As of 2019, approximately 460 drugs targeting GPCRs

are approved by the Food and Drug Administration (FDA)- accounting for ~35% of all FDA approved drugs [11-13]. These drugs bind at over 100 unique GPCR targets and are intended to treat numerous disease states, including diabetes, depression, migraines, Parkinson's, cardiovascular disease, schizophrenia, and allergenic symptoms **[13].**

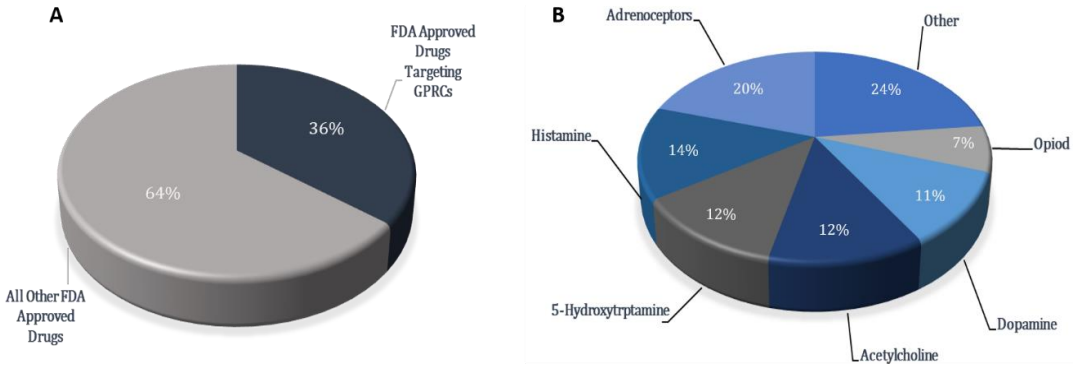

Figure 1.2 *A) GPCRs make up ~35% of all FDA approved drug targets. B) A pie chart shows the breakdown of which GPCR subfamilies compose the most FDA approved drug targets.*

Structural Discovery of GPCRs

The first crystal structure of a mammalian GPCR was that of bovine rhodopsin in 2000 [14]. Unfortunately, structures of other GPCRs proved difficult to obtain. First, unlike bovine rhodopsin, other GPCRs are not expressed in enough abundance to isolate from a natural source. This meant that recombinant protein expression must be performed. Secondly, rhodopsin is stabilized by a covalently bound 11-*cis*-retinol molecule, which greatly stabilizes an inactive conformation in dark environments. Other GPCRs are conformationally unstable and routinely sample large conformational spaces [15]. These issues were overcome in 2007 with the crystal structure of the β_2-Adrenergic receptor (β_2AR) [16]. The β_2AR was expressed at high levels using a baculovirus

expression system in insect (*sf9)* cells. Furthermore, conformational space was limited by both the incorporation of a fusion protein (T4-Lysozyme) into the 3rd intracellular loop of the receptor as well as purification in the presence of a high-affinity ligand carazolol [15]. Lipidic Cubic Phase (LCP) technology was also necessary for the crystallization of the β_2AR [17, 18]. LCP-crystallization is a method wherein the protein of interest is mixed with a lipid host, most typically monoolein. In the cubic phase, continuous bilayers form, providing a stable environment wherein the membrane protein can freely diffuse. LCP technology has since proved invaluable in the structural discovery of GPCRs and other membrane proteins [19]. Following the β_2AR structure, key technological advancements facilitated the structural discovery of many more GPCRs. These advancements include: Baculovirus Expression, LCP-Crystallization [17, 18], Advances in Receptor Engineering [20, 21], LCP-FRAP [22], LCP-Tm [23], Nanobody Stabilization [24], and other biophysical assays to probe receptor stability [25]. While crystallography has dominated the structural discovery of GPCRs, Cryo-Electron Microscopy (Cryo-EM) has recently been shown to be effective for structural elucidation of GPCR-G protein complexes [26-28]. Unfortunately, most receptors alone, at sizes of approximately 40-50 kDa, do not meet the size requirement to elucidate high-resolution structures from Cryo-EM. Still, Cryo-EM is valuable in studying protein-protein interactions within the complexed structures of GPCRs [27]. Altogether, there are 346 GPCR structures arising from 64 unique receptors in the GPCR database [13]. These structures have facilitated significant insights regarding GPCR function as well as structure-based drug design. However, with

over 800 receptors in the family and only 64 unique receptor structures, over 90% of GPCRs are still lacking high-resolution structural information.

A Brief Introduction to X-ray Crystallography

In 1912, the German physicist Paul Ewald described the optical properties of crystalline solids in his doctoral dissertation. While his interests were initially focused on the visible spectrum, his discussions with a colleague, Max Von Laue, inspired Laue to perform his own experiments. Laue believed that because the distance between atoms in a crystalline solid is on the same order of magnitude as the wavelength of X-rays, crystals could behave as a diffraction grating for an X-ray beam [29]. Laue's experiments soon showed that X-rays are elastically scattered in various directions upon striking a crystalline solid. With this discovery, the field of X-ray Crystallography was born and Laue was awarded the 1914 Nobel Prize. The 1915 Nobel Prize was then awarded to the father-son team of W.L Bragg and W.H Bragg, who described mathematics behind the angles necessary for the coherent or incoherent scattering of X-rays (termed Bragg's law). Yet another Nobel prize was awarded to John Kendrew and Max Perutz in 1962 for

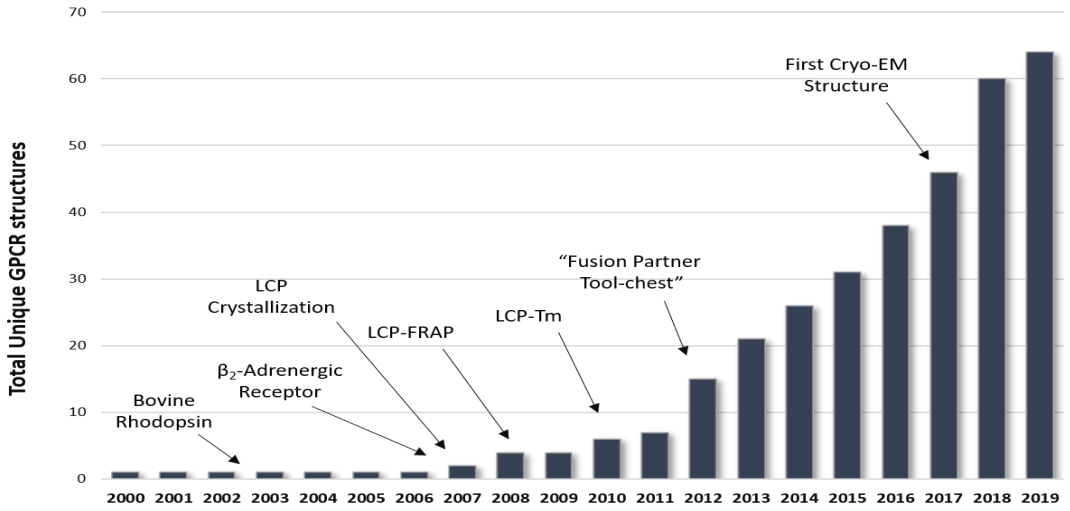

Figure 1.3 *Total number of Unique GPCR structure from 2000 – 2019. Interesting highlights or technical innovations are highlighted in the year of publication.*

their work on the first crystallographic protein structure of sperm whale myoglobin [30]. Since the first protein structure was solved in 1958, the crystallography of biological macromolecules has developed dramatically. To date, the Protein Data Bank (PDB) contains 149,238 protein structures, of which 134,187 were solved from X-ray diffraction [31].

Diffraction and Data Analysis

When X-rays are diffracted by a crystalline, the resultant waves can cancel each other out through destructive interference. However, the constructive interference, where the waves are added together occurs at specific distances as defined by Bragg's law, results in the diffraction spots that we see during data collection. The intensities of these diffraction spots (called Bragg spots) are related to the electron densities of the target molecule. While the overall patterns of these Bragg spots correlate with the unit cell of the crystal, the intensity yields information about the density of electrons in the crystal. Each diffraction spot is the intensity of the wave summation with a scattering angle at Bragg's condition. Unfortunately, diffraction patterns only yield information about the intensity (or the squared amplitude) of the Bragg spot, and the phase information is lost (coined the 'phase problem') [32]. Without phase information, it is impossible to determine the location from which the Bragg spot arose, and therefore impossible to solve the structure. The phase problem can be solved through either isomorphous replacement via Single-wavelength anomalous diffraction [33] [34]/Multi-wavelength anomalous diffraction (MAD), or through Molecular Replacement (MR) [35]. Isomorphous replacement is necessary when no closely related structures are available and requires two distinct datasets. First, from the native protein crystal, and second, from

crystals soaked with a heavy metal such as mercury, platinum, or gold [36]. The differences between the two datasets should be due to the heavy atoms; therefore, their position related to the rest of the protein atoms can be determined. The peaks generated from these heavy atoms provide a starting point for phasing the rest of the protein. MR is used when a model closely related to the protein of interest is available. This approach uses the known structure factors from the template model and fits the experimental data accordingly [36]. With both phase and amplitude information in hand, a structure model can soon follow. While the mathematics behind X-ray crystallography is rigorous, a series of programs and suites has allowed access to users from many areas of expertise.

Synchrotron Radiation

Synchrotron X-ray sources have traditionally been the workhorse of protein crystallography. However, a few bottlenecks have plagued the method. First, is the need for large, well-diffracting crystals. Traditionally, to generate a structure model at better than 3.5 Å resolution, crystals commonly have to be at least 20 µm in each dimension [37]. Optimizing crystallization conditions is a difficult and time-consuming process. Therefore, the need for large protein crystals is generally the greatest bottleneck that is elucidating a structure of a protein target. Second is the radiation damage that occurs

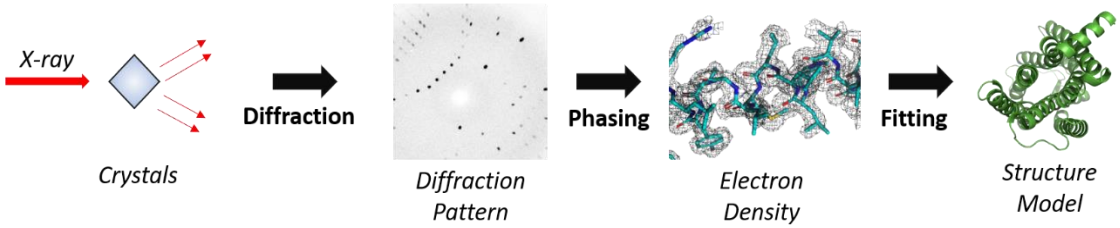

Figure 1.4 *Typical workflow during X-ray crystallography. Diffraction patterns are collected from crystal samples. The phase problem is fixed via isomorphous replacement or molecular replacement. Solving the phase problem yields electron density maps that a model is fitted to. After numerous rounds of refinement, the final structure model is determined.*

during data collection. Primary radiation damage is dependent on the X-ray "dose" and involves the breaking of bonds or damage to the molecule due to exposure to the X-ray. Secondary damage, however, is dependent on time and temperature and is related to the propagation of those species from primary radiation damage (e.g., free radicals) through the crystal sample causing more damage [38]. To limit the spread of secondary radiation damage, crystals are cooled and processed at cryogenic temperatures [38]. Despite these drawbacks, synchrotron radiation has resulted in most protein structures to date. When performing diffraction experiments at a synchrotron, single protein crystals are harvested and immediately flash-frozen in liquid nitrogen. These cryo-cooled crystals are then shipped to the beamline and mounted in front of the beam. It is commonly necessary to grow and harvest numerous crystals to collect a complete dataset [39]. Synchrotron X-rays are generated from electrons that have been accelerated to near the speed of light in a circular storage ring. Interactions with various magnets change the direction of the electrons – causing them to emit powerful radiation in the form of X-rays. The resultant X-rays are directed toward various beamlines at the facility.

X-Ray Free Electron Laser (XFEL) Radiation

The first X-ray Free Electron Laser (XFEL) was the Linac Coherent Light Source (LCLS) at Stanford University [40]. Soon after, protein structures from nanocrystals were solved using the Serial Femtosecond Crystallography (SFX) [41]. At an XFEL, electrons are accelerated to high speed and then passed through a long series of magnets called an undulator. Like a synchrotron, as the electrons are affected by the magnetic field, they emit X-rays. However, these X-rays interact with the electrons, speeding some up and slowing some down. The result is a "packing" of the electrons in discrete "bundles," a

process called Self-Amplified Spontaneous Emission (SASE) [42]. This "bundling" of the electrons imparts a very important property to XFEL radiation, the electrons in a bundle emit their radiation in phase with one another (the resulting X-rays are called "coherent"). Moreover, X-rays from FELs are thousands of times brighter than those generated at synchrotron sources. There are multiple benefits of using an XFEL compared to traditional synchrotron radiation. First the femtosecond X-ray pulses that originate from these beams are faster than the time it takes for atoms to move. This means that diffraction patterns from each pulse are recorded before radiation damage has a chance to interfere with data collection, a phenomenon that has been termed "diffraction before destruction" [43]. Secondly, small crystals (e.g. < 5 μm^3) are capable of diffracting to high resolutions [41, 43-45]. This is due to the fact that the beams generated from XFELs are thousands of times more intense than those generated by synchrotrons [43]. Unlike data collection at a synchrotron, Serial Femtosecond Crystallography (SFX) at an XFEL utilizes thousands of nanocrystals that are injected directly into the beam. Technological advancements concerning sample injectors and different viscous media have allowed both soluble and membrane proteins to be studied at XFELs [46-49]. Furthermore, SFX has been especially effective in the structural elucidation of GPCRs as growing large crystals is especially difficult given the dynamic nature of the proteins [45, 50, 51]. To date, there are only six XFELs in the world, making beamtimes at these facilities a hot commodity. To be sure, the greatest obstacle in performing SFX is getting access to the XFEL itself.

Molecular Dynamics

While crystallographic structures of proteins are vital in our understanding of protein biochemistry, there are many important questions that can't be answered from static pictures. Though crystal structures may clearly identify specific residues involved in ligand binding, other processes, such as the conformational changes or mechanisms behind binding/signaling events, are difficult (if not impossible) to determine via traditional crystallography. Molecular Dynamics (MD) simulations give researchers the ability to investigate these kinds of questions. The first MD simulations were published in 1957 by Alder and Wainwright [52]. These simulations probed the phase transition of hard spheres. However, it would be 20 years before McCammon *et al.* published the first protein simulations outlining the dynamics of the bovine pancreatic trypsin inhibitor [53]. Since these initial simulations, the last 40 years have seen many innovations in MD. Today, a multitude of forcefields have been developed that allow scientists to accurately model solvents, proteins, lipids, and more. While some scientists dedicate their entire careers to developing new and better forcefields, many simulators focus on utilizing available programs to probe interesting physical phenomena. It is the responsibility of researchers to choose the best forcefield for their own experimental needs.

MD is based on Newton's second law of motion, F = ma, where F is the force on a given particle, m is the particle's mass, and a is the acceleration of the particle. If we know the force on each atom, the acceleration can be calculated as well. Furthermore, the

integration of Newton's second law yields information about the position, velocity, and acceleration of each atom in a simulation (Eq.1b).

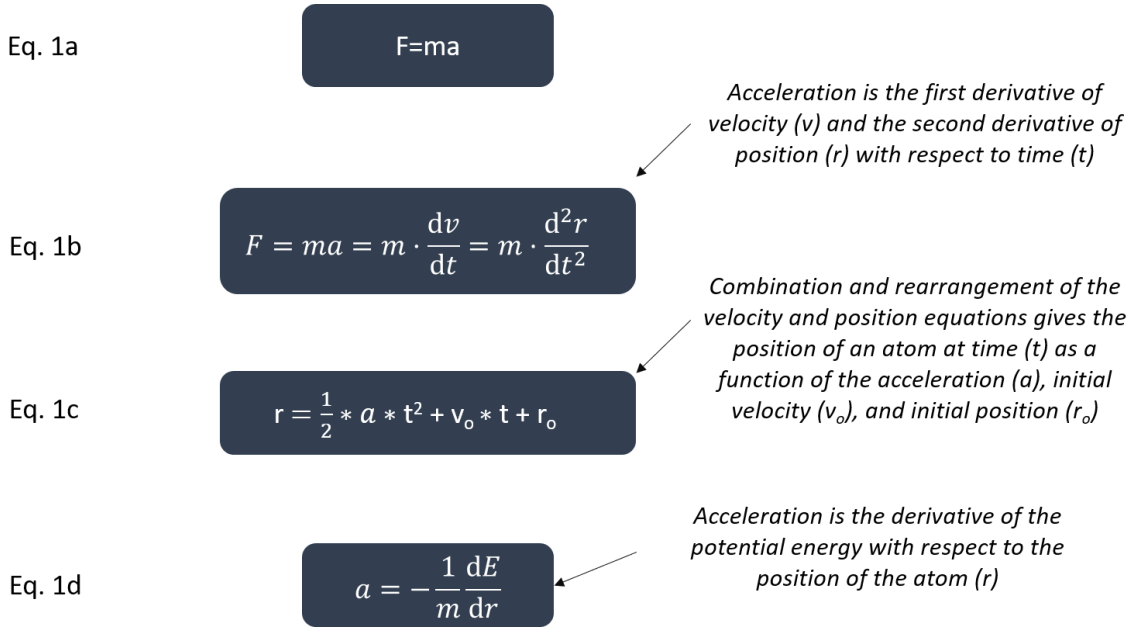

A further derivation of Newton's second law provides insight into how information is collected in MD. In equation 1C, we can see that the position of an atom at any given time can be calculated as a function of the acceleration (a), initial velocity (v_o), and initial position (r_o) [28]. The acceleration of the atom is given by the derivative of the potential energy with respect to the atom's position (eq. 1D). A consequence of equation 1C is that MD simulations are deterministic, meaning that a particle's velocity and position at any time is determined by the initial starting velocity/position. For proteins, the initial positions of each atom can be obtained from known structures (determined by crystallography, NMR, or Cryo-EM) or homology models, and the initial velocities are typically generated randomly from the Gaussian distribution of a given temperature.

Finally, to calculate the trajectories of atoms in a simulation, Newton's laws of motion must be integrated. Integration methods are based on a Taylor series (Eq. 2A-C).

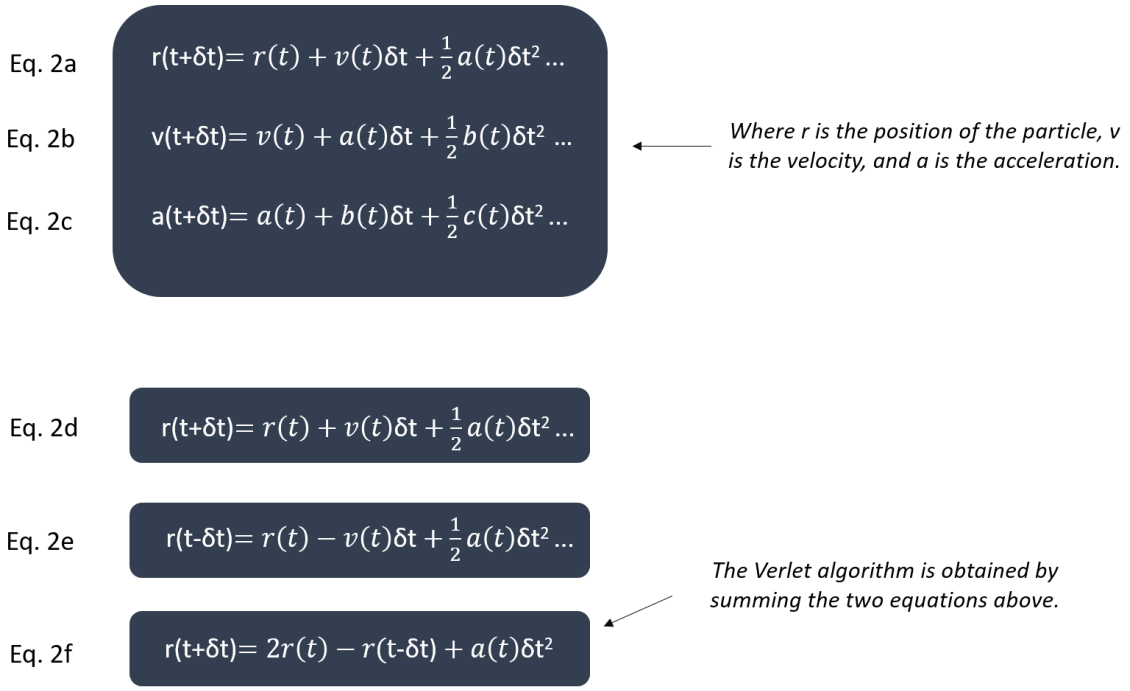

The Verlet algorithm, commonly used in MD simulations, utilizes the positions and velocities from time (t) and the positions and velocities from time (t -Δt), to calculate the new positions at time (t +Δt) (Eq. 2f). Many different integration algorithms have been developed and have their own set of strengths and weaknesses. Likewise, many different potential energy functions have been developed, such as the commonly used CHARRM [54] and AMBER [55] forcefields. Moreover, numerous programs have been developed to run and analyze MD simulations, including GROMACS [56], NAMD [57], and OpenMM [58]. The basic algorithm for MD follows a workflow described here. First, atoms are given initial positions, velocities, and acceleration and time is set to zero. Next, the forces on each atom are calculated from the potential energy function

(forcefield). Newton's equations of motion are then solved for each atom, and the atoms are moved to their new positions with new velocities. The properties of the system (energy, temperature...etc.) are then calculated and saved. Lastly, the time step is moved forward, and the process repeats for as many time steps as specified by the simulator. This cycle is outlined in detail in figure 5.

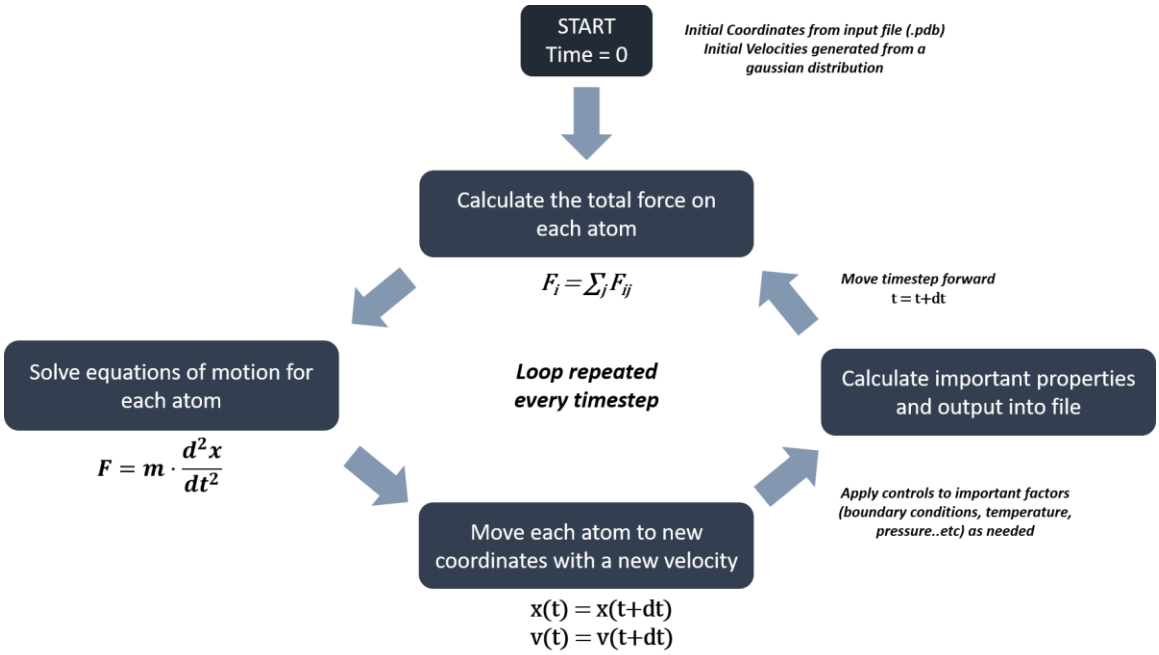

Figure 1.5. A general outline for MD simulations.

MD simulations, while different for every hypothesis being tested, will generally follow the same basic workflow: 1) System Preparation, 2) Minimization/Relaxation, 3) Equilibration, and 4) Production [33]. System preparation is focused on preparing the starting state of the system of interest. For example, to simulate a membrane protein, a structure model of the protein would need to be inserted into a lipid bilayer and a forcefield (potential energy function) would be applied to the new system. System preparation consists of two important components, building the system in the correct starting state (e.g., placing a protein in a membrane or solvating a protein in water) and applying appropriate

forcefields. After the system is prepared, a minimization/relaxation run must be performed. When proteins crystallize, the atoms may be locked in certain configurations that are not energetically favorable in the solvated state. Because most structure models used for MD originate from crystal structures, minimization allows these potentially high-energy interactions to "relax" as the system seeks a local free-energy minimum in which to settle. Failure to run minimization during MD could result in the system "blowing up" and the simulation fails. Changes from the initial starting state, if included in the simulation data, could make an analysis of the simulation difficult. Moreover, the simulations are generally considered in a specific macrostate of the whole ensemble with defined thermodynamic parameters, such as pressure, temperature, and system volume. In energetic terms, simulators want to ensure that any local minima are avoided and start from the most probable and energetically favorable configuration in the thermodynamic ensemble of interest. For these reasons, the system must be thoroughly equilibrated before the simulation begins. The equilibration phase may also be useful to ensure a constant temperature, pressure, or anything other metric depending on the simulation parameters. Determining whether the system has been sufficiently equilibrated is not trivial. In general, the simulator will ensure that important characteristics of the system are no longer changing with respect to the starting state. Though small changes and variations may be recorded in important characteristics (equilibrium is not a static state), an equilibrated system will fluctuate around a set value. For example, Root Mean Squared Deviation (RMSD) from the starting structure is an important metric when simulating proteins. Upon starting the simulation, one would expect the protein to sample different conformations from the starting state and eventually settle into the most energetically favorable. An RMSD plot for

a fully equilibrated protein would increase from the first time point and eventually level off when the most probable state is reached. After equilibration, a production run is performed, and the data is stored and analyzed.

References

1. Alexander SPH CA, Davenport AP, Kelly E, Mathie A, Peters JA, Veale EL, Armstrong JF, Faccenda E, Harding SD, Pawson AJ, Sharman JL, Southan C, Davies JA; CGTP Collaborators. . The Concise Guide to PHARMACOLOGY 2019/20: G protein-coupled receptors. . Br J Pharmacology2019;176 (S1):S21-S141.

2. Mahoney JP, Sunahara RK. Mechanistic insights into GPCR-G protein interactions. Curr Opin Struct Biol. 2016;41:247-54. Epub 2016/11/18. doi: 10.1016/j.sbi.2016.11.005. PubMed PMID: 27871057.

3. Weis WI, Kobilka BK. The Molecular Basis of G Protein-Coupled Receptor Activation. Annu Rev Biochem. 2018;87:897-919. doi: 10.1146/annurev-biochem-060614-033910. PubMed PMID: 29925258.

4. Oldham WM, Hamm HE. Heterotrimeric G protein activation by G-protein-coupled receptors. Nature Reviews Molecular Cell Biology. 2008;9(1):60-71. doi: 10.1038/nrm2299.

5. Gurevich VV, Gurevich EV. GPCR Signaling Regulation: The Role of GRKs and Arrestins. Frontiers in Pharmacology. 2019;10:125.

6. Ribas C, Penela P, Murga C, Salcedo A, García-Hoz C, Jurado-Pueyo M, et al. The G protein-coupled receptor kinase (GRK) interactome: Role of GRKs in GPCR regulation and signaling. Biochimica et Biophysica Acta (BBA) - Biomembranes. 2007;1768(4):913-22. doi: https://doi.org/10.1016/j.bbamem.2006.09.019.

7. Smith JS, Rajagopal S. The β-Arrestins: Multifunctional Regulators of G Protein-coupled Receptors. Journal of Biological Chemistry. 2016;291(17):8969-77.

8. Simon MI, Strathmann MP, Gautam N. Diversity of G proteins in signal transduction. Science. 1991;252(5007):802. doi: 10.1126/science.1902986.

9. González-Maeso J, Meana JJ. Heterotrimeric g proteins: insights into the neurobiology of mood disorders. Curr Neuropharmacol. 2006;4(2):127-38. doi: 10.2174/157015906776359586. PubMed PMID: 18615130.

10. Okashah N, Wan Q, Ghosh S, Sandhu M, Inoue A, Vaidehi N, et al. Variable G protein determinants of GPCR coupling selectivity. Proceedings of the National Academy of Sciences. 2019;116(24):12054. doi: 10.1073/pnas.1905993116.

11. Hauser AS, Chavali S, Masuho I, Jahn LJ, Martemyanov KA, Gloriam DE, et al. Pharmacogenomics of GPCR Drug Targets. Cell. 2018;172(1-2):41-54.e19. Epub

2017/12/14. doi: 10.1016/j.cell.2017.11.033. PubMed PMID: 29249361.

12. Insel PA, Sriram K, Gorr MW, Wiley SZ, Michkov A, Salmerón C, et al. GPCRomics: An Approach to Discover GPCR Drug Targets. Trends in Pharmacological Sciences. 2019;40(6):378-87. doi: 10.1016/j.tips.2019.04.001.

13. Pándy-Szekeres G, Munk C, Tsonkov TM, Mordalski S, Harpsøe K, Hauser AS, et al. GPCRdb in 2018: adding GPCR structure models and ligands. Nucleic Acids Research. 2017;46(D1):D440-D6. doi: 10.1093/nar/gkx1109.

14. Palczewski K, Kumasaka T, Hori T, Behnke CA, Motoshima H, Fox BA, et al. Crystal Structure of Rhodopsin: A G Protein-Coupled Receptor. Science. 2000;289(5480):739. doi: 10.1126/science.289.5480.739.

15. Cherezov V, Rosenbaum DM, Hanson MA, Rasmussen SGF, Thian FS, Kobilka TS, et al. High-Resolution Crystal Structure of an Engineered Human β₂-Adrenergic G Protein–Coupled Receptor. Science. 2007;318(5854):1258. doi: 10.1126/science.1150577.

16. Rosenbaum DM, Cherezov V, Hanson MA, Rasmussen SGF, Thian FS, Kobilka TS, et al. GPCR Engineering Yields High-Resolution Structural Insights into β₂-Adrenergic Receptor Function. Science. 2007;318(5854):1266. doi: 10.1126/science.1150609.

17. Caffrey M. Crystallizing Membrane Proteins for Structure Determination: Use of Lipidic Mesophases. Annual Review of Biophysics. 2009;38(1):29-51. doi: 10.1146/annurev.biophys.050708.133655.

18. Johansson LC, Wöhri AB, Katona G, Engström S, Neutze R. Membrane protein crystallization from lipidic phases. Curr Opin Struct Biol. 2009;19(4):372-8. doi: https://doi.org/10.1016/j.sbi.2009.05.006.

19. Caffrey M. A comprehensive review of the lipid cubic phase or in meso method for crystallizing membrane and soluble proteins and complexes. Acta Crystallographica Section F. 2015;71(1):3-18. doi: doi:10.1107/S2053230X14026843.

20. Chun E, Thompson Aaron A, Liu W, Roth Christopher B, Griffith Mark T, Katritch V, et al. Fusion Partner Toolchest for the Stabilization and Crystallization of G Protein-Coupled Receptors. Structure. 2012;20(6):967-76. doi: https://doi.org/10.1016/j.str.2012.04.010.

21. Heydenreich FM, Vuckovic Z, Matkovic M, Veprintsev DB. Stabilization of G protein-coupled receptors by point mutations. Frontiers in Pharmacology. 2015;6:82.

22. Cherezov V, Liu J, Griffith M, Hanson MA, Stevens RC. LCP-FRAP Assay for

Pre-Screening Membrane Proteins for in Meso Crystallization. Cryst Growth Des. 2008;8(12):4307-15. doi: 10.1021/cg800778j. PubMed PMID: 19234616.

23. Liu W, Hanson MA, Stevens RC, Cherezov V. LCP-Tm: an assay to measure and understand stability of membrane proteins in a membrane environment. Biophys J. 2010;98(8):1539-48. doi: 10.1016/j.bpj.2009.12.4296. PubMed PMID: 20409473.

24. Manglik A, Kobilka BK, Steyaert J. Nanobodies to Study G Protein-Coupled Receptor Structure and Function. Annu Rev Pharmacol Toxicol. 2017;57:19-37. Epub 2016/12/07. doi: 10.1146/annurev-pharmtox-010716-104710. PubMed PMID: 27959623.

25. Alexandrov AI, Mileni M, Chien EYT, Hanson MA, Stevens RC. Microscale Fluorescent Thermal Stability Assay for Membrane Proteins. Structure. 2008;16(3):351-9. doi: https://doi.org/10.1016/j.str.2008.02.004.

26. García-Nafría J, Lee Y, Bai X, Carpenter B, Tate CG. Cryo-EM structure of the adenosine A2A receptor coupled to an engineered heterotrimeric G protein. eLife. 2018;7:e35946. doi: 10.7554/eLife.35946.

27. García-Nafría J, Tate CG. Cryo-EM structures of GPCRs coupled to Gs, Gi and Go. Molecular and Cellular Endocrinology. 2019;488:1-13. doi: https://doi.org/10.1016/j.mce.2019.02.006.

28. Tsai C-J, Marino J, Adaixo R, Pamula F, Muehle J, Maeda S, et al. Cryo-EM structure of the rhodopsin-Gαi-βγ complex reveals binding of the rhodopsin C-terminal tail to the gβ subunit. eLife. 2019;8:e46041. doi: 10.7554/eLife.46041.

29. Hauptman HA. History of X-ray crystallography. Chemometrics and Intelligent Laboratory Systems. 1991;10(1):13-8. doi: https://doi.org/10.1016/0169-7439(91)80029-P.

30. Kendrew JC, Bodo G, Dintzis HM, Parrish RG, Wyckoff H, Phillips DC. A Three-Dimensional Model of the Myoglobin Molecule Obtained by X-Ray Analysis. Nature. 1958;181(4610):662-6. doi: 10.1038/181662a0.

31. Berman HM, Westbrook J, Feng Z, Gilliland G, Bhat TN, Weissig H, et al. The Protein Data Bank. Nucleic Acids Research. 2000;28(1):235-42. doi: 10.1093/nar/28.1.235.

32. Taylor GL. Introduction to phasing. Acta Crystallogr D Biol Crystallogr. 2010;66(Pt 4):325-38. Epub 2010/03/24. doi: 10.1107/S0907444910006694. PubMed PMID: 20382985.

33. Braun E, , Gilmer J, , Mayes HB, , et al. Best Practices for Foundations in Molecular Simulations Best Practices 2018;1(1). doi: 10.33011. PubMed PMID: Braun2018Best.

34. Wang B-C. Resolution of phase ambiguity in macromolecular crystallography. Methods in Enzymology. 115: Academic Press; 1985. p. 90-112.

35. Rossmann MG, Blow DM. The detection of sub-units within the crystallographic asymmetric unit. Acta Crystallographica. 1962;15(1):24-31. doi: doi:10.1107/S0365110X62000067.

36. Smyth MS, Martin JH. x ray crystallography. Mol Pathol. 2000;53(1):8-14. doi: 10.1136/mp.53.1.8. PubMed PMID: 10884915.

37. Sliz P, Harrison SC, Rosenbaum G. How does Radiation Damage in Protein Crystals Depend on X-Ray Dose? Structure. 2003;11(1):13-9. doi: https://doi.org/10.1016/S0969-2126(02)00910-3.

38. Garman EF, Owen RL. Cryocooling and radiation damage in macromolecular crystallography. Acta Crystallographica Section D. 2006;62(1):32-47. doi: doi:10.1107/S0907444905034207.

39. Mitchell E, Kuhn P, Garman E. Demystifying the synchrotron trip: a first time user's guide. Structure. 1999;7(5):R111-R21. doi: 10.1016/S0969-2126(99)80063-X.

40. Emma P, Akre R, Arthur J, Bionta R, Bostedt C, Bozek J, et al. First lasing and operation of an ångstrom-wavelength free-electron laser. Nature Photonics. 2010;4(9):641-7. doi: 10.1038/nphoton.2010.176.

41. Chapman HN, Fromme P, Barty A, White TA, Kirian RA, Aquila A, et al. Femtosecond X-ray protein nanocrystallography. Nature. 2011;470(7332):73-7. doi: 10.1038/nature09750.

42. Zholents AA. Method of an enhanced self-amplified spontaneous emission for x-ray free electron lasers. Physical Review Special Topics - Accelerators and Beams. 2005;8(4):040701. doi: 10.1103/PhysRevSTAB.8.040701.

43. Chapman HN, Caleman C, Timneanu N. Diffraction before destruction. Philosophical Transactions of the Royal Society B: Biological Sciences. 2014;369(1647):20130313. doi: 10.1098/rstb.2013.0313.

44. Coe J, Ros A. Small Is Beautiful: Growth and Detection of Nanocrystals. In: Boutet S, Fromme P, Hunter MS, editors. X-ray Free Electron Lasers: A Revolution in Structural Biology. Cham: Springer International Publishing; 2018. p. 59-85.

45. Liu W, Wacker D, Gati C, Han GW, James D, Wang D, et al. Serial Femtosecond Crystallography of G Protein–Coupled Receptors. Science. 2013;342(6165):1521. doi: 10.1126/science.1244142.

46. Conrad CE, Basu S, James D, Wang D, Schaffer A, Roy-Chowdhury S, et al. A novel inert crystal delivery medium for serial femtosecond crystallography. IUCrJ. 2015;2(4):421-30. doi: doi:10.1107/S2052252515009811.

47. Echelmeier A, Sonker M, Ros A. Microfluidic sample delivery for serial crystallography using XFELs. Analytical and Bioanalytical Chemistry. 2019;411(25):6535-47. doi: 10.1007/s00216-019-01977-x.

48. Fromme R, Ishchenko A, Metz M, Chowdhury SR, Basu S, Boutet S, et al. Serial femtosecond crystallography of soluble proteins in lipidic cubic phase. IUCrJ. 2015;2(5):545-51. doi: doi:10.1107/S2052252515013160.

49. Weierstall U, James D, Wang C, White TA, Wang D, Liu W, et al. Lipidic cubic phase injector facilitates membrane protein serial femtosecond crystallography. Nature Communications. 2014;5(1):3309. doi: 10.1038/ncomms4309.

50. Stauch B, Cherezov V. Serial Femtosecond Crystallography of G Protein-Coupled Receptors. Annual review of biophysics. 2018;47:377-97. Epub 2018/03/15. doi: 10.1146/annurev-biophys-070317-033239. PubMed PMID: 29543504.

51. Schlichting I. Serial femtosecond crystallography: the first five years. IUCrJ. 2015;2(2):246-55. doi: doi:10.1107/S205225251402702X.

52. Alder BJ, Wainwright TE. Phase Transition for a Hard Sphere System. The Journal of Chemical Physics. 1957;27(5):1208-9. doi: 10.1063/1.1743957.

53. McCammon JA, Gelin BR, Karplus M. Dynamics of folded proteins. Nature. 1977;267(5612):585-90. doi: 10.1038/267585a0.

54. Brooks BR, Bruccoleri RE, Olafson BD, States DJ, Swaminathan S, Karplus M. CHARMM: A program for macromolecular energy, minimization, and dynamics calculations. Journal of Computational Chemistry. 1983;4(2):187-217. doi: 10.1002/jcc.540040211.

55. Hornak V, Abel R, Okur A, Strockbine B, Roitberg A, Simmerling C. Comparison of multiple Amber force fields and development of improved protein backbone parameters. Proteins. 2006;65(3):712-25. doi: 10.1002/prot.21123. PubMed PMID: 16981200.

56. Abraham MJ, Murtola T, Schulz R, Páll S, Smith JC, Hess B, et al. GROMACS: High performance molecular simulations through multi-level parallelism from laptops to

supercomputers. SoftwareX. 2015;1-2:19-25. doi: https://doi.org/10.1016/j.softx.2015.06.001.

57. Phillips JC, Braun R, Wang W, Gumbart J, Tajkhorshid E, Villa E, et al. Scalable molecular dynamics with NAMD. Journal of Computational Chemistry. 2005;26(16):1781-802. doi: 10.1002/jcc.20289.

58. Eastman P, Swails J, Chodera JD, McGibbon RT, Zhao Y, Beauchamp KA, et al. OpenMM 7: Rapid development of high performance algorithms for molecular dynamics. PLOS Computational Biology. 2017;13(7):e1005659. doi: 10.1371/journal.pcbi.1005659.

CHAPTER 2

UNDERSTANDING THE RELATIONSHIP BETWEEN GPCRS AND CHOLESTEROL

GPCRs Reside in Lipid Rafts

The plasma membrane, located on the outside of eukaryotic cells, is mainly comprised of phospholipids that form a bilayer based on the hydrophobic/hydrophilic dichotomy of the molecules. In practice, the plasma membrane is often visualized as a mostly empty bilayer that contains a few sporadically placed integral membrane proteins. In fact, the first plasma membrane models were hypothesized in this way, without even incorporating proteins [1]. However, this simple phospholipid model could not account for the observed membrane phenomenon, such as electric resistance. Until 1972, the best accepted models were the Davidson-Danielli Tri-Layer Model [1, 2] and Robertson's Unit Membrane Model [3, 4]. The Tri-Layer Model revolutionarily asserted that proteins were found in the plasma membrane and were the reason for the phenomena that Gorter's simple phospholipid model could not explain. This model consisted of a "protein-lipid-protein sandwich." Similarly, Robertson's model was comprised of four layers-two lipids and two protein. The overall width of Robertson's model was ~70 Ångstroms wide and consisted of two distinct zones (named the electron light and electron-dense zones) [4]. In 1972, Singer and Nicolson published the Fluid-Mosaic Model, the model that is accepted today [5] (Fig. 3.1). As constructed at the time, the Fluid-Mosaic Model was comprised of a simple phospholipid bilayer with integral membrane proteins and glycoproteins interspersed. Since the initial publication, the model has undergone subtle changes as new information has become available [3]. For example, one year after Singer and Nicolson's

model was published, hypotheses concerning compartmentalization of the membrane became popular after a study by Yu *et al.* showed that membranes could be sectioned into detergent resistance or friendly sections [6]. These observations led to the Lipid Raft hypothesis that is still being explored today [7]. Unfortunately, much of the data regarding lipid rafts and membrane sectioning is ambiguous, making it difficult to draw concrete conclusions. To ease this difficulty, a precise definition of lipid rafts was developed and released in 2006 [8]. The consensus was that lipid rafts are membrane domains that compartmentalize cellular processes and are characterized as heterogeneous, small (10-200 nm), dynamic, and cholesterol and sphingolipid rich. These small rafts can then form larger (microscopic >300 nm) domains upon protein-lipid or lipid-lipid interactions [8]. Though much of the function and many of the characteristics of lipid rafts are unknown, they play a clearly important role in human physiology [9, 10]. Cholesterol and saturated lipids change the biophysical properties of these lipid rafts. Cholesterol, for example, orders the membrane and modulates membrane fluidity and permeability [11, 12]. These changes can have large physiologic consequences as evidenced by Cooper *et al.*, who showed that an increase in membrane cholesterol shorted the survival of red blood cells in vivo [11]. Proteins that are post-translationally modified with lipid groups (palmitoylation, for example) are known to have an affinity for lipid rafts [13, 14]. G-Protein Coupled Receptors (GPCRs), the main focus of this dissertation, are palmitoylated after translation and are commonly found residing in lipid rafts [15-17]. Practically, it is hypothesized that membrane proteins are separated into these distinct rafts as a mechanism to keep each signal clean and unaffected by the various other pathways operating simultaneously. For GPCRs, one take-home message is

clear- receptors operate in ordered, cholesterol-rich domains of the membrane. It is therefore not surprising that cholesterol is ubiquitous in GPCR literature.

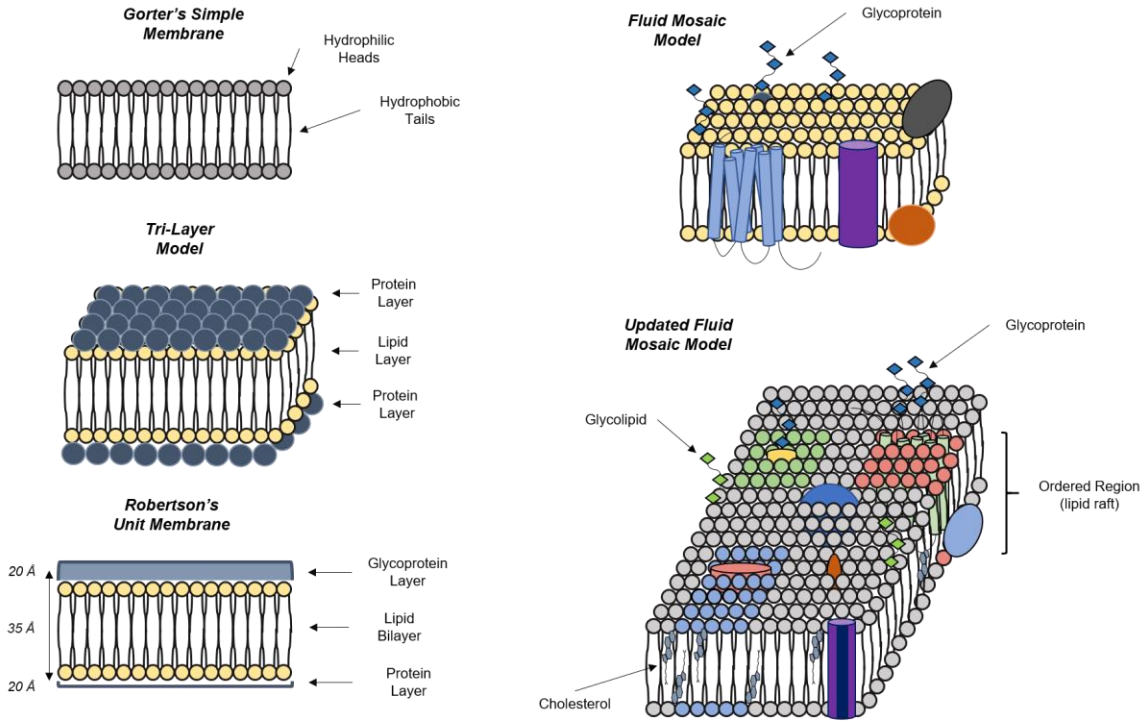

Figure 2.1 Models of the lipid bilayer throughout history. The first models were composed of a simple bilayer. Next, the Tri-Layer and Unit Membrane models had a "protein-lipid sandwich" system where proteins formed a layer on both the inside and outside of the membrane. The Fluid-Mosaic Model, the model accepted today incorporated integral membrane proteins into the bilayer. The updated Fluid-Mosaic Model shows an ordering or sectioning of the membrane into lipid rafts that house integral membrane proteins.

GPCRs are modulated by cholesterol

A short dive into the literature will quickly show that cholesterol is of utmost importance in GPCR physiology. Cholesterol hemi-succinate, a detergent derivative of cholesterol, is universally utilized to solubilize GPCRs from lipid bilayers as it imparts "bicelle" characteristics to the detergent and has been shown to stabilize receptors [18]. Furthermore, the addition of cholesterol into the host lipid during Lipidic Cubic Phase (LCP) crystallization has been shown to increase receptor thermal stability [19] and is

considered essential in the growth of well-diffracting GPCR crystals [20]. Furthermore, numerous receptors have been shown to be affected by the modulation of membrane cholesterol levels [21] (Table 1). Membrane cholesterol levels have been shown to affect the binding affinity of ligands at various receptors. Interestingly, there is evidence that a high cholesterol environment has caused receptors to show a decreased affinity for certain ligands while showing an increased affinity for others. It is therefore hypothesized that cholesterol could be involved in biased signaling (the receptor preferring to signal through a specific pathway/G-protein rather than another) or simply stabilize specific active/inactive conformations. Cholesterol is also known to modulate downstream signaling of receptors and has even been implicated to play a key role in the homo-dimerization of the β_2AR [22]. Unfortunately, little is understood about the mechanisms behind these modulations, and in many cases the scientific literature is difficult to rationalize. The type-1 cholecystokinin receptor (CCK_1R), for example, shows increased agonist affinity from cholesterol enrichment of the membrane while simultaneously showing a decrease in downstream signaling [23, 24]. The picture is made cloudier (but admittedly more interesting) when attention is brought to homologous receptors that behave differently regarding cholesterol. In short, despite the receptors sharing very high sequence homology and cholesterol recognition motifs, one receptor is modulated by cholesterol and the other is completely insensitive [24, 25].

Receptor	Effect of Cholesterol	References
β_2AR	Enhanced signaling upon cholesterol depletion/Thought to be involved in receptor homo-dimerization	[26-28]
5HT$_{1A}$	Ligand binding effected/Reduced G-protein coupling	[29-31]
Rhodopsin	Decreased receptor activation upon cholesterol modulation	[32, 33]
CCR5	Decreased downstream signaling upon removal of cholesterol	[34, 35]
CXCR4	Decreased downstream signaling upon removal of cholesterol / Conformational changes	[35, 36]
CB$_1$R	Removal of cholesterol increases ligand binding/Important in correct trafficking of the protein	[25, 37, 38]
CCK$_1$R	Cholesterol modulation affects ligand binding and downstream signaling	[23, 24, 39]
SMO	Cholesterol acts as an endogenous ligand to activate the receptor	[40]
GAL$_2$R	Reduced Cholesterol inhibited ligand binding	[41]
5HT$_{7A}$	Reduced Cholesterol inhibited ligand binding and downstream signaling	[42]
mGluR	Reduced cholesterol inhibited ligand binding	[43]
δ-Opioid	Reduced cholesterol modulated ligand binding	[44]
κ-Opioid	Reduced Cholesterol increased ligand affinity	[45]

μ-Opioid	Ergosterol found to lock receptor in an inactive state	[46]
OXTR	Cholesterol required for proper ligand binding	[47, 48]
NK_1R	Removal of cholesterol abolished signaling from the receptor	[49, 50]
M_2R	Cholesterol promotes antagonist binding	[51]
T_2R4	Cholesterol found necessary for optimal signaling	[52]
$A_{2a}AR$	Ligand binding is affected by cholesterol	[53, 54]
NTS1	Dimerization is promoted by cholesterol	[55]

Table 2.1. A list of receptors known to be sensitive to membrane cholesterol levels

Evidence suggests that both specific receptor-cholesterol interactions and the more general effects of the membrane could be responsible for receptor modulation, leading experts to conclude that a general rule concerning cholesterol-based modulation of GPCRs would be arbitrary, and it could be that both specific and general cholesterol effects are involved in the effects described above [56]. The strongest evidence for specific receptor-cholesterol interaction is seen at the smoothened receptor (SMO). The structure of the SMO revealed a cholesterol molecule bound in the extracellular cysteine-rich region of Class-F receptors [57]. Furthermore, cholesterol is known to act as the endogenous ligand for SMO and activate the frizzled signaling pathway [58]. Recently, in silico research (and in vitro validation) have yielded evidence that oxysterols bind specifically to and modulate GPR183, PY and CXCR2 [59, 60]. It is hypothesized that cholesterol (or oxidized cholesterol derivatives) may act as allosteric "ligands" that modulate the function of some receptors. Molecular Dynamics (MD) simulations have also shown evidence of cholesterol entering the binding pocket of the A_{2a} Adenosine

receptor [61]. However, most affinities may fall under that category of “slippery hot spots” coined by Sarkar and Chattopadhyay [62]. In other words, receptor-cholesterol interactions may be mostly transient with very quick off-rate. Still, these transient affinities are centered around specific regions and motifs on the receptor.

The general effects of cholesterol on lipid bilayers are also known to modulate GPCR function. Rhodopsin, a photoceptor in the eyes, is known to be regulated between inactive and active states by cholesterol [63]. Specifically, the equilibrium between these states was found to be due to the cholesterol-induced changes in the free volume available for molecular motion inside the hydrophobic core of the bilayer [64, 65]. Additionally, changes in bilayer thickness and membrane curvature have been found to be enough to modulate the function of Rhodopsin [66], both of which are known consequences of cholesterol on a biological membrane [67, 68]. Thus, in the case of Rhodopsin, general effects on the bilayer are sufficient to explain the modulation of the receptor. Cholesterol’s effects on membrane viscosity and dipole potential can be used to explain the modulation of the 5HT-1A serotonin receptor [56]. Though much evidence suggests that the 5HT-1A interacts specifically which cholesterol molecules, again, the general effect on the membranes is sufficient to explain much of cholesterol’s effect on receptor function [56]. Additionally, membrane fluidity was found to be of major importance in the function of the CCK_1R [47]. After the removal of cholesterol, sterol analogs were used to restore membrane fluidity. Restoration of membrane fluidity in the absence of cholesterol was found to support CCK_1R function, allowing for the hypothesis that cholesterols' effects on the fluidity of the membrane were more important in the sensitivity of the CCK_1R than specific allosteric modulation via cholesterol.

There is little consensus on how cholesterol induces changes in receptor function, and it would be irrational to apply one mechanism of action to every GPCR found in the human genome. It may be that some receptors are modulated by the general effects, while others rely on specific cholesterol binding events. Moreover, it is entirely plausible that receptor sensitivity could be due to a combination of both general and specific effects of cholesterol [56].

Structural Data and Binding Motifs

Cholesterol is essential for the crystallization of GPCRs in LCP [20]. In nearly every published crystal structure of GPCRs, the receptor was crystalized in a host lipid (typically monoolein) supplemented with 10% cholesterol. Unsurprisingly, cholesterol densities are commonly found in the crystallographic datasets arising from GPCRs (Table 2). Over 60 structures arising from 14 different GPCRs in the PDB contain at least one cholesterol molecule near the receptor. It is worthwhile to note that while receptors are commonly crystallized from lipid bilayers, the cholesterol interactions found in structure models may not represent physiological conditions. Still, the first important structural information regarding receptor-cholesterol interactions was found on the β_2AR (PDB: 3D4S) and included two cholesterol molecules near the receptor. [69]. It was made particularly clear during structural analysis that these cholesterol molecules were not involved in crystal packing and so the hypothesis was developed that cholesterol was interacting specifically with the β_2AR. Subsequent analysis lead to the discovery of the Cholesterol Consensus Motif (CCM), a cholesterol recognition site that is well conserved across Class-A GPCRs [69]. The CCM motif is located in a cleft between transmembrane helices 2 and 4 and consists of 4 amino acids: W/Y$^{4.50}$ (94% conserved in Class-A

GPCRs), R/K$^{4.39\text{-}4.43}$, I/L/V$^{4.46}$, and F/Y$^{2.41}$ (Ballesteros/Weinstein numbering (Ballesteros, 1995 #60)) (Fig. 3.2). Altogether, 21% of Class-A GCPRs contain the strict form of the CCM. However, a slightly revised CCM does not require an aromatic amino acid at position 2.41 and is conserved across 44% of Class-A GPCRs. Since its discovery, the structures of other receptors have shown cholesterol at the CCM, including the CB_1R and the $P2Y_{12}R$ [70, 71]. Interestingly, a similar motif was found to be essential for correct trafficking and incorporation into lipid rafts for a hemagglutinin from the Influenza virus [72]. Beyond the other effects on GPCR physiology above, it is possible that the CCM motif could play an important role in the proper trafficking of GPCRs to lipid rafts.

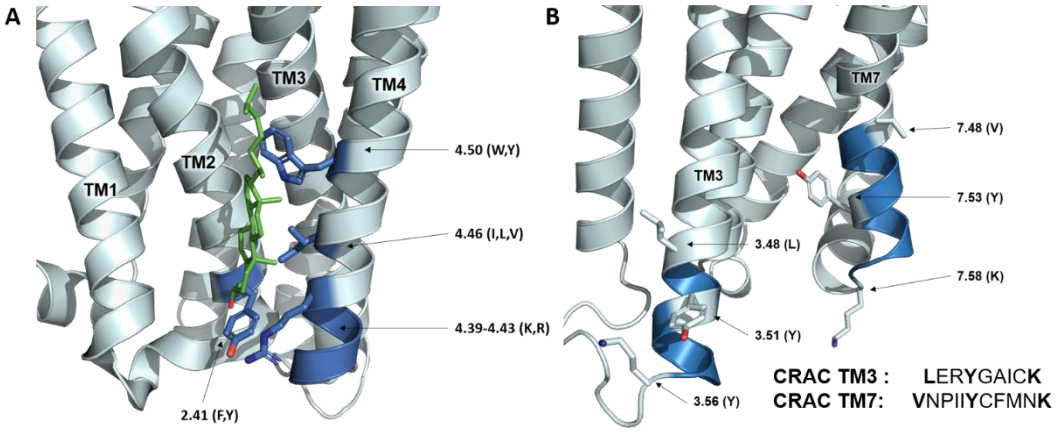

Figure 2.2. Cholesterol recognition motifs on GPCRs. A) The CCM motif is discovered on the β_2AR. The residues that make up the CCM motif are highlighted in dark blue. A cholesterol molecule bound to the CCM motif is shown in green. B) CRAC sequences are shown on a homology model of the CCK_1R. Residues that make the CRAC sequence are shown as sticks and bolded in the sequence. Residues in between these important residues are highlighted in blue.

Receptor	PDB ID
CB_1R	**5XRA, 5XR8**
$5HT_{2B}$	**4IB4, 4NC3, 5TVN, 6DSO, 6DRY, 6DRX, 6DRZ**
TP	**6IIV, 6IIU**
$A_{2a}AR$	**4EIY, 5IU7, 5IU8, 5IUA, 5IUB, 5IU4, 5K2D, 5K2B, 5K2C, 5K2A, 5UVI, 5JTB, 5MZJ, 5N2R, 5MZP, 5NLX, 5NM4, 5NM2, 5VRA, 6AQF, 5OLV, 5OLH, 5OLO, 5OM1, 5OLZ, 5OM4, 5OLG**
US28	**5WB2, 4XT1**
$mGluR_1$	**4OR2**
μ-Opioid	**4DKL, 5C1M**
CCR9	**5LWE**
κ-Opioid	**6B73**
ET_B	**5X93**
$P2Y_1$	**4XNV**
$P2Y_{12}$	**4PXZ, 4NTJ**
SMO	**5L7D, 6D35**
β_2AR	**2RH1, 3D4S, 3NY9, 3NY8, 3NYA, 3PDS, 5D5B, 5D5A, 5JQH', 5D6L, 5X7D**

Table 2.2. A list of GPCR structure models in the PDB that contain cholesterol

The Cholesterol Recognition Amino-acid Consensus (CRAC) is the most popular cholesterol binding motif in the literature and is regularly observed in membrane proteins [73]. A CRAC is a sequence of amino acids that may show an affinity for cholesterol

molecules and follows a simple form. First, a leucine or valine followed by 1-5 amino acids of any type, then a central tyrosine residue, again, followed by 1-5 amino acids of any type, and finally, an arginine or lysine to terminate the sequence ((L/V)-X_{1-5}-Y-X_{1-5}-(R/K)) (Fig.3.2). There is controversy in the literature over the predictive nature of the CRAC sequence. These issues arise from the "loose" nature of the motif and the wide variety of amino acids and length variations (5-13 amino acids long) that could theoretically bind cholesterol [74, 75]. Still, even skeptics have shown that protein-cholesterol interactions have been observed at CRAC sequences and mutation of key residues have been found to affect those interactions [74, 76]. These evidences support that CRAC sequences can facilitate specific protein-cholesterol binding. However, other research has shown that these observations cannot be applied to all cases. For example, the central tyrosine residue, considered essential for cholesterol binding at CRAC sequences by some studies [74], has been shown to be unimportant for cholesterol binding at CRAC sequences on other proteins [76]. It seems, therefore, that while CRAC sequences have little predictive value for cholesterol binding, the best view is that they are regions of proteins with potential affinity for cholesterol as they contain the proper hydrophobic, aromatic, and polar groups necessary to facilitate cholesterol binding. CRAC sequences are most commonly found on the upper and lower ends of transmembrane helices. This positioning allows the terminal charged residue of the CRAC sequence, as well as the hydroxyl group of the cholesterol molecule, to be placed in the hydrophilic, charged environment at the end of the membrane. On proteins with multiple transmembrane helices, CRAC sequences can be found on both the inner and outer leaflets of the membrane. A lesser known motif, called the CARC sequence, is also

known to interact with cholesterol. Simply put, the CARC sequence is simply a reversed sequence of the CRAC sequence ((R/K)-X_{1-5}-(Y)-X_{1-5}-(L/V)).

CRAC sequences are commonly found on GPCRs and may have important functional implications [77]. It is undeniable that some receptors are affected by the presence of these CRAC sequences. The $5HT_{1A}$ receptor contains numerous CRAC sequences that are evolutionarily conserved and thought to be important for the function of the receptor [78]. The CB_1R contains a CRAC sequence on transmembrane helix 7 that was shown to be the cause of the differential sensitivity of the CB_1 and CB_2 receptors. Strikingly, the removal of this CRAC sequence via mutation abolished the cholesterol sensitivity of the CB_1R [25]. Mutations of a CRAC sequence on the CCK_1R has been implicated to be important in the cholesterol sensitivity of the receptor [23]. Furthermore, a taste receptor, T2R4, known to be modulated by cholesterol was made insensitive to changes in membrane cholesterol levels upon mutagenesis of a CRAC sequence on helix 3 [79]. It is important to note, however, that the presence of a CRAC sequence does not ensure cholesterol binding or sensitivity. The CCK subfamily of Class-A GPCRs is a perfect example. Despite sharing nearly identical cholesterol recognition motifs with the cholesterol sensitive CCK_1R, the CCK_2R is completely insensitive to the amount of cholesterol in the membrane [24]. So, evidence from one subfamily ($CB_{1/2}R$) shows that a specific CRAC sequence is vital in the cholesterol sensitivity of the receptor. However, evidence from a different subfamily ($CCK_{1/2}R$) shows that their shared CRAC sequences may not be the reason for the cholesterol sensitivity of the receptor. Clearly, a one-size-fits-all approach to cholesterol-GPCR interactions is a poor tactic.

Methods to identify cholesterol sensitivity of GPCRs

Nearly every study probing cholesterol sensitivity of GPCRs relies on the modulation of membrane cholesterol levels or limiting the availability of cholesterol in the host cells. After cholesterol is modulated, numerous assays can be run to quantitatively analyze receptor function. These assays often include competitive ligand binding to analyze the receptor's ability to bind endogenous/exogenous ligands or downstream signaling assays to measure the levels of various signaling species that arise after receptor activation (such as Ca^{2+} or cAMP).

Researchers have been able to modulate membrane cholesterol content through an array of techniques. Perhaps the most common of which is the use of a specific carrier molecule such as Methyl-β-cyclodextrin (MβCD). MβCD is a cyclodextrin oligomer of glucose that preferentially chelates cholesterol [80] (Fig. 3.3). One particular benefit of using cyclodextrins is the ability to preload the molecules with cholesterol or other sterols to supplement back into the membrane [81]. This allows researchers to both remove and supplement cholesterol. MβCD has been used to analyze the sensitivity of numerous GPCRS, including cannabinoid[37, 38], CCK [24], 5HT-1A [30], galanin [41], rhodopsin [65], and oxytocin [47].

Another technique involves the oxidation of membrane cholesterol with cholesterol oxidase [82]. This strategy allows researchers to change the nature of cholesterol in the membrane without physically removing cholesterol. Thus, treatment

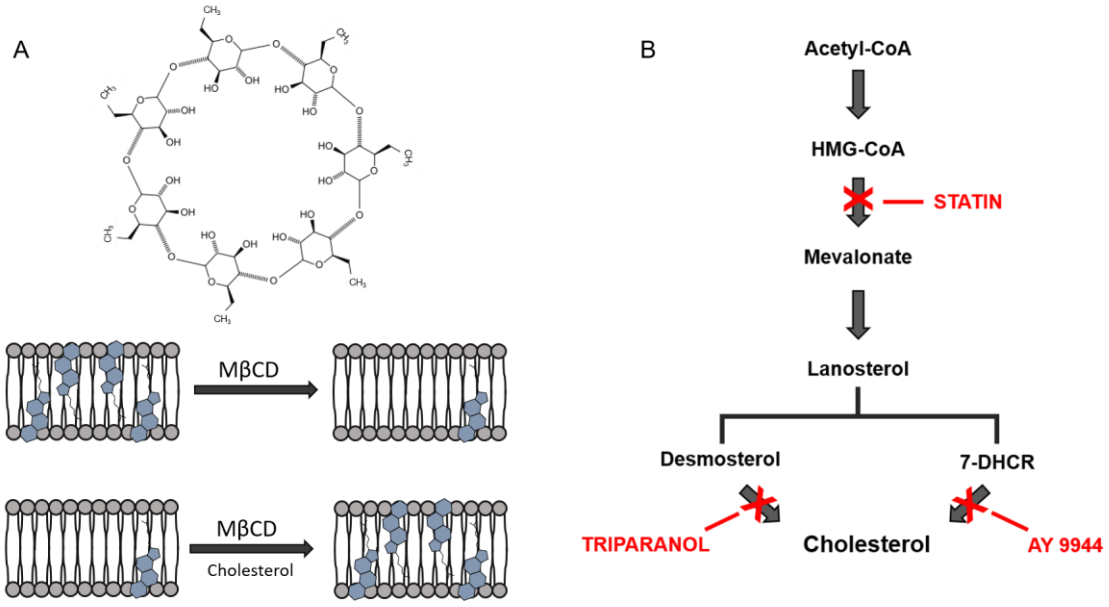

Figure 2.3 A) The structure of MβCD allows for it to preferentially bind cholesterol and other sterols. MβCD alone removes cholesterol from membranes. MβCD preloaded with cholesterol will supplement the cholesterol in a membrane. B) Cholesterol synthesis pathway. Inhibitors that are commonly used to reduce cellular cholesterol are shown in red.

with cholesterol oxidase is associated with only mild effects on the membrane, which could be better when probing for the specific effects of cholesterol on receptor function. Additionally, this approach changes cholesterol at the hydroxyl group, making it valuable for studies interested in the function of the hydroxyl. Modulation via cholesterol oxidase has been used to study the CCK [47], galanin [41], and chemokine receptors [35], among others.

Yet another technique to control membrane cholesterol content is the inhibition of cholesterol biosynthesis by selectively inhibiting different enzymes in the cholesterol synthesis pathway. Statins are commonly used to lower cellular cholesterol levels as they

inhibit HMG-CoA reductase, the enzyme responsible for the rate-limiting step in the biosynthesis of cholesterol [83, 84] (Fig.3.3). AY 9944, which inhibits the formation of cholesterol from 7-DHCR, and triparanol, which inhibits cholesterol synthesis from 24-DHCR interfere with the final steps in the Kandutsch-Russell pathway and Bloch pathway, respectively [85, 86]. Additionally, cholesterol can be controlled via the addition of complexing agents into the membrane. These do not change the actual concentration of cholesterol in the membrane, instead they sequester cholesterol into specific regions of the bilayer, thus inhibiting interactions with receptors of interest.

In Silico methods to measure receptor-cholesterol interactions

The above *in vitro* experiments have yielded great insight into the modulations of GPCRs. Yet, they cannot yield information about if, how, and where cholesterol interacts with receptors. Computational methods, specifically Molecular Dynamics (MD) simulations, can yield insights into binding locations and receptor conformational changes. Briefly, in vitro experiments commonly tell us that a given receptor is modulated by cholesterol. In contrast, MD can give us information on why or how a receptor is modulated.

In standard GPCR-lipid simulations, course-grained simulations are preferred because of their better sampling efficiency. Effectively sampling lipid (or cholesterol) diffusion and binding require long-time scales (>1 μs). Fully atomistic simulations, while providing more explicit details than coarse-grain, are computationally expensive and difficult to push past the microsecond timescale. The most commonly used forcefield for coarse-grain GPCR-lipid simulation is the MARTINI forcefield [87]. The MARTINI forcefield has been shown to be computationally efficient while accurately reproducing

protein-lipid interactions [88]. Furthermore, the forcefield has been extensively validated to reproduce similar results to accepted *in vivo/vitro* assays [89]. However, there are a few documented limitations of the MARTINI model. First, lower resolution due to the course-grain model. Second, because entropies are generally lower due to coarse-graining, free energies and enthalpies can differ from true results. Lastly, the method wherein MARTINI generates its coarse-grain model greatly limits real conformational changes in proteins during simulations [89].

The MARTINI forcefield is generated based on a four-to-one-mapping. In other words, four heavy atoms (plus any hydrogens associated with them) are represented as one interaction center, here called a martini particle [89]. Ring-like molecules (like benzene rings or cholesterol) are modeled with a 2:1 ratio for nonhydrogen atoms to martini particles (Fig. 3.4). Martini particles are divided into four main types: polar, non-polar, apolar, and charged. Each main type of particle is then divided into subtypes indicating either the degree of polarity (1-5) or hydrogen bonding capability (donor, acceptor, both, none) [89]. Altogether, there are 18 martini particles in the model.

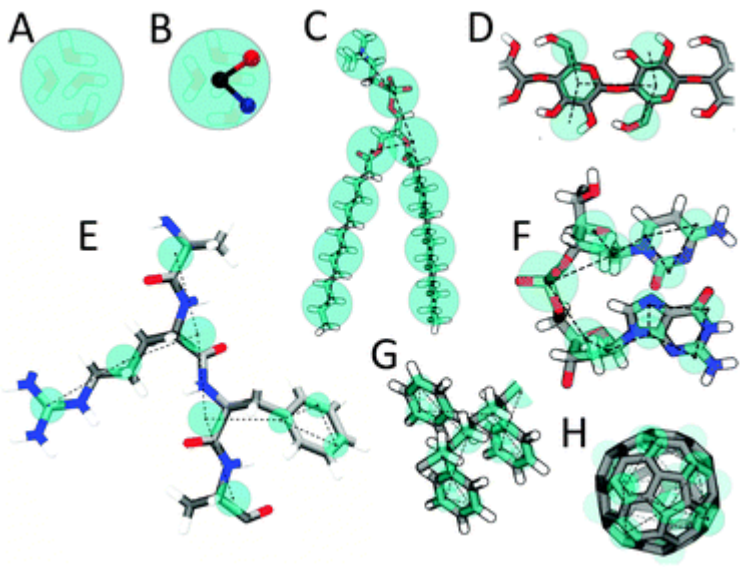

Fig. 2.4 Martini mapping examples of selected molecules. (A) Standard water particle representing four water molecules. (B) Polarizable water molecule with embedded charges. (C) DMPC lipid. (D) Polysaccharide fragment. (E) Peptide. (F) DNA fragment. (G) Polystyrene fragment. (H) Fullerene molecule. In all cases Martini CG beads are shown as cyan transparent beads overlaying the atomistic structure.

Aside from the validation listed above, one of the largest benefits of the MARTINI forcefield is the limited parameters required for a converged solution during the simulation course. The key parameters are timestep, cut-off radii for non-bonded potentials, updating the neighbor list, and determining a switch function. Time-steps of 20-40 fs are commonly utilized [89]. MARTINI uses a Lennard-Jones [90] 12-6 potential to characterize non-bonded potentials and a switch function that pushes all non-bonded interactions (Lennard-Jones and Coulombic) to zero at a distance of 1.2 nm [87]. Additionally, MARTINI support suggests a neighbor list cut-off of 1.2 nm that updates every 10 timesteps. Though originally developed for use with GROMACS [91], MARTINI has been made compatible with numerous other simulation programs such as NAMD [92], Desmond [93], and GROMOS [94]. MARTINI has been shown to be

effective at simulating GPCR-cholesterol interactions at numerous receptors. Evidence supporting the role of cholesterol in the homo-dimerization of the β_2AR came from simulations with MARTINI [22]. MARTINI was also used to map cholesterol binding sites on the 5HT-1A [95]. Similarly, binding pockets on the β_2AR and the A_{2a}AR were discovered from simulations utilizing a MARTINI forcefield [96].

Before simulations can be run, structure models must be prepared and inserted into a membrane. If no structure is available, a homology model must be created. Numerous software packages are available to create homology models, such as Modeller [97]. Even if a structure of the receptor is available, care should be taken before running simulations as structure models of GPCRs are commonly generated from crystals of highly engineered receptors. Often the incorporation of fusion proteins into intracellular loops or the addition of an antibody during purification can lock the receptor into specific conformations that could introduce bias into the simulation. In the case of the former, fusion proteins should be removed and the endogenous loop can be modeled with the software described above. After quality structure models are generated, they are inserted into a bilayer. CHARMM-GUI is a trusted program that is commonly seen in the literature and has been extensively validated [98]. CHARMM-GUI allows users to choose a wide variety of lipid compositions for their own experimental needs. Typically, GPCRs are inserted into a 1-palmitoyl-2-oleoyl-*sn*-glycero-3-phosphocholine (POPC) bilayer [28, 95, 96]. This POPC bilayer can then be supplemented with whatever concentration of cholesterol as deemed necessary by the simulators. Additional parameters, such as water molecules and intra/extra cellular salt atoms, can be added to mimic physiological conditions. An additional benefit of CHARMM-GUI is its ability to

export results compatible with a wide variety of simulation packages [99]. An overview of the preparation for GPCR-cholesterol simulations is outlined in figure 3.5.

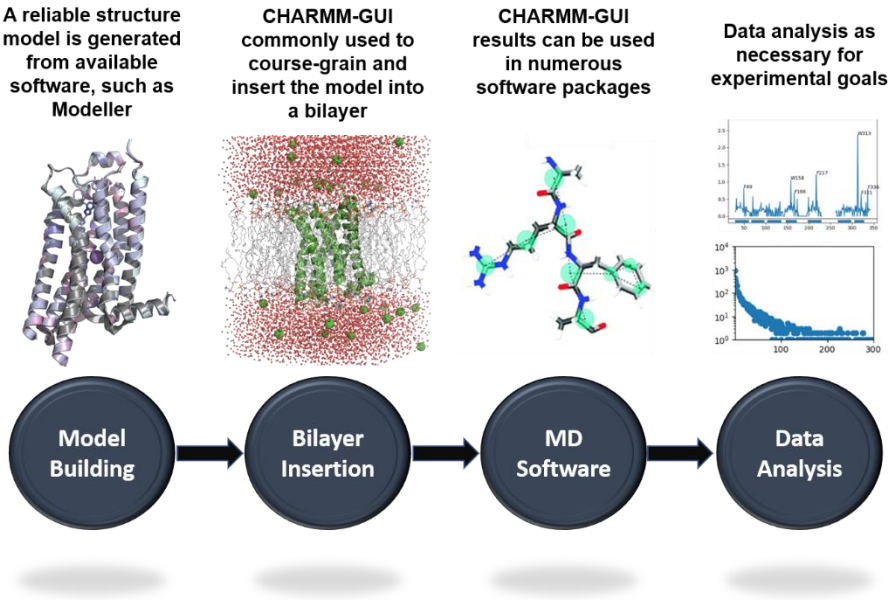

Fig. 2.5 A general workflow for simulating GPCR-cholesterol interactions. After structure models are built. They are course-grained and inserted into a bilayer using software such as CHARMM-GUI. CHARMM-GUI outputs can be used in a variety of MD software packages. After the simulation is run, data can be analyzed as necessary for the experiment.

Conclusion and Take-Home Messages

Cholesterol undeniably plays an important role in GPCR function. Unfortunately, much is still unclear concerning this important molecule. Recognition motifs seem to be a poor predictor of how/if cholesterol will interact with the receptor, and even if cholesterol is found to have an affinity for these motifs, it is not guaranteed that those interactions will manifest themselves in the physiology of the receptor. Experts have called for new computational and experimental developments to better understand these recognition motifs and how they may affect GPCR function [62]. This is the aim of the next chapter of this dissertation. To be sure, cholesterol interactions will vary from one receptor to another and it may be difficult to come to one consensus on how GPCRs function with

regards to this molecule. However, one take-home message is certain – GPCRs have a strong association with cholesterol, and in some cases this relationship is critical in receptor function.

References

1. Gorter E, Grendel F. ON BIMOLECULAR LAYERS OF LIPOIDS ON THE CHROMOCYTES OF THE BLOOD. Journal of Experimental Medicine. 1925;41(4):439-43. doi: 10.1084/jem.41.4.439.

2. Danielli JF, Davson H. A contribution to the theory of permeability of thin films. Journal of Cellular and Comparative Physiology. 1935;5(4):495-508. doi: 10.1002/jcp.1030050409.

3. Nicolson GL. The Fluid—Mosaic Model of Membrane Structure: Still relevant to understanding the structure, function and dynamics of biological membranes after more than 40years. Biochimica et Biophysica Acta (BBA) - Biomembranes. 2014;1838(6):1451-66. doi: https://doi.org/10.1016/j.bbamem.2013.10.019.

4. Robertson JD. The ultrastructure of cell membranes and their derivatives. Biochem Soc Symp. 1959;16:3-43. PubMed PMID: 13651159.

5. Singer SJ, Nicolson GL. The Fluid Mosaic Model of the Structure of Cell Membranes. Science. 1972;175(4023):720. doi: 10.1126/science.175.4023.720.

6. Yu J, Fischman DA, Steck TL. Selective solubilization of proteins and phospholipids from red blood cell membranes by nonionic detergents. Journal of Supramolecular Structure. 1973;1(3):233-48. doi: 10.1002/jss.400010308.

7. Sezgin E, Levental I, Mayor S, Eggeling C. The mystery of membrane organization: composition, regulation and roles of lipid rafts. Nature Reviews Molecular Cell Biology. 2017;18(6):361-74. doi: 10.1038/nrm.2017.16.

8. Pike LJ. Rafts defined: a report on the Keystone symposium on lipid rafts and cell function. Journal of Lipid Research. 2006;47(7):1597-8.

9. Alonso MA, Millán J. The role of lipid rafts in signalling and membrane trafficking in T lymphocytes. Journal of Cell Science. 2001;114(22):3957.

10. Simons K, Ehehalt R. Cholesterol, lipid rafts, and disease. (0021-9738 (Print)).

11. Cooper RA. Influence of increased membrane cholesterol on membrane fluidity and cell function in human red blood cells. Journal of supramolecular structure. 1978;8(4):413-30. doi: 10.1002/jss.400080404. PubMed PMID: 723275.

12. Raffy S, Teissié J. Control of lipid membrane stability by cholesterol content. Biophys J. 1999;76(4):2072-80. doi: 10.1016/S0006-3495(99)77363-7. PubMed PMID: 10096902.

13. Calder PC, Yaqoob P. Lipid Rafts—Composition, Characterization, and Controversies. The Journal of Nutrition. 2007;137(3):545-7. doi: 10.1093/jn/137.3.545.

14. Goluszko P, Nowicki B. Membrane Cholesterol: a Crucial Molecule Affecting Interactions of Microbial Pathogens with Mammalian Cells. Infection and Immunity. 2005;73(12):7791. doi: 10.1128/IAI.73.12.7791-7796.2005.

15. Barnett-Norris J, Lynch D, Reggio PH. Lipids, lipid rafts and caveolae: Their importance for GPCR signaling and their centrality to the endocannabinoid system. Life Sciences. 2005;77(14):1625-39. doi: https://doi.org/10.1016/j.lfs.2005.05.040.

16. Goddard AD, Watts A. Regulation of G protein-coupled receptors by palmitoylation and cholesterol. BMC Biol. 2012;10:27-. doi: 10.1186/1741-7007-10-27. PubMed PMID: 22429402.

17. Villar VAM, Cuevas S, Zheng X, Jose PA. Chapter 1 - Localization and signaling of GPCRs in lipid rafts. In: K. Shukla A, editor. Methods in Cell Biology. 132: Academic Press; 2016. p. 3-23.

18. Thompson AA, Liu JJ, Chun E, Wacker D, Wu H, Cherezov V, et al. GPCR stabilization using the bicelle-like architecture of mixed sterol-detergent micelles. Methods. 2011;55(4):310-7. doi: https://doi.org/10.1016/j.ymeth.2011.10.011.

19. Liu W, Hanson MA, Stevens RC, Cherezov V. LCP-Tm: An Assay to Measure and Understand Stability of Membrane Proteins in a Membrane Environment. Biophys J. 2010;98(8):1539-48. doi: 10.1016/j.bpj.2009.12.4296.

20. Gimpl G. Interaction of G protein coupled receptors and cholesterol. Chemistry and Physics of Lipids. 2016;199:61-73. doi: https://doi.org/10.1016/j.chemphyslip.2016.04.006.

21. Paila YD, Chattopadhyay A. The function of G-protein coupled receptors and membrane cholesterol: specific or general interaction? Glycoconjugate Journal. 2008;26(6):711. doi: 10.1007/s10719-008-9218-5.

22. Prasanna X, Chattopadhyay A, Sengupta D. Cholesterol modulates the dimer interface of the β_2-adrenergic receptor via cholesterol occupancy sites. Biophysical journal. 2014;106(6):1290-300. doi: 10.1016/j.bpj.2014.02.002. PubMed PMID: 24655504.

23. Desai AJ, Harikumar KG, Miller LJ. A Type 1 Cholecystokinin Receptor Mutant That Mimics the Dysfunction Observed for Wild Type Receptor in a High Cholesterol Environment. 2014;289(26):18314-26. doi: 10.1074/jbc.M114.570200.

24. Potter RM, Harikumar KG, Wu SV, Miller LJ. Differential sensitivity of types 1

and 2 cholecystokinin receptors to membrane cholesterol. 2012;53(1):137-48. doi: 10.1194/jlr.M020065.

25. Oddi S, Dainese E, Fezza F, Lanuti M, Barcaroli D, De Laurenzi V, et al. Functional characterization of putative cholesterol binding sequence (CRAC) in human type-1 cannabinoid receptor. Journal of Neurochemistry. 2011;116(5):858-65. doi: 10.1111/j.1471-4159.2010.07041.x.

26. Kirilovsky J, Schramm M. Delipidation of a beta-adrenergic receptor preparation and reconstitution by specific lipids. Journal of Biological Chemistry. 1983;258(11):6841-9.

27. Paila YD, Jindal E, Goswami SK, Chattopadhyay A. Cholesterol depletion enhances adrenergic signaling in cardiac myocytes. Biochimica et Biophysica Acta (BBA) - Biomembranes. 2011;1808(1):461-5. doi: https://doi.org/10.1016/j.bbamem.2010.09.006.

28. Prasanna X, Chattopadhyay A, Sengupta D. Cholesterol modulates the dimer interface of the β_2-adrenergic receptor via cholesterol occupancy sites. (1542-0086 (Electronic)).

29. Paila YD, Pucadyil Tj Fau - Chattopadhyay A, Chattopadhyay A. The cholesterol-complexing agent digitonin modulates ligand binding of the bovine hippocampal serotonin 1A receptor. (0968-7688 (Print)).

30. Pucadyil TJ, Chattopadhyay A. Cholesterol modulates ligand binding and G-protein coupling to serotonin1A receptors from bovine hippocampus. Biochimica et Biophysica Acta (BBA) - Biomembranes. 2004;1663(1):188-200. doi: https://doi.org/10.1016/j.bbamem.2004.03.010.

31. Pucadyil TJ, Chattopadhyay A. Cholesterol modulates the antagonist-binding function of hippocampal serotonin1A receptors. Biochimica et Biophysica Acta (BBA) - Biomembranes. 2005;1714(1):35-42. doi: https://doi.org/10.1016/j.bbamem.2005.06.005.

32. Albert AD, Boesze-Battaglia K. The role of cholesterol in rod outer segment membranes. Progress in Lipid Research. 2005;44(2):99-124. doi: https://doi.org/10.1016/j.plipres.2005.02.001.

33. Mitchell DC, Straume M, Miller JL, Litman BJ. Modulation of metarhodopsin formation by cholesterol-induced ordering of bilayer lipids. Biochemistry. 1990;29(39):9143-9. doi: 10.1021/bi00491a007.

34. Nguyen DH, Taub D. Cholesterol is essential for macrophage inflammatory protein 1β binding and conformational integrity of CC chemokine receptor 5. Blood. 2002;99(12):4298-306. doi: 10.1182/blood-2001-11-0087.

35. Nguyen DH, Taub DD. Inhibition of chemokine receptor function by membrane cholesterol oxidation. Experimental Cell Research. 2003;291(1):36-45. doi: https://doi.org/10.1016/S0014-4827(03)00345-8.

36. Nguyen DH, Taub D. CXCR4 Function Requires Membrane Cholesterol: Implications for HIV Infection. The Journal of Immunology. 2002;168(8):4121. doi: 10.4049/jimmunol.168.8.4121.

37. Bari M, Battista N, Fezza F, Finazzi-Agrò A, Maccarrone M. Lipid Rafts Control Signaling of Type-1 Cannabinoid Receptors in Neuronal Cells: IMPLICATIONS FOR ANANDAMIDE-INDUCED APOPTOSIS. Journal of Biological Chemistry. 2005;280(13):12212-20.

38. Bari M, Paradisi A, Pasquariello N, Maccarrone M. Cholesterol-dependent modulation of type 1 cannabinoid receptors in nerve cells. Journal of Neuroscience Research. 2005;81(2):275-83. doi: 10.1002/jnr.20546.

39. Miller LJ, Desai AJ. Metabolic Actions of the Type 1 Cholecystokinin Receptor: Its Potential as a Therapeutic Target. Trends in Endocrinology & Metabolism. 2016;27(9):609-19. doi: 10.1016/j.tem.2016.04.002.

40. Luchetti G, Sircar R, Kong JH, Nachtergaele S, Sagner A, Byrne EF, et al. Cholesterol activates the G-protein coupled receptor Smoothened to promote Hedgehog signaling. eLife. 2016;5:e20304. doi: 10.7554/eLife.20304. PubMed PMID: 27705744.

41. Pang L, Graziano M, Wang S. Membrane Cholesterol Modulates Galanin−GalR2 Interaction. Biochemistry. 1999;38(37):12003-11. doi: 10.1021/bi990227a.

42. Sjögren B, Hamblin MW, Svenningsson P. Cholesterol depletion reduces serotonin binding and signaling via human 5-HT7(a) receptors. European Journal of Pharmacology. 2006;552(1):1-10. doi: https://doi.org/10.1016/j.ejphar.2006.08.069.

43. Eroglu Ç, Brügger B, Wieland F, Sinning I. Glutamate-binding affinity of Drosophila metabotropic glutamate receptor is modulated by association with lipid rafts. Proceedings of the National Academy of Sciences. 2003;100(18):10219. doi: 10.1073/pnas.1737042100.

44. Huang P, Xu W, Yoon S-I, Chen C, Chong PL-G, Liu-Chen L-Y. Cholesterol reduction by methyl-β-cyclodextrin attenuates the delta opioid receptor-mediated signaling in neuronal cells but enhances it in non-neuronal cells. Biochemical Pharmacology. 2007;73(4):534-49. doi: https://doi.org/10.1016/j.bcp.2006.10.032.

45. Xu W, Yoon S-I, Huang P, Wang Y, Chen C, Chong PL-G, et al. Localization of the κ Opioid Receptor in Lipid Rafts. Journal of Pharmacology and Experimental

Therapeutics. 2006;317(3):1295. doi: 10.1124/jpet.105.099507.

46. Lagane B, Gaibelet G, Meilhoc E, Masson J-M, Cézanne L, Lopez A. Role of Sterols in Modulating the Human μ-Opioid Receptor Function in Saccharomyces cerevisiae. Journal of Biological Chemistry. 2000;275(43):33197-200.

47. Gimpl G, Burger K, Fahrenholz F. Cholesterol as Modulator of Receptor Function. Biochemistry. 1997;36(36):10959-74. doi: 10.1021/bi963138w.

48. Gimpl G, Wiegand V, Burger K, Fahrenholz F. Chapter 4 Cholesterol and steroid hormones: modulators of oxytocin receptor function. Progress in Brain Research. 139: Elsevier; 2002. p. 43-55.

49. Meyer BH, Segura J-M, Martinez KL, Hovius R, George N, Johnsson K, et al. FRET imaging reveals that functional neurokinin-1 receptors are monomeric and reside in membrane microdomains of live cells. Proceedings of the National Academy of Sciences. 2006;103(7):2138. doi: 10.1073/pnas.0507686103.

50. Monastyrskaya K, Hostettler A, Buergi S, Draeger A. The NK1 Receptor Localizes to the Plasma Membrane Microdomains, and Its Activation Is Dependent on Lipid Raft Integrity. Journal of Biological Chemistry. 2005;280(8):7135-46.

51. Colozo AT, Park PSH, Sum CS, Pisterzi LF, Wells JW. Cholesterol as a determinant of cooperativity in the M2 muscarinic cholinergic receptor. Biochemical Pharmacology. 2007;74(2):236-55. doi: https://doi.org/10.1016/j.bcp.2007.04.009.

52. Pydi SP, Jafurulla M, Wai L, Bhullar RP, Chelikani P, Chattopadhyay A. Cholesterol modulates bitter taste receptor function. Biochimica et Biophysica Acta (BBA) - Biomembranes. 2016;1858(9):2081-7. doi: https://doi.org/10.1016/j.bbamem.2016.06.005.

53. Guixà-González R, Albasanz JL, Rodriguez-Espigares IA-O, Pastor M, Sanz F, Martí-Solano M, et al. Membrane cholesterol access into a G-protein-coupled receptor. (2041-1723 (Electronic)).

54. O'Malley MA, Helgeson ME, Wagner NJ, Robinson AS. The Morphology and Composition of Cholesterol-Rich Micellar Nanostructures Determine Transmembrane Protein (GPCR) Activity. Biophys J. 2011;100(2):L11-L3. doi: 10.1016/j.bpj.2010.12.3698.

55. Oates J, Faust B, Attrill H, Harding P, Orwick M, Watts A. The role of cholesterol on the activity and stability of neurotensin receptor 1. Biochimica et Biophysica Acta (BBA) - Biomembranes. 2012;1818(9):2228-33. doi: https://doi.org/10.1016/j.bbamem.2012.04.010.

56. Jafurulla M, Aditya Kumar G, Rao BD, Chattopadhyay A. A Critical Analysis of Molecular Mechanisms Underlying Membrane Cholesterol Sensitivity of GPCRs. In: Rosenhouse-Dantsker A, Bukiya AN, editors. Cholesterol Modulation of Protein Function: Sterol Specificity and Indirect Mechanisms. Cham: Springer International Publishing; 2019. p. 21-52.

57. Byrne EFX, Sircar R, Miller PS, Hedger G, Luchetti G, Nachtergaele S, et al. Structural basis of Smoothened regulation by its extracellular domains. (1476-4687 (Electronic)).

58. Luchetti G, Sircar R, Kong JH, Nachtergaele S, Sagner A, Byrne EFX, et al. Cholesterol activates the G-protein coupled receptor Smoothened to promote Hedgehog signaling. eLife. 2016;5:e20304. doi: 10.7554/eLife.20304.

59. Benned-Jensen T, Norn C Fau - Laurent S, Laurent S Fau - Madsen CM, Madsen Cm Fau - Larsen HM, Larsen Hm Fau - Arfelt KN, Arfelt Kn Fau - Wolf RM, et al. Molecular characterization of oxysterol binding to the Epstein-Barr virus-induced gene 2 (GPR183). (1083-351X (Electronic)).

60. Sensi C, Daniele S, Parravicini C, Zappelli E, Russo V, Trincavelli ML, et al. Oxysterols act as promiscuous ligands of class-A GPCRs: in silico molecular modeling and in vitro validation. (1873-3913 (Electronic)).

61. Guixà-González R, Albasanz JL, Rodriguez-Espigares I, Pastor M, Sanz F, Martí-Solano M, et al. Membrane cholesterol access into a G-protein-coupled receptor. Nature Communications. 2017;8(1):14505. doi: 10.1038/ncomms14505.

62. Sarkar P, Chattopadhyay A. Cholesterol interaction motifs in G protein-coupled receptors: Slippery hot spots? WIREs Systems Biology and Medicine. 2020;12(4):e1481. doi: 10.1002/wsbm.1481.

63. Brown MF. Modulation of rhodopsin function by properties of the membrane bilayer. (0009-3084 (Print)).

64. Mitchell DC, Straume M Fau - Miller JL, Miller Jl Fau - Litman BJ, Litman BJ. Modulation of metarhodopsin formation by cholesterol-induced ordering of bilayer lipids. (0006-2960 (Print)).

65. Niu SL, Mitchell Dc Fau - Litman BJ, Litman BJ. Manipulation of cholesterol levels in rod disk membranes by methyl-beta-cyclodextrin: effects on receptor activation. (0021-9258 (Print)).

66. Soubias O, Gawrisch K. The role of the lipid matrix for structure and function of the GPCR rhodopsin. Biochim Biophys Acta. 2012;1818(2):234-40. Epub 2011/09/05. doi: 10.1016/j.bbamem.2011.08.034. PubMed PMID: 21924236.

67. Chen Z, Rand RP. The influence of cholesterol on phospholipid membrane curvature and bending elasticity. Biophys J. 1997;73(1):267-76. doi: 10.1016/S0006-3495(97)78067-6. PubMed PMID: 9199791.

68. Nezil FA, Bloom M. Combined influence of cholesterol and synthetic amphiphillic peptides upon bilayer thickness in model membranes. (0006-3495 (Print)).

69. Hanson MA, Cherezov V, Griffith MT, Roth CB, Jaakola V-P, Chien EYT, et al. A specific cholesterol binding site is established by the 2.8 A structure of the human beta2-adrenergic receptor. Structure. 2008;16(6):897-905. doi: 10.1016/j.str.2008.05.001. PubMed PMID: 18547522.

70. Hua T, Vemuri K, Nikas SP, Laprairie RB, Wu Y, Qu L, et al. Crystal structures of agonist-bound human cannabinoid receptor CB1. Nature. 2017;547(7664):468-71. doi: 10.1038/nature23272.

71. Zhang J, Zhang K, Gao Z-G, Paoletta S, Zhang D, Han GW, et al. Agonist-bound structure of the human P2Y12 receptor. Nature. 2014;509(7498):119-22. doi: 10.1038/nature13288.

72. de Vries M, Herrmann A, Veit M. A cholesterol consensus motif is required for efficient intracellular transport and raft association of a group 2 HA from influenza virus. (1470-8728 (Electronic)).

73. Li H, Papadopoulos V. Peripheral-type benzodiazepine receptor function in cholesterol transport. Identification of a putative cholesterol recognition/interaction amino acid sequence and consensus pattern. (0013-7227 (Print)).

74. Epand RM. Cholesterol and the interaction of proteins with membrane domains. (0163-7827 (Print)).

75. Palmer M. Cholesterol and the activity of bacterial toxins. (0378-1097 (Print)).

76. Fantini J, Barrantes F. How cholesterol interacts with membrane proteins: an exploration of cholesterol-binding sites including CRAC, CARC, and tilted domains. Frontiers in Physiology. 2013;4:31.

77. Jafurulla M, Tiwari S, Chattopadhyay A. Identification of cholesterol recognition amino acid consensus (CRAC) motif in G-protein coupled receptors. Biochemical and Biophysical Research Communications. 2011;404(1):569-73. doi: https://doi.org/10.1016/j.bbrc.2010.12.031.

78. Fatakia SN, Sarkar P, Chattopadhyay A. A collage of cholesterol interaction motifs in the serotonin(1A) receptor: An evolutionary implication for differential

cholesterol interaction. (1873-2941 (Electronic)).

79. Pydi SP, Jafurulla M, Wai L, Bhullar RP, Chelikani P, Chattopadhyay A. Cholesterol modulates bitter taste receptor function. (0006-3002 (Print)).

80. Zidovetzki R, Levitan I. Use of cyclodextrins to manipulate plasma membrane cholesterol content: Evidence, misconceptions and control strategies. Biochimica et Biophysica Acta (BBA) - Biomembranes. 2007;1768(6):1311-24. doi: https://doi.org/10.1016/j.bbamem.2007.03.026.

81. Chattopadhyay A, Rao BD, Jafurulla M. Solubilization of G protein-coupled receptors: a convenient strategy to explore lipid-receptor interaction. (1557-7988 (Electronic)).

82. Sampson NS, Vrielink A. Cholesterol oxidases: a study of nature's approach to protein design. (0001-4842 (Print)).

83. Istvan ES, Deisenhofer J. Structural mechanism for statin inhibition of HMG-CoA reductase. (0036-8075 (Print)).

84. Levitt ES, Clark Mj Fau - Jenkins PM, Jenkins Pm Fau - Martens JR, Martens Jr Fau - Traynor JR, Traynor JR. Differential effect of membrane cholesterol removal on mu- and delta-opioid receptors: a parallel comparison of acute and chronic signaling to adenylyl cyclase. (0021-9258 (Print)).

85. Kolf-Clauw M, Chevy F Fau - Wolf C, Wolf C Fau - Siliart B, Siliart B Fau - Citadelle D, Citadelle D Fau - Roux C, Roux C. Inhibition of 7-dehydrocholesterol reductase by the teratogen AY9944: a rat model for Smith-Lemli-Opitz syndrome. (0040-3709 (Print)).

86. Mizuno GR, Chapman CJ, Chipault JR, Pfeiffer DR. Lipid composition and (Na+ + K+)-ATPase activity in rat lens during triparanol-induced cataract formation. Biochimica et Biophysica Acta (BBA) - Biomembranes. 1981;644(1):1-12. doi: https://doi.org/10.1016/0005-2736(81)90052-3.

87. Marrink SJ, Risselada Hj Fau - Yefimov S, Yefimov S Fau - Tieleman DP, Tieleman Dp Fau - de Vries AH, de Vries AH. The MARTINI force field: coarse grained model for biomolecular simulations. (1520-6106 (Print)).

88. Monticelli L, Kandasamy SK, Periole X, Larson RG, Tieleman DP, Marrink SJ. The MARTINI Coarse-Grained Force Field: Extension to Proteins. (1549-9618 (Print)).

89. Marrink SJ, Tieleman DP. Perspective on the Martini model. (1460-4744 (Electronic)).

90. Ye L, Neale C, Sljoka A, Lyda B, Pichugin D, Tsuchimura N, et al. Mechanistic insights into allosteric regulation of the A\textsubscript2A adenosine G protein-coupled receptor by physiological cations. Nature Communications. 2018;9(1):1372. doi: 10.1038/s41467-018-03314-9.

91. Van Der Spoel D, Lindahl E, Hess B, Groenhof G, Mark AE, Berendsen HJC. GROMACS: Fast, flexible, and free. Journal of Computational Chemistry. 2005;26(16):1701-18. doi: 10.1002/jcc.20291.

92. Shih AY, Arkhipov A, Freddolino PL, Schulten K. Coarse Grained Protein−Lipid Model with Application to Lipoprotein Particles. The Journal of Physical Chemistry B. 2006;110(8):3674-84. doi: 10.1021/jp0550816.

93. Proceedings of the 2006 ACM/IEEE conference on Supercomputing2006; Tampa, Florida: Association for Computing Machinery.

94. Baron R, Trzesniak D, de Vries AH, Elsener A, Marrink SJ, van Gunsteren WF. Comparison of Thermodynamic Properties of Coarse-Grained and Atomic-Level Simulation Models. ChemPhysChem. 2007;8(3):452-61. doi: 10.1002/cphc.200600658.

95. Sengupta D, Chattopadhyay A. Identification of Cholesterol Binding Sites in the Serotonin1A Receptor. The Journal of Physical Chemistry B. 2012;116(43):12991-6. doi: 10.1021/jp309888u.

96. Genheden S, Essex JW, Lee AG. G protein coupled receptor interactions with cholesterol deep in the membrane. Biochimica et Biophysica Acta (BBA) - Biomembranes. 2017;1859(2):268-81. doi: https://doi.org/10.1016/j.bbamem.2016.12.001.

97. Webb B, Sali A. Comparative Protein Structure Modeling Using MODELLER. (1934-340X (Electronic)).

98. Jo S, Kim T, Iyer VG, Im W. CHARMM-GUI: A web-based graphical user interface for CHARMM. Journal of Computational Chemistry. 2008;29(11):1859-65. doi: 10.1002/jcc.20945.

99. Lee J, Cheng X, Swails JM, Yeom MS, Eastman PK, Lemkul JA, et al. CHARMM-GUI Input Generator for NAMD, GROMACS, AMBER, OpenMM, and CHARMM/OpenMM Simulations Using the CHARMM36 Additive Force Field. Journal of Chemical Theory and Computation. 2016;12(1):405-13. doi: 10.1021/acs.jctc.5b00935.

CHAPTER 3

EVIDENCE THAT SPECIFIC INTERACTIONS PLAY A ROLE IN THE CHOLESTEROL SENSITIVITY OF G PROTEIN-COUPLED RECEPTORS

James Geiger [1¶], Rick Sexton [2¶], Zina Al-Sahouri [1], Ming-Yue Lee [1], Eugene Chun [1], Kaleeckal G. Harikumar [3], Laurence J. Miller [3], Oliver Beckstein [2*], and Wei Liu [1*]

[1] Center for Applied Structural Discovery at the Biodesign Institute, Arizona State University, Tempe, Arizona, United States of America

[2] Department of Physics and Center for Biological Physics, Arizona State University, Tempe, Arizona, United States of America

[3] Department of Molecular Pharmacology and Experimental Therapeutics, Mayo Clinic, Scottsdale, Arizona, United States of America

* Corresponding authors

¶These authors contributed equally.

This is chapter is a manuscript that we have submitted at BBA Biomembranes. I wrote most of the text in the manuscript. I was responsible for project planning, data analysis, and performed the biochemical assays. I performed the majority of editing and handled the peer review process. The manuscript utilizes molecular dynamics outlined in chapter 2 and highlights specific, differential cholesterol binding at the CCK receptors.

Abstract:

G protein-coupled receptors (GPCRs) are known to be modulated by membrane cholesterol levels, but whether or not the effects are caused by specific receptor-cholesterol interactions or cholesterol's general effects on the membrane is not well-understood. We performed coarse-grained molecular dynamics (CGMD) simulations coupled with structural bioinformatics approaches on the β_2-adrenergic receptor (β_2AR) and the cholecystokinin (CCK) receptor subfamily. The β_2AR has been shown to be sensitive to membrane cholesterol and cholesterol molecules have been clearly resolved in numerous β_2AR crystal structures. The two CCK receptors are highly homologous and preserve similar cholesterol recognition motifs but despite their homology, CCK_1R shows functional sensitivity to membrane cholesterol while CCK_2R does not. Our results offer new insights into how cholesterol modulates GPCR function by showing cholesterol interactions with β_2AR that agree with previously published data; additionally, we observe differential and specific cholesterol binding in the CCK receptor subfamily while revealing a previously unreported Cholesterol Recognition Amino-acid Consensus (CRAC) sequence that is also conserved across 38% of class A GPCRs. A thermal denaturation assay (LCP-T_m) shows that mutation of a conserved CRAC sequence on TM7 of the β_2AR affects cholesterol stabilization of the receptor in a lipid bilayer. The results of this study provide a better understanding of receptor-cholesterol interactions that can contribute to novel and improved therapeutics for a variety of diseases.

Introduction:

G protein-coupled receptors (GPCRs) are the largest family of integral membrane proteins in eukaryotic cells. Characterized by a conserved seven transmembrane (TM) helical bundle, GPCRs are classified into five distinct phylogenetic families: class A/rhodopsin, class B/secretin, class C/glutamate, class F/frizzled, and Adhesion, with the vast majority of receptors being found in class A (1) (Fig. 3.1A). GPCRs play essential roles in physiological pathways and cell signaling events, making them important potential drug targets (2).

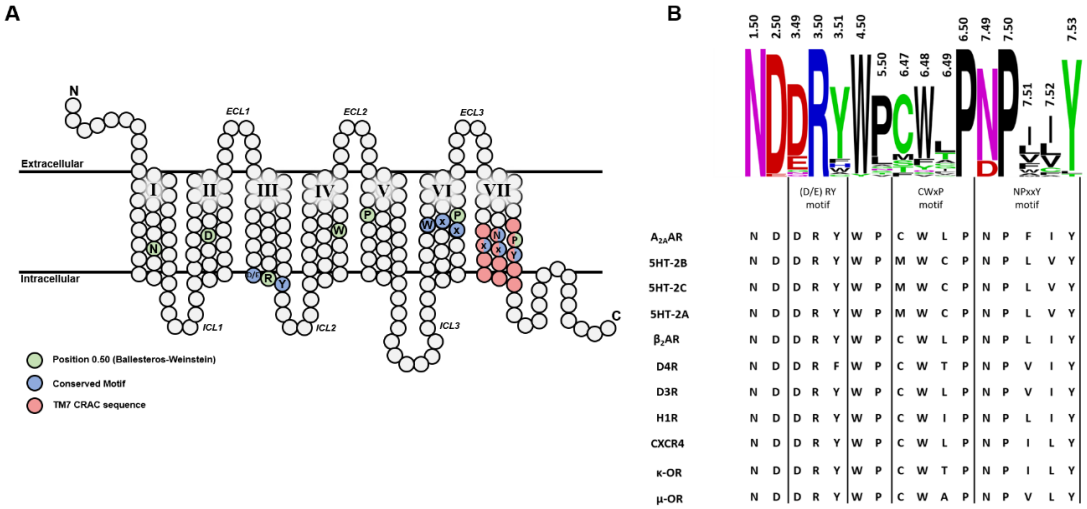

Figure 3.1. Location and conservation of important residues across Class A GPCRs. (A) Snake plot shows the location of well-conserved residues and motifs in class A GPCRs in the transmembrane bundle. B) Cartoon visualization of the most conserved residues on each transmembrane helix as well as well-conserved motifs. Eleven well-studied GPCRs are shown.

GPCRs are commonly found residing in lipid rafts, which are highly ordered regions of the bilayer due to their high cholesterol content (3). GPCR sequestration to these ordered microdomains had led to the hypothesis that cholesterol acts as an allosteric modulator for GPCR functions. Studies involving membrane cholesterol depletion showed

specific altered signaling for the β_2 Adrenergic Receptor (β_2AR) (4), the cannabinoid receptor CB_1 (5), and serotonin receptor $5HT_{1A}$ (6, 7); while cholesterol presence is required for the high affinity active state of the oxytocin receptor (8, 9). Molecular spatial distribution analysis showed high density distribution of cholesterol around $Pro^{7.48}$ (Ballesteros-Weinstein numbering) (10) at the bottom of TM7 of rhodopsin associated with receptor activation (11) (Fig. 3.1A).

Additional evidence suggested that other receptors (e.g. Smoothened, chemokine receptor CXCR2, and GPR183) may directly bind cholesterol through specific interactions (12-15) with multiple specific GPCR-cholesterol interaction sites having been identified (16-19). The CCM motif, first characterized from a structure of the β_2AR, is strictly conserved in 21% of class A GPCRs with 44% of class A receptors containing a slightly relaxed form of the motif (19). CRAC sequences, defined as (–(L/V)-(X_{1-5})-Y-(X_{1-5})-(R/K)-), where X_{1-5} represents 1-5 residues of any amino acid, are considered the most well-known cholesterol recognition motif in literature and are found on many GPCRs (17). Cholesterol molecules were clearly resolved in the crystal structures of numerous receptors (18), but questions remain regarding whether the cholesterol molecules found in these crystal structures represent physiologically relevant and specific interactions, or if they are simply crystallization artifacts due to the abundance of cholesterol in the lipid bilayer and proximity to receptor molecules.

Alternatively, there is evidence suggesting that the observed cholesterol effects arise indirectly through the physical effects of cholesterol on the lipid bilayer (20). Cholesterol is known to alter membrane fluidity (21), thickness (22), and curvature (23). Membrane fluidity was shown to have a direct effect on ligand binding at the $5HT_{1A}$ (24)

and the type-1 cholecystokinin receptor (CCK_1R) (8). Similarly, membrane thickness and curvature is known to affect the active/inactive equilibrium of Rhodopsin (25). Taken together, there is a critical need to address and reconcile the apparent ambiguities in how cholesterol exerts its effect on GPCR functions.

Here, we set out to probe the specificity of cholesterol-GPCR interactions through a combination of coarse-grained molecular dynamics (CGMD) simulations (26, 27) with structural bioinformatics and experimental validation using β_2AR as the model system., and apply the structural dynamics and bioinformatics approaches to the CCK receptor family. CGMD has been widely used to predict and elucidate detailed interactions of GPCRs with lipids (26, 28, 29), in particular the interaction of cholesterol with GPCRs (30-33). Further, we focus the study on the CCK receptor family due to the differential effects cholesterol exerts: the CCK_1R ligand binding and downstream signaling are both modulated by membrane cholesterol levels, while the highly homologous (53% identity overall, and 69% in the transmembrane regions) gastrin receptor (CCK_2R) is unaffected by cholesterol (34). Even though both CCK receptor subtypes share cholesterol recognition motif sites, the functional implications of membrane cholesterol composition are quite distinct. Our results show that the CCK receptors interact with cholesterol through different motifs despite similar recognition sequences on the primary level. The CRAC motif at the bottom of TM3 has been identified as the functionally important site in CCK_1R (35). The CCK_1R has been implicated as a potential therapeutic target to treat metabolic syndrome and obesity, with an allosteric modulator designed that can prevent the inhibitory effects of the high cholesterol environment associated with obese patients (36, 37).

Lastly, we discover a new CRAC motif near the end of transmembrane-helix seven (TM7) that is conserved across 38% of class A GPCRs (Fig. 3.1A). The results reported herein elucidate GPCR-cholesterol interactions in greater detail and could prove insightful in the development of additional allosteric therapeutics specifically targeting the CCK_1R.

Results:

Simulations on the β_2AR revealed receptor-cholesterol interactions consistent with previously published literature results (19, 31, 38, 39). We analyzed 11 β_2AR structures in the PDB and observed that pockets around structurally resolved cholesterol molecules showed high residency times in our simulations (Fig. 3.2). Residues from the CCM motif including $W158^{4.50}$ and $I153^{4.45}$ showed peaks, indicating longer cholesterol residency. $I55^{1.54}$ also showed significant interaction times with cholesterol molecules. In certain structure models (e.g., PDB: 2RH1) a cholesterol molecule is found within 5 Å from this residue. A pair of the strongest signals arose from $T164^{4.56}$ and $W313^{7.40}$. Though not observed in crystal structures, both residues have been have been implicated to interact with cholesterol (38, 39). Additional residues, such as $F217^{5.56}$, are in close proximity to CRAC sequences with one site on the intracellular end of TM7 already characterized on the β_2AR, CB_1R, and $5\text{-}HT_{1A}$ (31). This motif is especially important on the CB_1R where a mutation in this site, $K402G^{4.58}$, abolished the cholesterol sensitivity of the receptor showing the critical role the CRAC motif plays in CB_1R-cholesterol interaction (5).

With the successful application of our CGMD approach to β_2AR, we next used the same methods to study the CCKRs. On the CCK_1R, we observed strong receptor-cholesterol interactions at $F130^{3.41}$ with the highest residency time out of all of the receptor

targets in this study. Furthermore, few CCK_1R residues have residency times higher than the background signal. A binding pocket at this $F130^{3.41}$ location is further supported by slightly weaker interactions at $S169^{4.53}$ (Fig. 3.2). Short residency times were also observed on TM7 at residues $I369^{7.52}$ and $F372^{7.55}$ (Fig. 3.3A/B).

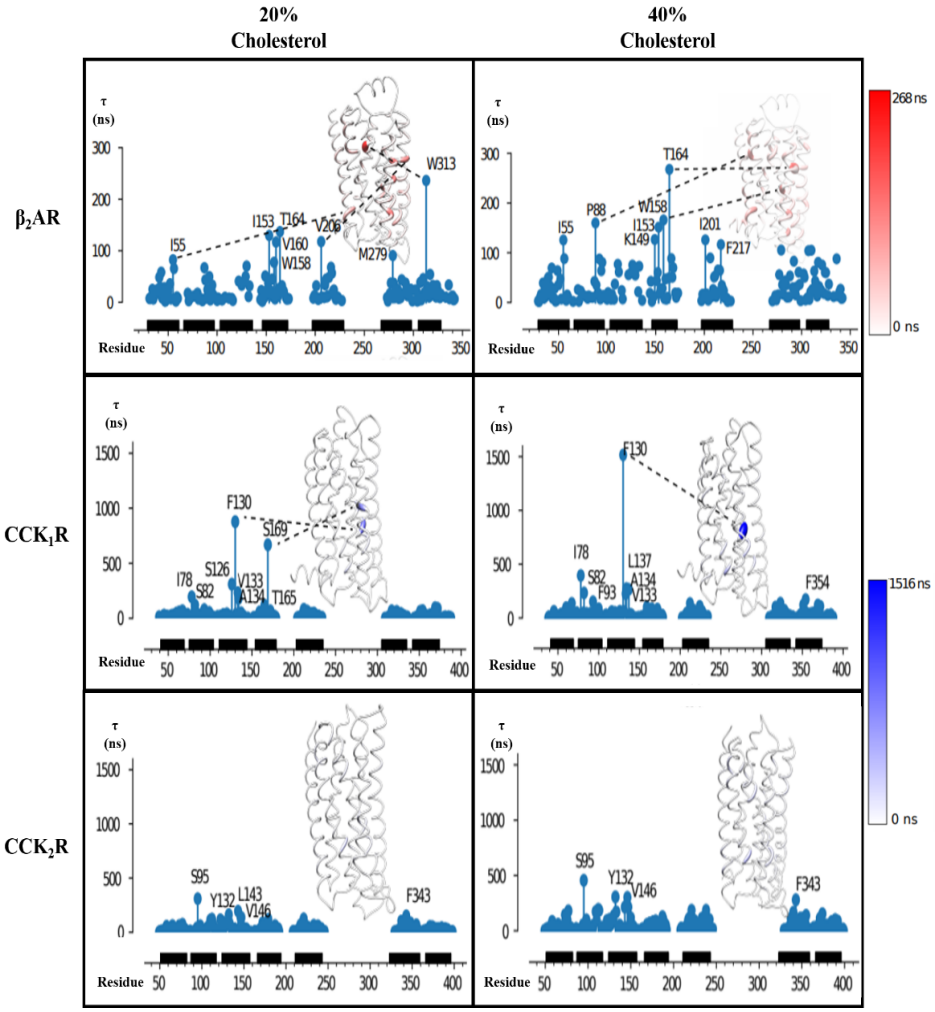

Figure 3.2. Residency data from the simulations by residue. Residency times at the β_2AR, CCK_1R, and CCK_2R in 20% and 40% cholesterol membranes. Structure models highlight residues with long residency times. The color on the structure models reflects average residency according to the bars on the right.

While the CCK_1R-cholesterol interactions were mainly centered around TM3, the CCK_2R interactions were more spread throughout the receptor and residency times were

all close to background, although some interactions (such as at S95$^{2.45}$) suggest that CCK$_2$R may also interact with cholesterol molecules via the CCM motif mentioned above (Fig. 3.3C). Direct comparison of the residency times for structurally equivalent residues between the two receptors demonstrated that residues in the CCK$_1$R typically bound cholesterol longer than the corresponding residues in CCK$_2$R (Fig. 3.3B). These results were consistent regardless of the simulated cholesterol concentrations, implying that the CGMD simulations are able to differentiate which of the two homologous receptors interacts preferentially with cholesterol.

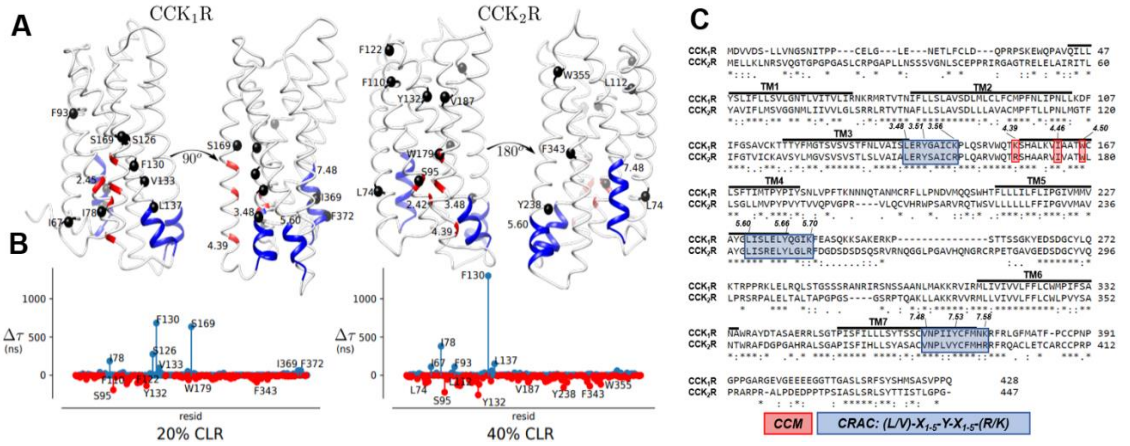

Figure 3.3. Differential interactions with cholesterol in the CCK subfamily. (A) Structure models of the CCK receptors. CRAC sequences are shown in blue and the CCM motif is shown in red. Black dots represent residues that showed cholesterol residency during the simulation. (B) Simulation data from the CCK receptors plotted together. Blue represents the CCK$_1$R and red represents the CCK$_2$R. Residencies at the CCK$_1$R are much stronger than those at the CCK$_2$R. Furthermore, despite conserved recognition motifs, the CCK receptors interact much differently with cholesterol. (C) A sequence alignment of the two CCK receptors. The CCM motif is highlighted in red and CRAC sequences are highlighted in blue.

With the small interactions observed on TM7 of the CCK$_1$R, we performed a sequence alignment to identify a previously unreported TM7 CRAC sequence consisting of V365$^{7.48}$, Y370$^{7.53}$, and K374$^{7.57}$ on the CCK$_1$R, and V385$^{7.48}$, Y390$^{7.53}$, and R394$^{7.57}$ on the CCK$_2$R (Fig. 3.3C). This novel CRAC site is centered around the highly conserved

NPxxY motif in class A GPCRs (40). Thus, we aligned all class A GPCRs (excluding olfactory receptors) using the structure-based alignment tool from the GPCR database (41) to see if this new CRAC site is also present in other class A GPCRs (41). 38% of the 285 class A GPCRs that were aligned and analyzed were found to contain a CRAC sequence surrounding the NPxxY motif, including β_2AR (S1).

To better understand cholesterol interactions on TM7, we performed a series of mutations on the β_2AR and used the LCP-T_m assay to quantify the stabilizing effects of cholesterol binding to the receptor (42). We analyzed single point mutations at the newly discovered CRAC sequence along with other residues on TM7. A summary of all mutations tested is shown in Table 1. Two mutations, Y326A$^{7.53}$ and F336A$^{8.54}$, nearly abolished protein expression completely. Of the β_2AR constructs with reasonable expression, four of the seven remaining mutants were highly aggregated after purification in the presence of the high-affinity ligand timolol (Table 3.1). Due to poor protein expression and aggregation of most of the mutants, we were only able to collect LCP-T_m data on two mutant receptors alongside an unmutated receptor control sample. The first, F321A$^{7.48}$ (located two helix turns near W313$^{7.40}$, see Fig. 3.2A) was included as it could potentially interact with cholesterol molecules on the TM7 CRAC site. Similarly, R328A$^{7.55}$ was incorporated due to its position in the TM7 CRAC sequence (Fig. 3.4C). Previous studies showed the unmutated β_2AR to be stabilized by 2.3°C when 10% (w/w) cholesterol was added to the host lipid monoolein relative to the monoolein-only sample (42). In our experiments, the T_m of unmutated β_2AR is 43.45 ± 0.65 °C (monoolein-only) and 45.15 ± 0.54 °C (monoolein with 10% cholesterol) resulting in a ΔT_m of 1.71 ± 0.85°C (Fig. 3.4A/B). The F321A and R328A mutations showed similar transition temperatures to the unmutated

control in cholesterol-free assays, with T_m values of 42.65 ± 0.21 and 43.10 ± 0.74 °C, respectively. In the cholesterol, the F321A mutant had a very slight increase in stability with a ΔT_m value of 0.46 ± 0.77 °C. Surprisingly, the R328A mutant had the largest ΔT_m value at 5.75 ± 1.65 °C with the addition of cholesterol into the host lipid. A summary of the data is included in Fig. 3.4.

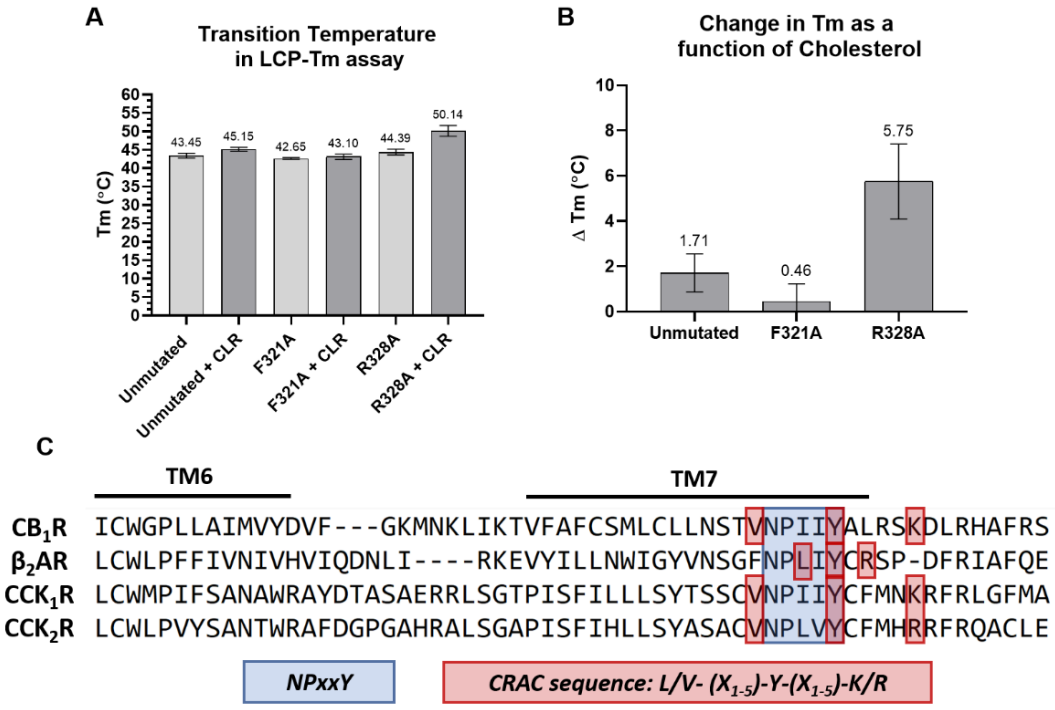

Figure 3.4. A conserved CRAC sequence modulates cholesterol-induced stability on the β2AR. (A) Mean transition temperatures from LCP-Tm assay with and without cholesterol in the LCP. (B) ΔT_m values for each mutant. (C) Alignment of CB_1R, β_2AR, and the CCK receptors. The conserved NPxxY motif on helix 7 is shown in blue. Residues fulfilling the CRAC sequence are shown in red.

TABLE 3.1. Summary of the mutations on the β_2AR and their results.

Construct	Purpose	Behavior	ΔTm(°C)
Unmutated	Control	Good	1.71±0.85
W313A	Flagged in simulation	High Aggregation	-
S319A	Control mutation	Slight aggregation. Biphasic data could not be fit to Boltzmann curve in LCP-Tm	-
I319A	Control mutation	Heavily Aggregated	-
F321A	Theoretical interaction with cholesterol on TM7	Good	0.46±0.77
L324A	Part of CRAC sequence on TM7	Heavily Aggregated	-
I325A	Control Mutation	Heavily Aggregated	-
Y326A	CRAC sequence	Expression Abolished	-
R328A	CRAC sequence	Good	5.75±1.65
F336A	Theoretical interaction with cholesterol	Expression Abolished	-

Discussion:

The β_2 adrenergic receptor (β_2AR) was initially used as the model system to initially test and validate the methods outlined in this study. The structure, function, and cholesterol sensitivity of the β_2AR have been extensively characterized with multiple cholesterol recognition motifs (CCM, CRAC) already identified on this receptor (31). The results from our study identified cholesterol interaction sites consistent with previously reported motifs. A clear binding pocket was observed at the CCM motif in our simulations. Furthermore, CRAC sequences found on TM5 and 7, were consistent with the higher residency times observed in our simulations. Overall, we found that our simulations agreed with the established literature on cholesterol interactions with the β_2AR (19, 31, 38, 39).

Our simulations on the CCK receptor family showed differential cholesterol binding despite a high sequence homology between these receptors (34). Experiments on chimeras of the two receptors showed that the CRAC motif at the bottom of TM3 is responsible for the differential cholesterol sensitivity between the two receptors (34), consistent with our simulation data. Furthermore, the CCK_1R Y140A mutation at the bottom of TM3 within this CRAC motif has been shown to mimic the wildtype CCK_1R conformation in a high cholesterol environment along with the loss of cholesterol sensitivity (34, 35). Our simulations predict that the CCK_1R mainly interacts with cholesterol molecules via $F130^{3.41}$. Taken together, our results along with the previously published data suggest that cholesterol binds the CCK_1R on TM3. Strong cholesterol interactions around position 3.41 are intriguing as mutation of this position to tryptophan is commonly performed during receptor engineering for structural studies, and has been included in the thermo-stabilization of numerous receptors for crystallization (43-45). Initially discovered on β_2AR, mutation of the residue at this position (3.41) decreased affinity for small molecule ligands 2-fold while increasing recombinant expression by nearly 4-fold and purified monomer yield by 5-fold (44). Position 3.41 mutations to tryptophan have also been successfully extended to chemokine, serotonin, and dopamine receptor structural studies (43). Taken together, the ability to affect receptor expression, yield, and stability as well as broadly being applicable to other GPCRs underscore the potential importance of this residue in GPCR physiology. Therefore, it is not unreasonable to presume that cholesterol interactions at 3.41 could be responsible for the cholesterol sensitivity of the CCK_1R.

The CCK_2R appears to mainly interact with cholesterol via the CCM as the strongest signal was from $S95^{2.45}$ at the bottom of TM2 but it appears to interact with cholesterol with lower specificity and affinity than CCK_1R. In the CGMD simulations, CCK_1R interacted with cholesterol for much longer and at more specific residues than its insensitive homolog CCK_2R (Fig. 3.3B). These results imply that specific cholesterol-receptor binding and interaction could be responsible for the difference in physiological effects between the two CCK receptors seen in a high cholesterol environment. Although indirect effects of cholesterol on membrane curvature could be responsible for modulating receptor functions, our data suggest that CCKRs bind cholesterol specifically and differentially. Thus, for the CCKRs they may be insensitive to the global effects of cholesterol on lipid bilayer curvature, fluidity, and microdomain-receptor sequestration. Our simulations agree with previous literature results that TM3, and specifically F130, is responsible for the differential effect of membrane cholesterol on the CCK receptors (34, 35).

As part of this study on the CCKRs, we had discovered a new CRAC site on TM7 that overlaps with the highly conserved class A GPCR NPxxY motif; subsequent sequence alignment with all 285 class A GPCRs showed that 38% share a CRAC sequence in this region (S1). $Tyr^{7.53}$ of the NPxxY motif plays an essential role in class A GPCR activation, as mutation of $Tyr^{7.53}$ on numerous receptors has shown a decrease or elimination of downstream signaling (46). Upon ligand binding, conformational changes in the transmembrane helices result in a water-mediated hydrogen-bond network that links $Tyr^{7.53}$ to $Tyr^{5.58}$. This interaction helps facilitate the outward swing of helix VI which in turn allows for the G_α subunit to bind the receptor and activate the signaling cascade. The

importance of both the NPxxY motif and cholesterol in GPCR physiology have been extensively supported in the literature and it is well established that the NPxxY motif plays a significant role in stabilizing active state receptors (46). Our mutations on the β_2AR reinforce the importance of this region in receptor stability and function as mutations to Y326A$^{7.53}$ and F336A^{helix8} nearly abolished expression of the protein (Table 3.1).

Our LCP-T_m assay on the unmutated receptor showed that incorporating 10% cholesterol into the host lipid increased the T_m by 1.71 ± 0.85°C. F321$^{7.48}$ is located on TM7 three amino acids above the novel CRAC sequence. We expected that mutating this residue (F321A) would alter cholesterol binding at this location and would thus decrease the ΔT_m value in the LCP-T_m assay. However, our ΔT_m value of 0.46 ± 0.77 °C was not found to be statistically significant from the unmutated receptor at a 95% confidence interval (p = 0.1310). R328$^{7.55}$ is a key part of the CRAC sequence outlined above. Like our F321A mutation, we hypothesized that the R328A mutation would inhibit cholesterol interactions and lower the ΔT_m value of the receptor. Surprisingly, the R328A mutant's T_m value increased from 44.39 ± 0.76 to 50.14 ± 1.47°C with the addition of cholesterol, yielding a ΔT_m 5.75 ± 1.65 °C. This result was found to be significant from the unmutated receptor at a 95% confidence interval (p=0.0194). This result is counterintuitive as we expected that the positively charged arginine residue should interact favorably with the hydroxyl group of cholesterol molecules, and thus the R328A mutation would result in a smaller ΔT_m than the unmutated control. One potential explanation is that, from the crystal structure model (PDB: 2RH1), the R328$^{7.55}$ sidechain participates in several hydrogen bond interactions with the sidechains of T274$^{6.36}$, backbone carbonyl of K270$^{6.32}$, and a sulfate ion. Therefore, the R328A mutation would disrupt these hydrogen bond interactions and

potentially destabilize the local region. However, upon further examination, the hydrogen bond interactions outlined above could have instead made the entry of the cholesterol binding cleft inaccessible from the membrane environment. Thus, removing the bulky Arg sidechain would disrupt the existing hydrogen bond network, and potentially make the binding cleft accessible to favorable receptor-cholesterol interactions resulting in the higher ΔT_m value for R328A. Alternatively, the ΔT_m of R328A could be explained by the physical impact of cholesterol on lipid bilayers (21, 47, 48). A mismatch between the length of the hydrophobic transmembrane helix and the width of the lipid bilayer is known to destabilize proteins (45). Hypothetically, these physical changes in the bilayer upon the addition of cholesterol could place the charged arginine residue into an environment that destabilizes the receptor (i.e. further into the hydrophobic membrane). Therefore, mutation to alanine would remove the potentially destabilizing effect of the charged arginine in the bilayer. Nevertheless, the difference in the ΔT_m values between the R328A mutant and the unmutated control were found to be statistically significant. Although the results were unexpected, and do not definitively show cholesterol binding at this CRAC, the data may suggest that $R328^{7.55}$ affects the receptor's behavior in a membrane with modulated cholesterol levels.

It should be noted that CRAC sequences, as well as CCM and other cholesterol-recognition motifs, provide little predictive value in how cholesterol will interact with the protein (17, 49). Indeed, CRAC sequences are ubiquitous in membrane proteins and the presence of a CRAC sequence does not ensure cholesterol binding. Instead, cholesterol molecules may have an affinity for the region surrounding a CRAC sequence as the correct

hydrophobic, aromatic, and polar groups are in place to facilitate protein-cholesterol interactions (16, 17, 49).

Our study has shown that cholesterol interacts stronger with specific regions of cholesterol-sensitive receptors compared to their insensitive homologs. These data imply that specific receptor-cholesterol interactions play an important role in the modulation of receptors as a function of membrane cholesterol content. More detailed experimentation to determine the conformational changes associated with cholesterol binding would be very helpful in understanding these phenomena. We have identified a CRAC sequence that is conserved at the bottom of TM7 in 38% of class A GPCRs. Due to its overlap with the NPxxY motif, it is interesting to hypothesize that receptor-cholesterol interactions at TM7 could play an important role in cholesterol-mediated modulation throughout this family and detailed studies on other cholesterol sensitive receptors could yield more information. Additionally, downstream signaling assays could shed light on how these CRAC sequences affect receptor function. Regarding the CCK subfamily, our data agrees with previously published literature and could be helpful in the development of allosteric modulators to treat metabolic syndrome and obesity.

Materials and Methods:

Model Preparation and Simulations

Models for CCK_1R and CCK_2R were generated using Modeller (50, 51) with the orexin receptors 1 and 2 (OX_1R and OX_2R) as templates (PDB codes: OX_1R: 4zj8 and 4zjc (52); OX_2R: 4s0v (53), 5wqc and 5ws3 (54)). Fusion protein inserts were removed from the crystal structures and a multi-sequence alignment was performed using Jalview (55) with the CCK_1R and CCK_2R sequences (Uniprot (https://www.uniprot.org) accession numbers

P32238 and P32239, respectively) independently. Modeller was used to create twenty models for each protein and the structure with the lowest normalized DOPE score (56) for each was chosen (-0.52 and -0.40 for CCK_1R and CCK_2R, respectively). The system setup for the β2-adrenergic receptor (β_2AR) began with removing the T4-lysozyme fusion from the third intracellular loop (ICL3) in the crystal structure (PDB 2rh1 (57)). Modeller was used to fix the resulting gap in the structure by joining the short loop segments left after removing the insert. Using the CHARMM-GUI server (58), each of the three models was coarse-grained using the MARTINI force field (59, 60) with the ElNeDyn secondary structure restraints and inserted into a membrane. Two separate systems were created for each protein: one with a 1:4 cholesterol:1-palmitoyl-2-oleoyl-sn-glycero-3-phosphocholine (POPC) membrane ("20% cholesterol") and one with a 2:3 cholesterol:POPC membrane ("40% cholesterol"). Coarse-grained molecular dynamics (CGMD) was performed using Gromacs 2019 (61) at 303.15 K and 1 bar using semiisotropic Parrinello-Rahman pressure coupling (62) and stochastic velocity-rescale temperature coupling (63) with a 20 fs time step. A reaction-field with a 1.1 nm cutoff was used for the electrostatic interactions and a single cutoff of 1.215 nm was used for the van der Waal interactions (64). Constraints were added according to the MARTINI force field (65). Two MD runs were performed on each system and concatenated for analysis. Simulation lengths for each system are reported in Table 3.2.

Time series of the cholesterol-protein contacts were collected on a per residue basis for each trajectory using functionality in the MDAnalysis package (66), where a contact was defined with a 7 Å cutoff. Survival functions were calculated from a histogram of the

waiting times for each residue. The survival functions were least-square-fitted with relative weights to a two-term hyperexponential with the form

$$s(t) = ae^{-\alpha t} + (1-a)e^{-\beta t} \quad (1)$$

using the *curve_fit()* function in SciPy (67). Artifacts from the cutoff manifest themselves as spurious contacts with short waiting times, i.e., higher rates, so only the slower rates from the longer waiting times were taken to be indicative of cholesterol-protein interactions. Specifically, the slower of the two rates was used to calculate a mean waiting time τ for each residue, termed the "residency time", as

$$\tau = \frac{1}{\min(\alpha,\beta)} \quad (2)$$

Further technical details on the methods will be published elsewhere (Sexton et al, in preparation). τ was plotted against the residue number to compare mean waiting times across the protein using Matplotlib (68). VMD (69) and Chimera (70) were used for molecular visualizations.

TABLE 3.2. Run times for the simulations in microseconds (μs)

20% Cholesterol	**β_2AR**	**CCK$_1$R**	**CCK$_2$R**
Run 1	19.71	88.71	89.41
Run 2	83.01	11.41	36.21
Total	102.71	100.11	125.61
40% Cholesterol			
Run 1	24.61	86.71	87.81
Run 2	75.51	14.51	49.41
Total	100.11	101.21	137.11

Mutant Receptor Preparation

Site-directed mutagenesis was performed on β_2AR using primers with internal mismatches (IDT) and Phusion polymerase (Thermo Fisher Scientific). Mutant receptors were verified via Sanger sequencing (Genewiz). Receptors were expressed and purified as

previously described (19). Receptors were analyzed for total and surface expression on a Guava flow cytometer (Millipore). Purified receptors were analyzed for purity and homogeneity via analytical size exclusion chromatography. Homogeneous receptors were further analyzed using the LCP-T_m assay.

LCP-T_m Assay

Cholesterol binding to mutant receptors was quantified via a thermal denaturation assay in LCP as described (42). Briefly, purified receptors were mixed in an approximately 35% (v/v) ratio with molten monoolein (Nu-check) containing either 0 or 10% cholesterol. Final protein concentrations were 0.015 mg/mL for each assay. Fluorescence signal was recorded using a Cary Eclipse Emission Spectrophotometer (Agilent). Background signal from a blank LCP sample was subtracted from the protein sample and the inner filter effect was corrected for as described (42). CPM (7-Diethylamino-3-(4'-Maleimidylphenyl)-4-Methylcoumarin (Sigma)) probe was added to the protein at a final concentration of 0.004 mg/mL and allowed to incubate on ice, and in the dark, for 30 minutes before incorporation into the LCP matrix. The excitation wavelength for fluorescence was 387 nm and emissions were recorded via scanning between 400 and 500 nm with a step size of 1 nm. Mathematical fitting and statistics were carried out in Prism version 8.3.1(GraphPad) as described (42). The effects of cholesterol were quantified as the change in denaturation temperature as a function of the addition of cholesterol into the LCP matrix. ΔT_m values for mutant receptors were compared to an unmutated control.

Acknowledgements:

Research reported in this publication was supported by the National Institute of General Medical Sciences of the National Institutes of Health under Award Number 1R15GM124623-01A (O.B.), the National Institutes of Health grants R21DA042298 (W.L.) and R01GM124152 (W.L.), the STC Program of the National Science Foundation through BioXFEL (No. 1231306; W.L.), a Mayo Clinic ASU Collaborative Seed Grant Award (W.L.), and the Flinn Foundation Seed Grant (W.L.)

The funders had no role in study design, data collection and analysis, decision to publish, or preparation of the manuscript.

References:

1. Fredriksson R, Lagerström MC, Lundin L-G, Schiöth HB. The G-Protein-Coupled Receptors in the Human Genome Form Five Main Families. Phylogenetic Analysis, Paralogon Groups, and Fingerprints. 2003;63(6):1256-72.

2. Hauser AS, Attwood MM, Rask-Andersen M, Schiöth HB, Gloriam DE. Trends in GPCR drug discovery: new agents, targets and indications. Nature Reviews Drug Discovery. 2017;16(12):829-42.

3. Villar VAM, Cuevas S, Zheng X, Jose PA. Chapter 1 - Localization and signaling of GPCRs in lipid rafts. In: K. Shukla A, editor. Methods in Cell Biology. 132: Academic Press; 2016. p. 3-23.

4. Paila YD, Jindal E, Goswami SK, Chattopadhyay A. Cholesterol depletion enhances adrenergic signaling in cardiac myocytes. Biochimica et Biophysica Acta (BBA) - Biomembranes. 2011;1808(1):461-

5. Oddi S, Dainese E, Fezza F, Lanuti M, Barcaroli D, De Laurenzi V, et al. Functional characterization of putative cholesterol binding sequence (CRAC) in human type-1 cannabinoid receptor. Journal of Neurochemistry. 2011;116(5):858-65.

6. Pucadyil TJ, Chattopadhyay A. Cholesterol modulates ligand binding and G-protein coupling to serotonin1A receptors from bovine hippocampus. Biochimica et Biophysica Acta (BBA) - Biomembranes. 2004;1663(1):188-200.

7. Pucadyil TJ, Chattopadhyay A. Cholesterol modulates the antagonist-binding function of hippocampal serotonin1A receptors. Biochimica et Biophysica Acta (BBA) - Biomembranes. 2005;1714(1):35-42.

8. Gimpl G, Burger K, Fahrenholz F. Cholesterol as Modulator of Receptor Function. Biochemistry. 1997;36(36):10959-74.

9. Gimpl G, Wiegand V, Burger K, Fahrenholz F. Chapter 4 Cholesterol and steroid hormones: modulators of oxytocin receptor function. Progress in Brain Research. 139: Elsevier; 2002. p. 43-55.

10. Ballesteros JA, Weinstein H. Integrated methods for the construction of three-dimensional models and computational probing of structure-function relations in G protein-coupled receptors. In: Sealfon SC, editor. Methods in Neurosciences. 25: Academic Press; 1995. p. 366-428.

11. Khelashvili G, Grossfield A, Feller SE, Pitman MC, Weinstein H. Structural and dynamic effects of cholesterol at preferred sites of interaction with rhodopsin identified from microsecond length molecular dynamics simulations. Proteins. 2009;76(2):403-17.

12. Benned-Jensen T, Norn C Fau - Laurent S, Laurent S Fau - Madsen CM, Madsen Cm Fau - Larsen HM, Larsen Hm Fau - Arfelt KN, Arfelt Kn Fau - Wolf RM, et al. Molecular characterization of oxysterol binding to the Epstein-Barr virus-induced gene 2 (GPR183). (1083-351X (Electronic)).

13. Byrne EFX, Sircar R, Miller PS, Hedger G, Luchetti G, Nachtergaele S, et al. Structural basis of Smoothened regulation by its extracellular domains. (1476-4687 (Electronic)).

14. Luchetti G, Sircar R, Kong JH, Nachtergaele S, Sagner A, Byrne EF, et al. Cholesterol activates the G-protein coupled receptor Smoothened to promote Hedgehog signaling. Elife. 2016;5:e20304.

15. Sensi C, Daniele S, Parravicini C, Zappelli E, Russo V, Trincavelli ML, et al. Oxysterols act as promiscuous ligands of class-A GPCRs: in silico molecular modeling and in vitro validation. (1873-3913 (Electronic)).

16. Bukiya AN, Dopico AM. Common structural features of cholesterol binding sites in crystallized soluble proteins. 2017;58(6):1044-54.

17. Fantini J, Barrantes F. How cholesterol interacts with membrane proteins: an exploration of cholesterol-binding sites including CRAC, CARC, and tilted domains. Frontiers in Physiology. 2013;4:31.

18. Gimpl G. Interaction of G protein coupled receptors and cholesterol. Chemistry and Physics of Lipids. 2016;199:61-73.

19. Hanson MA, Cherezov V, Griffith MT, Roth CB, Jaakola V-P, Chien EYT, et al. A Specific Cholesterol Binding Site Is Established by the 2.8 A Structure of the Human beta2-adrenergic Receptor. Structure. 2008;16(6):897-905.

20. Jafurulla M, Aditya Kumar G, Rao BD, Chattopadhyay A. A Critical Analysis of Molecular Mechanisms Underlying Membrane Cholesterol Sensitivity of GPCRs. In: Rosenhouse-Dantsker A, Bukiya AN, editors. Cholesterol Modulation of Protein Function: Sterol Specificity and Indirect Mechanisms. Cham: Springer International Publishing; 2019. p. 21-52.

21. Cooper RA. Influence of increased membrane cholesterol on membrane fluidity and cell function in human red blood cells. Journal of Supramolecular Structure. 1978;8(4):413-30.

22. Nezil FA, Bloom M. Combined influence of cholesterol and synthetic amphiphillic peptides upon bilayer thickness in model membranes. (0006-3495 (Print)).

23. Chen Z, Rand RP. The influence of cholesterol on phospholipid membrane curvature and bending elasticity. (0006-3495 (Print)).

24. Pal S, Chakraborty H, Bandari S, Yahioglu G, Suhling K, Chattopadhyay A. Molecular rheology of neuronal membranes explored using a molecular rotor: Implications for receptor function. Chemistry and physics of lipids. 2016;196:69-75.

25. Soubias O, Gawrisch K. The role of the lipid matrix for structure and function of the GPCR rhodopsin. Biochimica et Biophysica Acta (BBA) - Biomembranes. 2012;1818(2):234-40.

26. Stansfeld PJ, Sansom MSP. Molecular simulation approaches to membrane proteins. Structure. 2011;19(11):1562-72.

27. Ingólfsson HI, Lopez CA, Uusitalo JJ, de Jong DH, Gopal SM, Periole X, et al. The power of coarse graining in biomolecular simulations. WIREs Computational Molecular Science. 2014;4(3):225-48.

28. Sengupta D, Chattopadhyay A. Molecular dynamics simulations of GPCR–cholesterol interaction: An emerging paradigm. Biochimica et Biophysica Acta (BBA) - Biomembranes. 2015;1848(9):1775 - 82.

29. Hedger G, Sansom MSP. Lipid interaction sites on channels, transporters and receptors: Recent insights from molecular dynamics simulations. Biochimica et Biophysica Acta (BBA) - Biomembranes. 2016;1858(10):2390 - 400.

30. Genheden S, Essex JW, Lee AG. G protein coupled receptor interactions with cholesterol deep in the membrane. Biochimica et Biophysica Acta (BBA) - Biomembranes. 2017;1859(2):268 - 81.

31. Jafurulla M, Tiwari S, Chattopadhyay A. Identification of cholesterol recognition amino acid consensus (CRAC) motif in G-protein coupled receptors. Biochemical and Biophysical Research Communications. 2011;404(1):569-73.

32. Prasanna X, Chattopadhyay A, Sengupta D. Cholesterol modulates the dimer interface of the β_2-adrenergic receptor via cholesterol occupancy sites. Biophysical journal. 2014;106(6):1290-300.

33. Rouviere E, Arnarez C, Yang L, Lyman E. Identification of Two New Cholesterol Interaction Sites on the A_{2A} Adenosine Receptor. Biophysical Journal. 2017;113(11):2415 - 24.

34. Potter RM, Harikumar KG, Wu SV, Miller LJ. Differential sensitivity of types 1 and 2 cholecystokinin receptors to membrane cholesterol. 2012;53(1):137-48.

35. Desai AJ, Harikumar KG, Miller LJ. A Type 1 Cholecystokinin Receptor Mutant That Mimics the Dysfunction Observed for Wild Type Receptor in a High Cholesterol Environment. 2014;289(26):18314-26.

36. Miller LJ, Desai AJ. Metabolic Actions of the Type 1 Cholecystokinin Receptor: Its Potential as a Therapeutic Target. Trends in Endocrinology & Metabolism. 2016;27(9):609-19.

37. Miller LJ, Holicky EL, Ulrich CD, Wieben ED. Abnormal processing of the human cholecystokinin receptor gene in association with gallstones and obesity. Gastroenterology. 1995;109(4):1375-80.

38. Cang X, Du Y, Mao Y, Wang Y, Yang H, Jiang H. Mapping the Functional Binding Sites of Cholesterol in β2-Adrenergic Receptor by Long-Time Molecular Dynamics Simulations. The Journal of Physical Chemistry B. 2013;117(4):1085-94.

39. Lee AG. Interfacial Binding Sites for Cholesterol on G Protein-Coupled Receptors. Biophysical Journal. 2019;116(9):1586-97.

40. Mirzadegan T, Benkö G, Filipek S, Palczewski K. Sequence Analyses of G-Protein-Coupled Receptors: Similarities to Rhodopsin. Biochemistry. 2003;42(10):2759-67.

41. Pándy-Szekeres G, Munk C, Tsonkov TM, Mordalski S, Harpsøe K, Hauser AS, et al. GPCRdb in 2018: adding GPCR structure models and ligands. Nucleic Acids Research. 2017;46(D1):D440-D6.

42. Liu W, Hanson MA, Stevens RC, Cherezov V. LCP-Tm: An Assay to Measure and Understand Stability of Membrane Proteins in a Membrane Environment. Biophysical Journal. 2010;98(8):1539-48.

43. Heydenreich FM, Vuckovic Z, Matkovic M, Veprintsev DB. Stabilization of G protein-coupled receptors by point mutations. Frontiers in Pharmacology. 2015;6:82.

44. Roth CB, Hanson MA, Stevens RC. Stabilization of the Human β2-Adrenergic Receptor TM4–TM3–TM5 Helix Interface by Mutagenesis of Glu1223.41, A Critical Residue in GPCR Structure. Journal of Molecular Biology. 2008;376(5):1305-19.

45. Webb RJ, East JM, Sharma RP, Lee AG. Hydrophobic Mismatch and the Incorporation of Peptides into Lipid Bilayers: A Possible Mechanism for Retention in the Golgi. Biochemistry. 1998;37(2):673-9.

46. Ragnarsson L, Andersson Å, Thomas WG, Lewis RJ. Mutations in the NPxxY motif stabilize pharmacologically distinct conformational states of the α_{1B}- and β_2-adrenoceptors. Science Signaling. 2019;12(572):eaas9485.

47. Raffy S, Teissié J. Control of Lipid Membrane Stability by Cholesterol Content. Biophysical Journal. 1999;76(4):2072-80.

48. Cherezov V, Clogston J, Misquitta Y, Abdel-Gawad W, Caffrey M. Membrane Protein Crystallization In Meso: Lipid Type-Tailoring of the Cubic Phase. Biophysical Journal. 2002;83(6):3393-407.

49. Baier CJ, Fantini J, Barrantes FJ. Disclosure of cholesterol recognition motifs in transmembrane domains of the human nicotinic acetylcholine receptor. Scientific Reports. 2011;1(1):69.

50. Fiser A, Do RKG, Šali A. Modeling of loops in protein structures. Protein Science. 2000;9(9):1753-73.

51. Sali A, Blundell TL. Comparative protein modelling by satisfaction of spatial restraints. (0022-2836 (Print)).

52. Yin J, Babaoglu K, Brautigam CA, Clark L, Shao Z, Scheuermann TH, et al. Structure and ligand-binding mechanism of the human OX1 and OX2 orexin receptors. Nature Structural & Molecular Biology. 2016;23(4):293-9.

53. Yin J, Mobarec JC, Kolb P, Rosenbaum DM. Crystal structure of the human OX2 orexin receptor bound to the insomnia drug suvorexant. Nature. 2015;519(7542):247-50.

54. Suno R, Kimura KT, Nakane T, Yamashita K, Wang J, Fujiwara T, et al. Crystal Structures of Human Orexin 2 Receptor Bound to the Subtype-Selective Antagonist EMPA. Structure. 2018;26(1):7-19.e5.

55. Waterhouse AM, Procter JB, Martin DMA, Clamp M, Barton GJ. Jalview Version 2—a multiple sequence alignment editor and analysis workbench. Bioinformatics. 2009;25(9):1189-91.

56. Eramian D, Eswar N, Shen M-Y, Sali A. How well can the accuracy of comparative protein structure models be predicted? Protein Science. 2008;17(11):1881-93.

57. Rosenbaum DM, Cherezov V, Hanson MA, Rasmussen SGF, Thian FS, Kobilka TS, et al. GPCR Engineering Yields High-Resolution Structural Insights into β_2-Adrenergic Receptor Function. Science. 2007;318(5854):1266.

58. Qi Y, Ingólfsson HI, Cheng X, Lee J, Marrink SJ, Im W. CHARMM-GUI Martini Maker for Coarse-Grained Simulations with the Martini Force Field. Journal of Chemical Theory and Computation. 2015;11(9):4486-94.

59. de Jong DH, Singh G, Bennett WFD, Arnarez C, Wassenaar TA, Schäfer LV, et al. Improved Parameters for the Martini Coarse-Grained Protein Force Field. Journal of Chemical Theory and Computation. 2013;9(1):687-97.

60. Periole X, Cavalli M, Marrink S-J, Ceruso MA. Combining an Elastic Network With a Coarse-Grained Molecular Force Field: Structure, Dynamics, and Intermolecular Recognition. Journal of Chemical Theory and Computation. 2009;5(9):2531-43.

61. Abraham MJ, Murtola T, Schulz R, Páll S, Smith JC, Hess B, et al. GROMACS: High performance molecular simulations through multi-level parallelism from laptops to supercomputers. SoftwareX. 2015;1-2:19-25.

62. Parrinello M, Rahman A. Polymorphic transitions in single crystals: A new molecular dynamics method. Journal of Applied Physics. 1981;52(12):7182-90.

63. Bussi G, Donadio D Fau - Parrinello M, Parrinello M. Canonical sampling through velocity rescaling. (0021-9606 (Print)).

64. de Jong DH, Baoukina S, Ingólfsson HI, Marrink SJ. Martini straight: Boosting performance using a shorter cutoff and GPUs. Computer Physics Communications. 2016;199:1 - 7.

65. Monticelli L, Kandasamy SK, Periole X, Larson RG, Tieleman DP, Marrink S-J. The MARTINI Coarse-Grained Force Field: Extension to Proteins. Journal of Chemical Theory and Computation. 2008;4(5):819-34.

66. R. J. Gowers ML, J. Barnoud, T. J. E. Reddy, M. N. Melo, S. L. Seyler, D. L. Dotson, J. Domanski, S. Buchoux, I. M. Kenney, and O. Beckstein. . MDAnalysis: A Python package for the rapid analysis of molecular dynamics simulations. . Proceedings of the 15th Python in Science Conference,. 2016:98/105.

67. Virtanen P, Gommers R, Oliphant TE, Haberland M, Reddy T, Cournapeau D, et al. SciPy 1.0: fundamental algorithms for scientific computing in Python. Nature Methods. 2020;17(3):261-72.

68. Hunter JD. Matplotlib: A 2D Graphics Environment. Computing in Science Engineering. 2007;9(3):90-5.

69. Humphrey W, Dalke A, Schulten K. VMD: Visual molecular dynamics. Journal of Molecular Graphics. 1996;14(1):33-8.

70. Pettersen EF, Goddard TD, Huang CC, Couch GS, Greenblatt DM, Meng EC, et al. UCSF Chimera—A visualization system for exploratory research and analysis. Journal of Computational Chemistry. 2004;25(13):1605-12.

3.3. Alignment of Class-A GPCRs shows 38% conservation of TM7 CRAC sequence

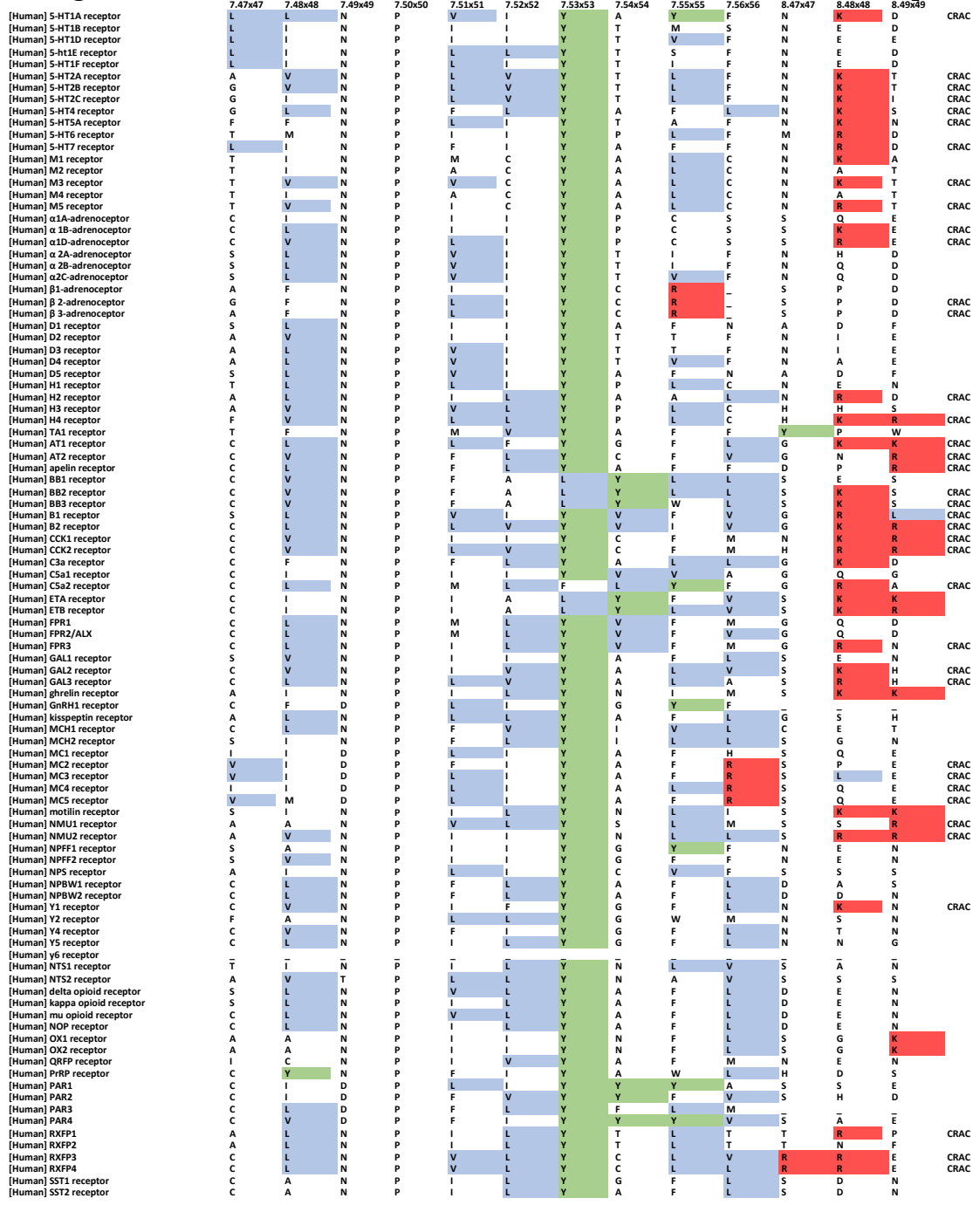

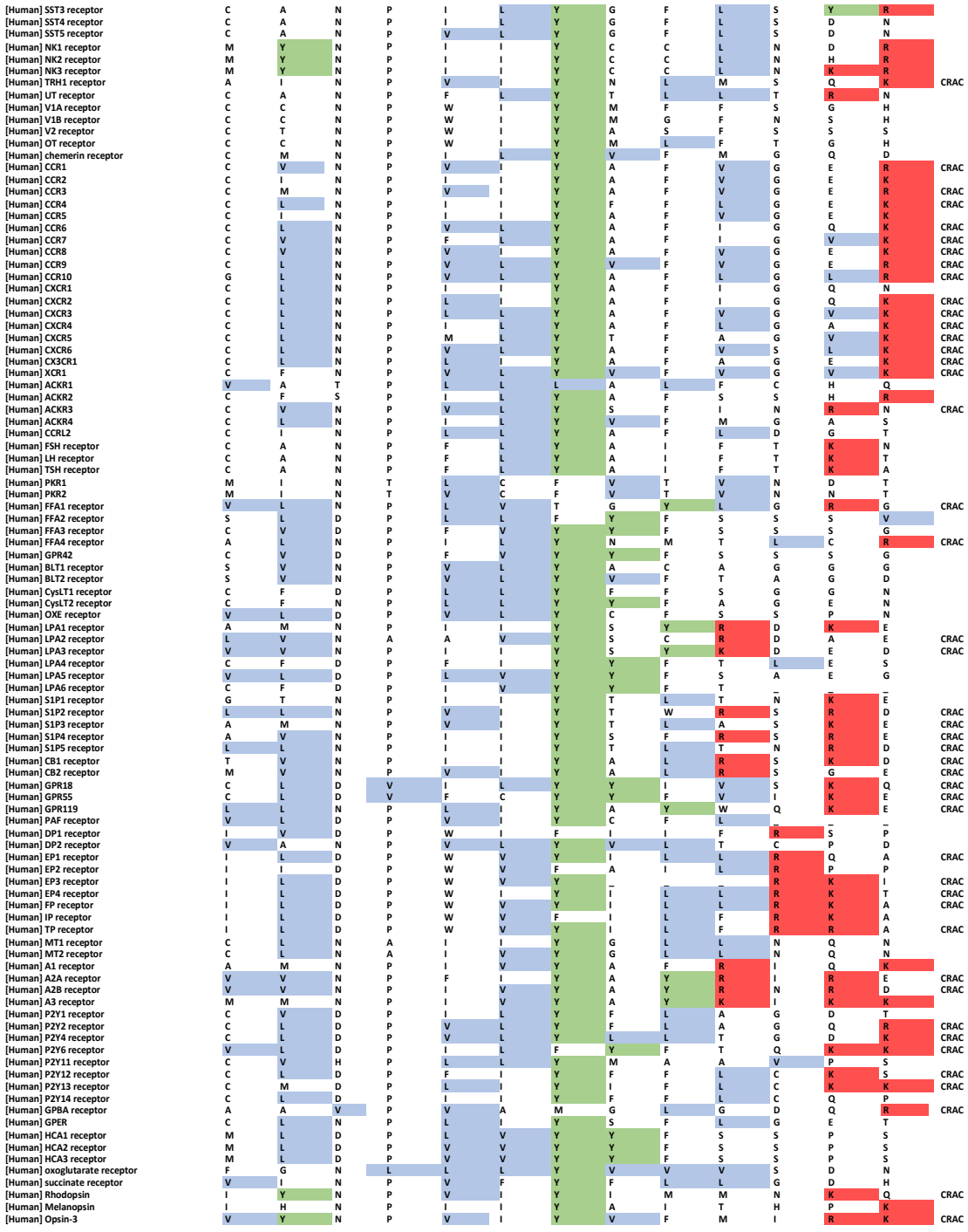
[Human] SST3 receptor
[Human] SST4 receptor
[Human] SST5 receptor
[Human] NK1 receptor
[Human] NK2 receptor
[Human] NK3 receptor
[Human] TRH1 receptor
[Human] UT receptor
[Human] V1A receptor
[Human] V1B receptor
[Human] V2 receptor
[Human] OT receptor
[Human] chemerin receptor
[Human] CCR1
[Human] CCR2
[Human] CCR3
[Human] CCR4
[Human] CCR5
[Human] CCR6
[Human] CCR7
[Human] CCR8
[Human] CCR9
[Human] CCR10
[Human] CXCR1
[Human] CXCR2
[Human] CXCR3
[Human] CXCR4
[Human] CXCR5
[Human] CXCR6
[Human] CX3CR1
[Human] XCR1
[Human] ACKR1
[Human] ACKR2
[Human] ACKR3
[Human] ACKR4
[Human] CCRL2
[Human] FSH receptor
[Human] LH receptor
[Human] TSH receptor
[Human] PKR1
[Human] PKR2
[Human] FFA1 receptor
[Human] FFA2 receptor
[Human] FFA3 receptor
[Human] FFA4 receptor
[Human] GPR42
[Human] BLT1 receptor
[Human] BLT2 receptor
[Human] CysLT1 receptor
[Human] CysLT2 receptor
[Human] OXE receptor
[Human] LPA1 receptor
[Human] LPA2 receptor
[Human] LPA3 receptor
[Human] LPA4 receptor
[Human] LPA5 receptor
[Human] LPA6 receptor
[Human] S1P1 receptor
[Human] S1P2 receptor
[Human] S1P3 receptor
[Human] S1P4 receptor
[Human] S1P5 receptor
[Human] CB1 receptor
[Human] CB2 receptor
[Human] GPR18
[Human] GPR55
[Human] GPR119
[Human] PAF receptor
[Human] DP1 receptor
[Human] DP2 receptor
[Human] EP1 receptor
[Human] EP2 receptor
[Human] EP3 receptor
[Human] EP4 receptor
[Human] FP receptor
[Human] IP receptor
[Human] TP receptor
[Human] MT1 receptor
[Human] MT2 receptor
[Human] A1 receptor
[Human] A2A receptor
[Human] A2B receptor
[Human] A3 receptor
[Human] P2Y1 receptor
[Human] P2Y2 receptor
[Human] P2Y4 receptor
[Human] P2Y6 receptor
[Human] P2Y11 receptor
[Human] P2Y12 receptor
[Human] P2Y13 receptor
[Human] P2Y14 receptor
[Human] GPBA receptor
[Human] GPER
[Human] HCA1 receptor
[Human] HCA2 receptor
[Human] HCA3 receptor
[Human] oxoglutarate receptor
[Human] succinate receptor
[Human] Rhodopsin
[Human] Melanopsin
[Human] Opsin-3
CRAC

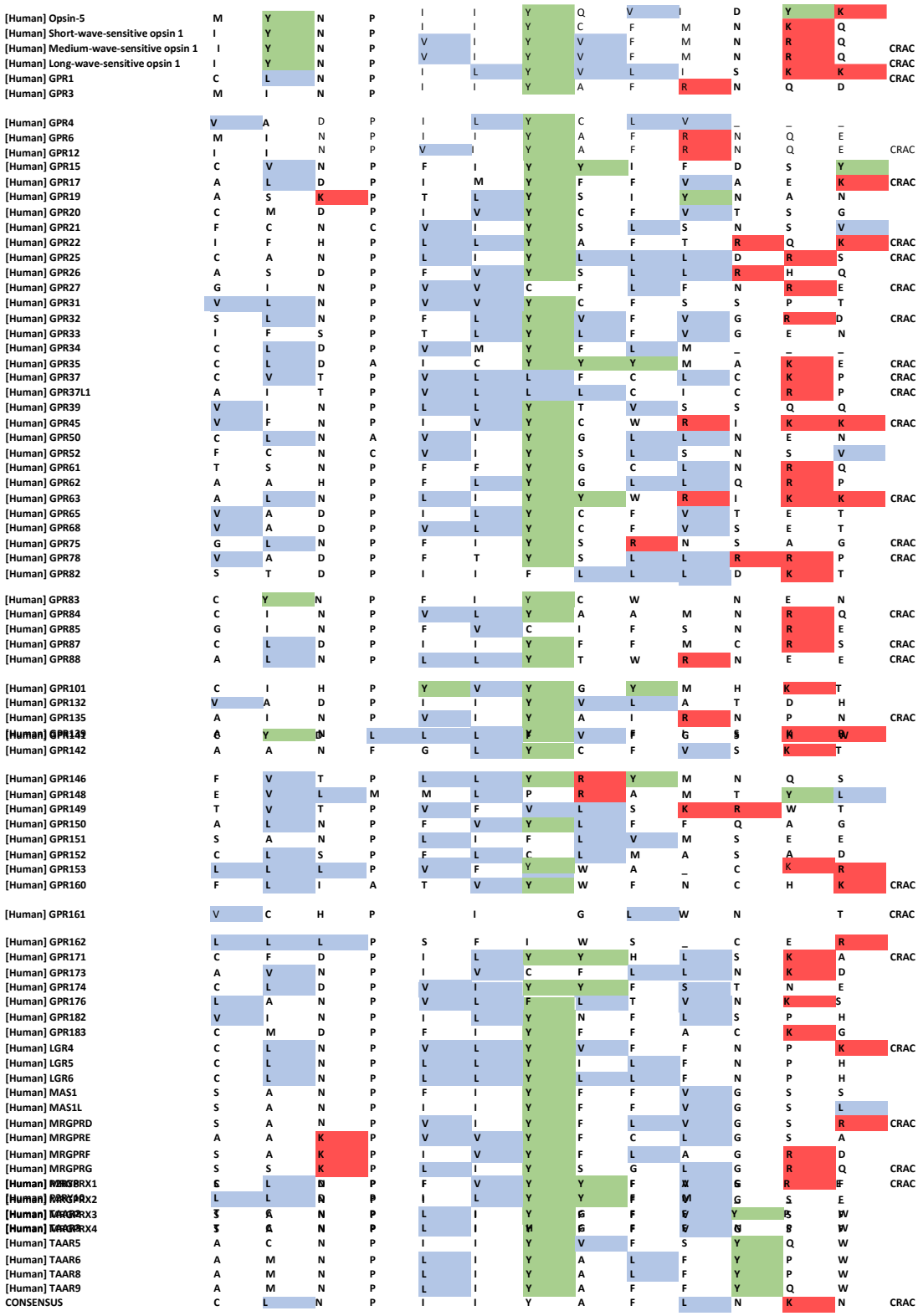
[Human] Opsin-5
[Human] Short-wave-sensitive opsin 1
[Human] Medium-wave-sensitive opsin 1
[Human] Long-wave-sensitive opsin 1
[Human] GPR1
[Human] GPR3
[Human] GPR4
[Human] GPR6
[Human] GPR12
[Human] GPR15
[Human] GPR17
[Human] GPR19
[Human] GPR20
[Human] GPR21
[Human] GPR22
[Human] GPR25
[Human] GPR26
[Human] GPR27
[Human] GPR31
[Human] GPR32
[Human] GPR33
[Human] GPR34
[Human] GPR35
[Human] GPR37
[Human] GPR37L1
[Human] GPR39
[Human] GPR45
[Human] GPR50
[Human] GPR52
[Human] GPR61
[Human] GPR62
[Human] GPR63
[Human] GPR65
[Human] GPR68
[Human] GPR75
[Human] GPR78
[Human] GPR82
[Human] GPR83
[Human] GPR84
[Human] GPR85
[Human] GPR87
[Human] GPR88
[Human] GPR101
[Human] GPR132
[Human] GPR135
[Human] GPR142
[Human] GPR146
[Human] GPR148
[Human] GPR149
[Human] GPR150
[Human] GPR151
[Human] GPR152
[Human] GPR153
[Human] GPR160
[Human] GPR161
[Human] GPR162
[Human] GPR171
[Human] GPR173
[Human] GPR174
[Human] GPR176
[Human] GPR182
[Human] GPR183
[Human] LGR4
[Human] LGR5
[Human] LGR6
[Human] MAS1
[Human] MAS1L
[Human] MRGPRD
[Human] MRGPRE
[Human] MRGPRF
[Human] MRGPRG
[Human] TAAR5
[Human] TAAR6
[Human] TAAR8
[Human] TAAR9
CONSENSUS
CRAC

CHAPTER 4

HARNESSING THE POWER OF AN X-RAY LASER FOR SERIAL CRYSTALLOGRAPHY OF MEMBRANE PROTEINS CRYSTALLIZED IN LIPIDIC CUBIC PHASE

Ming-Yue Lee[a‡], James Geiger[a‡], Andrii Ishchenko[b], Gye Won Han[b], Anton Barty[c], Thomas A. White[c], Cornelius Gati[d], Alexander Batyuk[d], Mark S. Hunter[d], Andrew Aquila[d], Sébastien Boutet[d], Uwe Weierstall[a], Vadim Cherezov[be*] and Wei Liu[af*]
[a]Center for Applied Structural Discovery at the Biodesign Institute, Arizona State University, Tempe, AZ, 85287-1604, USA
[b]Bridge Institute, Michelson Center for Convergent Bioscience, University of Southern California, 1002 W. Childs Way, Los Angeles, CA 90089, USA
[c]Center for Free-Electron Laser Science, Deutsches Elektronen-Synchrotron DESY, Notkestrasse 85, Hamburg, 22607, Germany
[d]LCLS, SLAC National Accelerator Laboratory, 2575 Sand Hill Road, Menlo Park, CA, 94025, USA
[e]Department of Chemistry, University of Southern California, Los Angeles, CA, 90089, USA
[f]School of Molecular Sciences, Arizona State University, Tempe, AZ, 85287, USA
Correspondence email: cherezov@usc.edu; w.liu@asu.edu
‡These authors contributed equally

This is a research letter that I co-first authored and published in the International Union of Crystallography Journal (IUCrJ). I was involved in data analysis, molecular replacement, and model refinement. I wrote and edited the introduction, results, discussion, and conclusion. The goal of this work to is streamline data collection during serial femtosecond crystallography (SFX) of GPCRs. This should allow researchers to determine GPCR structures with less experimental time, data, and sample consumption.

Abstract

Serial femtosecond crystallography (SFX) with X-ray free electron lasers (XFELs) has proven highly successful for structure determination of challenging membrane proteins crystallized in lipidic cubic phase, however, as most techniques, it has limitations. Here we attempted to address some of these limitations related to the use of a vacuum chamber and the need for attenuation of the XFEL beam, in order to further improve the efficiency of this method. Using an optimized SFX experimental setup in a helium atmosphere we determined the room temperature structure of the adenosine A_{2A} receptor (A_{2A}AR) at 2.0 Å resolution and compared it with previous A_{2A}AR structures determined in vacuum and/or at cryogenic temperatures. Specifically, we demonstrated the capability of utilizing high XFEL beam transmissions, in conjunction with a high dynamic range detector, to collect high-resolution SFX data while reducing crystalline material consumption and shortening the collection time required for a complete data set. The experimental setup presented herein can be applied to future SFX applications for protein nanocrystal samples to aid in structure-based discovery efforts of therapeutic targets that are difficult to crystallize.

Introduction

Elucidating high-resolution X-ray structures of G protein-coupled receptors (GPCRs) and other membrane proteins using synchrotron radiation sources has been limited by the difficulty of obtaining high-quality crystals that can withstand radiation damage. So far, only few GPCR structures had been resolved to better than 2.0 Å resolution using synchrotron radiation [1-5]. Several challenges must be overcome during crystallization and diffraction data collection to achieve high-resolution structure models. First, the size of a protein crystal suitable to resolve a 3.5 Å structural model using synchrotron diffraction should be at least 20 micrometers (µm) in each dimension [6]. Additionally, as secondary radiation damage propagates throughout the crystals, diffraction data quality deteriorates, resulting in decreased resolution, increased unit cell volume, B-factors, and mosaicity [7]. Typically, protein crystals are cryo-cooled to reduce secondary radiation damage during data collection. However, subjecting protein crystals to cryogenic conditions can potentially introduce non-physiological artifacts due to improper freezing and increase their mosaicity [8].

Recent advances at synchrotron microfocus beamlines have allowed room temperature serial diffraction data collection using crystals approximately 10 µm in size [9, 10]. Serial millisecond crystallography (SMX) techniques have enabled room temperature structure determination of GPCRs at moderate resolutions using synchrotron radiation sources [5, 11]. Nonetheless, the crystal sizes needed for collecting high-resolution SMX data are much larger than those required for SFX [5, 11]. An XFEL source with extremely bright femtosecond pulses allows for diffraction patterns to be collected from protein crystals with minimal deleterious effects outlined above,

specifically with the intent of minimizing radiation damage, termed “diffraction before destruction” [12, 13]. Also, SFX experiments are typically conducted at room temperature, permitting a more native-like temperature environment for the protein target of interest. Over the last several years, SFX demonstrated a clear advantage for structure determination of difficult for crystallization membrane proteins such as GPCRs [14].

Despite the numerous advantages offered by SFX, further technical advancements are critical to optimize data-collection. One major limitation observed in SFX experiments at the Linac Coherent Light Source (LCLS) using the Cornell-SLAC Pixel Array Detector (CSPAD) [15, 16] is the need to attenuate the beam to about 10% (a few hundred μJ/pulse at sample) of its full power [14, 17, 18]. This attenuation is required to avoid detector pixel saturation and possible damage by the strong low-resolution diffraction spots and to reduce the LCP flow disruption by the highly intense XFEL beam [14, 19]. Specifically, due to the viscous nature of the LCP matrix, interaction with a strong XFEL beam can lead to disruption of the LCP stream and sticking it to the injector nozzle, which requires stopping the experiment to clean the nozzle, thereby increasing the data collection time and negating any advantage in sample consumption that the method offers. Furthermore, beam attenuation is undesirable when attempting to collect high-resolution data (<2.0 Å), as the weaker, high-resolution diffraction spots become harder to detect [20] since each spot is recorded at a lower signal-to-background ratio. Since diffraction intensity typically scales with crystal size, attenuating beam fluence for SFX experiments further limits sample crystal sizes that can yield quality diffraction patterns as the signal to noise ratio decreases [18].

Lastly, since the available beam time at XFEL sources is scarce, it is critical to increase their usage efficiency. Therefore, in this experiment we tested a secondary chamber with helium atmosphere environment at the LCLS Coherent X-ray Imaging (CXI) instrument [21], in which the 1 μm focused XFEL beam that passed through the sample in the main vacuum sample chamber is re-focused by beryllium lens to a spot of <3 μm. While not done in our experiment, the refocused beam in the secondary helium chamber can be used for simultaneous data collection with the focused beam in the primary vacuum chamber, thus doubling the diffraction sample throughput during available XFEL beamtime [22, 23]. Additionally, the utilization of a high dynamic range Rayonix MX170-HS detector allowed for diffraction data to be collected using an unattenuated XFEL beam, although the beryllium lens and the diamond window allowing for the passage through the upstream chamber contributed to an overall beam attenuation by a factor of two. In this study, we present the 2.0 Å model of the human adenosine A_{2A} receptor (A_{2A}AR) using SFX data collected in a helium environment under atmospheric pressure and at room temperature. We compare this model with the 1.8 Å synchrotron structure (PDB: 4EIY [1]) as well as with other published A_{2A}AR structures from XFEL SFX (PDB: 5NM4 [5] and 5K2D [24]) and synchrotron SMX experiments (PDB: 5NLX [5]).

Results

Crystal sample generation and SFX experimental setup

Microcrystal samples of human $A_{2A}AR$ in complex with the antagonist ZM241385 for SFX experiments were generated using the same methodology and crystallization conditions as previously reported [1, 25]. At the LCLS CXI instrument, microcrystals measuring approximately 5×5×2 μm^3 were combined to produce 40 µL of densely packed LCP-crystal sample. The samples were loaded and injected into the XFEL beam using an LCP-injector as previously described [12], with the major exception being that the injector was housed in a helium-filled enclosure (Fig. 4.1A, details shown in Supplementary Fig.4.1) instead of the commonly used conventional vacuum chamber for SFX experiments at CXI. A Rayonix MX170-HS detector was used to collect the SFX data at a 2×2 binning mode with 10 Hz data acquisition rate. A representative diffraction image at approximately 1 mJ recorded to 2.0 Å at the edge of the detector is shown in Fig. 4.1B.

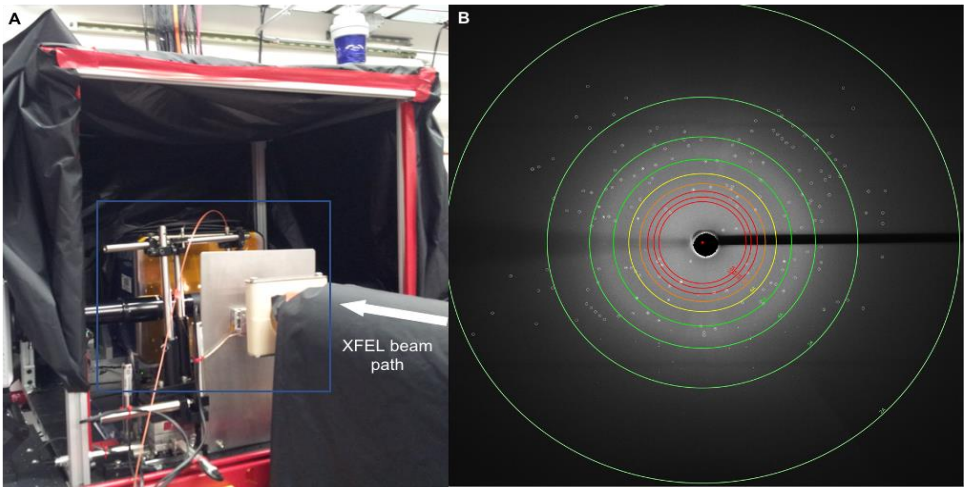

Figure 4.1. A) A view of the experimental setup for LCP-SFX data collection in helium at CXI. Detailed view of instrumentation in the blue inset from panel (A) are shown Supplementary Fig.1. B) Representative diffraction pattern during data collection. Diffraction spots located by *Cheetah* are

Diffraction data collection and processing

From approximately 2 hours of data collection, we had an average crystal hit rate of 37.5% resulting in 26,341 "hits" – defined as crystal diffraction patterns containing at least 15 peaks with the signal-to-noise ratio above 6. From 26,341 hits, 16,737 patterns were successfully indexed (63.5% indexing rate) and used to build the model presented here. After molecular replacement and refinement, the electron density maps revealed three clear densities corresponding to cholesterol molecules near the receptor and a density for the ligand ZM241385 consistent with previous structures (Fig. 4.2). Densities for lipid molecules, co-purified with the receptor or utilized in crystallization and sample delivery, as well as other molecules (polyethylene glycol and glycerol), were resolved as well. We also observed a sodium ion coordinated by three water molecules and residues Asp52$^{2.50}$ and Ser91$^{3.39}$ (superscript refers to the generic Ballesteros-Weinstein numbering scheme for class A GPCRs [26]) in the conserved allosteric site known to be important for receptor activation [1, 27] (Fig. 4.2). For a comprehensive comparison of our model with other existing models in the Protein Data Bank (PDB), we searched for all available A_{2A}AR structures bound to ZM241385 and containing the apocytochrome b_{562}RIL (BRIL) fusion protein at intracellular loop 3 (ICL3). We then separated these structures according to resolution and diffraction technique.

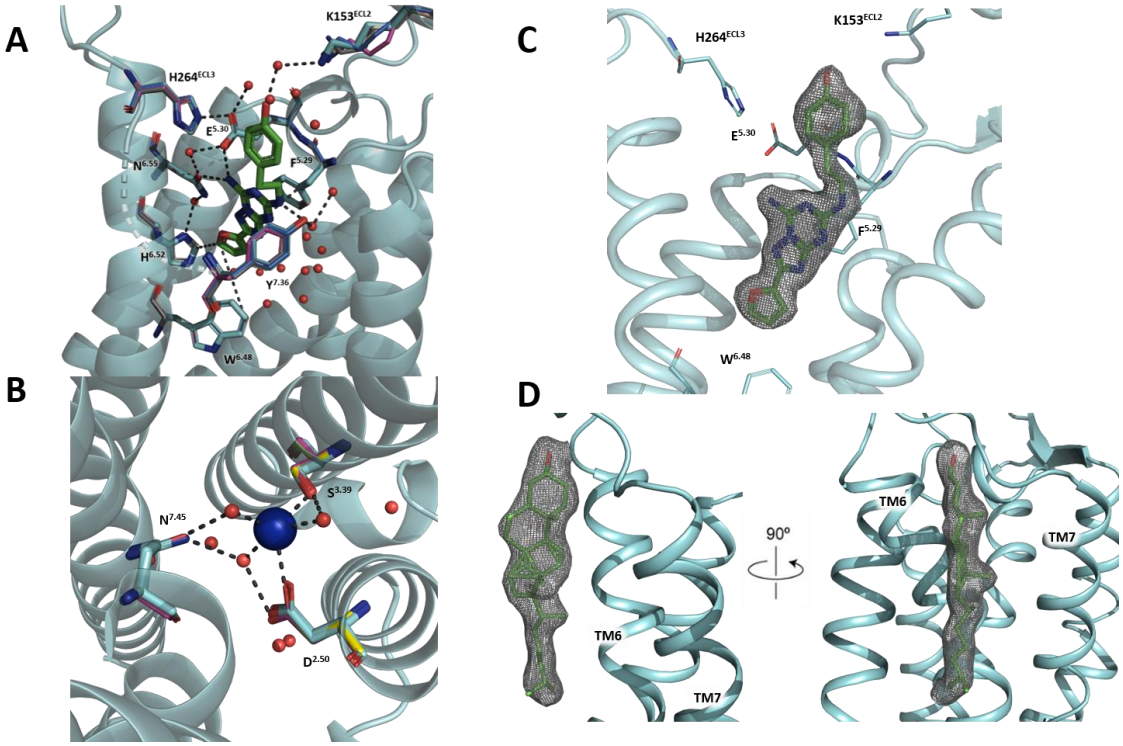

Figure 4.2. Quality and validation of the $A_{2A}AR$ model obtained in this study. A) ZM341385 binding site is conserved across all models. The ligand from our structure (green sticks) is shown with side chains from all structures aligned. B) Conservation of the sodium binding site. Side chains from all models are shown with the sodium (blue sphere) and waters (red spheres) from our current model. C) 2Fo-Fc map contoured at 1.0 σ shows density for ZM341385 in our model. D) 2Fo-Fc map contoured at 1.0 σ shows clear cholesterol densities in our model.

For the sake of brevity, structures with lower than 2.2 Å resolution were not analyzed in detail and are thus excluded from the present discussion. Table 4.1 compares the statistics for our model with four other previously published structures: 4EIY, a 1.8 Å structure from merging multiple single crystal synchrotron diffractions at cryo-conditions [1], 5NM4, a 1.7 Å structure obtained using SFX from an XFEL source [5], 5K2D, a 1.9 Å SFX structure with crystals delivered in vacuum [24], and 5NLX, a 2.14 Å synchrotron SMX structure [5]. Superimposition of our model with these high-resolution structures showed close alignment with low RMSD (root mean square deviation) values for C_α atoms (RMSD values for all-atoms in parenthesis): 0.281 (0.683) Å, 0.279 (0.651) Å, 0.193 (0.814) Å, and 0.082 (0.571) Å between the current structure and 5NM4, 5NLX,

4EIY, and 5K2D, respectively (Fig. 4.3A). Overall, all models were found to be in agreement with each other without any significant observable differences between the synchrotron single crystal diffraction method, SMX, and SFX structures. We observed similar crystallographic statistics between the models, with higher B factors for structures determined at room temperature compared to cryogenic conditions (4EIY), as expected (Table 4.1). Our final model was refined to 2.0 Å with similar crystallographic statistics as the other A_{2A}AR models (Table 4.1).

	Current Model	**4EIY**	**5NM4**	**5NLX**	**5K2D**
Data collection					
Method / Source	SFX / XFEL	Small wedge / Synchrotron	SFX / XFEL	SMX / Synchrotron	SFX / XFEL
Resolution Range (Å)	27.7-2.0 (2.07-2.00)	27.5-1.8 (1.86-1.80)	19.6-1.7 (1.76-1.70)	34.5-2.1 (2.22-2.14)	24.0-1.9 (2.00-1.90)
Space Group	$C222_1$	$C222_1$	$C222_1$	$C222_1$	$C222_1$
Cell dimensions (Å)					
a	40.4	39.4	39.9	40.3	40.4
b	180.5	179.5	179.2	180.1	180.7
c	142.7	140.3	141.2	142.7	142.8
Crystal Size (μm^3)	5×5×2	60×10×3	30×30×5	30×30×5	5×5×2

Unique Reflections	35,870 (3,486)	44,252 (4,100)	56,793 (3,437)	32,392 (2,761)	41,882 (2,933)
Mean I/σ (I)	4.1 (1.22)	17.7 (1.8)	2.93 (0.44)	13.17 (0.7)	6.0 (0.6)
Redundancy	205 (72)	4.0 (3.3)	23.3 (3.0)	1,007 (8.1)	291 (62)
R_{split} (%) or R_{merge} (%) (4EIY)	19.1 (211)	10 (81)	17.9 (315)	4.7 (212)	10.1 (197)
CC*	0.99 (0.50)	N/A	0.99 (0.45)	0.99 (0.47)	0.99 (0.58)
Completeness (%)	100.0 (100.0)	95.1 (92.8)	94.6 (61.8)	99.5 (95.7)	100.0 (100.0)
Wilson B-factor ($Å^2$)	33.3	23.7	40.4	45.2	41.5
Average B-factors ($Å^2$)					
Overall	48.0	34.0	62.8	69.9	58.5
A_{2A}AR	39.4	25.2	50.0	55.8	45.3
BRIL	82.6	55.9	90.4	117.0	92.3
Lipids	72.6	45.4	140.6	98.6	80.1
Ligand	32.9	20.4	37.6	40.5	35.6
Solvent	48.3	37.4	52.8	46.7	54.1
Number of indexed images used for dataset	16,737	-	3,563	128,086	72,753

Indexing Rate (%)	63.5	-	2.3	10.8	31.3
Number of Reflections used in refinement	35,862	42,032	53,302	27,734	39,840
Reflections used for R-free	2,000	2,221	2,606	1,430	1,988
R-work/R-free (%)	19.3 / 21.6	17.4 / 21.3	21.2 / 23.5	19.9 / 22.9	17.4 / 20.7
Number of non-hydrogen atoms					
Macromolecules	2,978	3,105	2,899	2,894	3,121
Lipids	392	456	174	138	397
Ligand	25	25	25	25	25
Solvent	85	185	59	33	93
Protein Residues	391	390	382	382	391
RMS bonds (Å) angles (°)	 0.010 1.06	 0.016 1.29	 0.014 1.35	 0.014 1.41	 0.010 1.20
Ramachandran Plot Analysis					
favoured (%)	98.2	99.0	98.2	96.6	99.0
allowed (%)	1.8	1.0	1.6	3.4	1.0
outliers (%)	0.0	0.0	0.3	0.0	0.0
Rotamer outliers (%)	4.01	0.31	1.37	3.08	2.20

Clashscore	1.30	2.69	3.33	4.51	3.20

Table 4.1. Data collection and refinement statistics for the $A_{2A}AR$ models discussed in the present study.

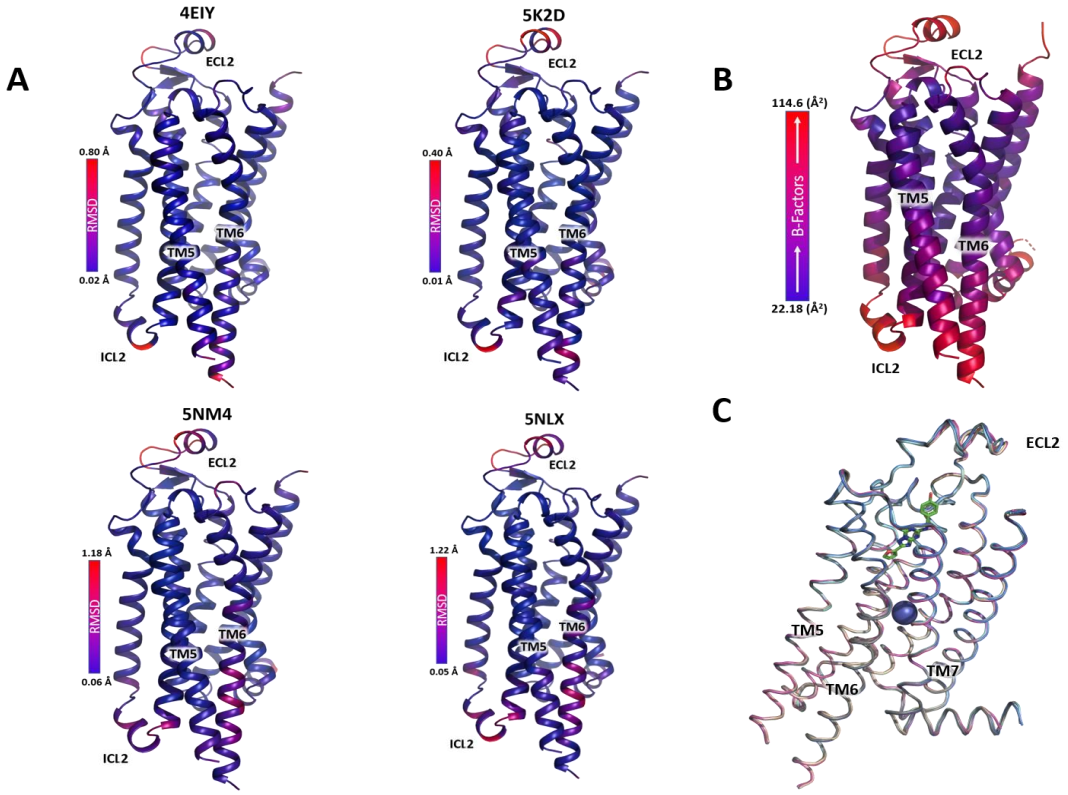

Figure 4.3. A) Cα RMSD values between the current $A_{2A}AR$ structure model and the compared models. Lower RMSD shown in blue, higher RMSD values shown in red. Scale bars included for maximum and minimum values. B) The current $A_{2A}AR$ structure model colored by B-factors. Lower B-factors shown in blue, higher B-factors in red. Scale bar shows minimum and maximum B-factors. C) Overlay of all $A_{2A}AR$ models compared in this study (Our model (cyan), 5NM4 (tan), 5NLX (purple), 4EIY (grey), 5K2D (blue). The BRIL fusion

Discussion

After refinement, we observed no significant differences in the $2mF_o$-DF_c maps between our model and previously published $A_{2A}AR$ structures (4EIY, 5K2D, 5NLX, and 5NM4). Analysis of structural characteristics such as disulfide bonds, the sodium binding

pocket, ligand binding residues, and cholesterol molecules showed similar quality between the $2mF_o$-DF_c maps (Suppl. Fig. 4.2). We observed slightly larger RMSD values in regions including ICL2, the intracellular portion of TM6, and ECL2 (Fig. 4.3A). Moreover, weaker densities were observed across all models for ICL2 and ECL2, potentially indicative of the dynamic nature of these loops. These regions of weaker density and higher RMSD also correlate to higher B-factors from the model (Fig. 4.3B). Nonetheless, all the structure models generated using different diffraction methods are comparable, with important structural characteristics clearly resolved (Fig. 4.2). Figure 4.3C shows a ribbon representation of all structure models aligned to our current model.

At the time of writing, the standard detector installed in the primary chamber of the LCLS CXI instrument is the Cornell-SLAC pixel array detector (CSPAD) capable of high speed readout at 120 Hz [21, 28]. The main advantage of this detector is that it is specifically made for LCLS applications; it has a large cross-sectional area (1,516×1,516 pixels at 110 μm per pixel; 167×167 mm), can count single photons, with a maximum signal of 2,700 photons (8 keV) / pixel, and a fast 120 Hz data acquisition rate, all of which are amenable for XFEL SFX experiments. The results reported here were recorded using the Rayonix MX170-HS detector. Beyond the technical differences (CCD vs. pixel arrays), which are outside the scope of this study, we mainly focus on the advantages the MX170-HS detector offers. During our SFX experiments, the MX170-HS detector was recording in a 2x2 binning mode (1,920×1,920 pixels at 89 μm per pixel ; 171×171 mm) which has a capacity of recording a max signal of 50,000 photons (12 keV) / pixel [28]; in comparison, the CSPAD detector can record either a max signal of 2,700 photons (8 keV) / pixel at the low gain mode, or 350 photons (8 keV) / pixel at the high gain mode,

significantly less than that of the MX170-HS. Additionally, the lower dynamic range of the CSPAD detector limits the amount of tolerable background noise since a detector readout must include a full LCLS pulse, elevated background can utilize all the dynamic range of the detector and lead to signals above background saturating the detector. Performing experiments in vacuum as regularly done at XFELs alleviates this problem. In contrast, our experiment was performed at ambient pressure in a helium atmosphere. Utilizing the high dynamic range of the MX170-HS detector allowed us to overcome the background scattering effects contributed by helium atoms.

Using the MX170-HS coupled with a full strength XFEL beam, we were able to resolve an A_{2A}AR structure model to 2.0 Å with reasonable statistics, demonstrating the capabilities of the hardware setup presented herein. The A_{2A}AR crystal sample used in this study was comprised of microcrystals that averaged approximately 5×5×2 μm^3 in size. In contrast, the crystals used to generate the 5NM4 model from SFX were reported to be 30×30×5 μm^3 [5]. Optimizing conditions to grow larger crystals is often a time-consuming process that may take months to years and is a significant bottleneck in protein structural studies. Our present method alongside established SFX methods have shown the potential in obtaining high-resolution diffraction data by focusing on optimizing crystal growth conditions to form dense, uniform showers of small crystals. Data collection under the conditions outlined here has numerous benefits: first, the high dynamic range detectors can record the intense diffraction signals at low resolution so the images can be collected using unattenuated beam without concerns for damaging the detector electronics. Second, although not tested explicitly here, when more diffraction spots are observed in each image, fewer images should be required for structure

determination which could reduce the sample consumption and data collection time. It has been common to collect >10^4 SFX diffraction images to enable the building of a quality structure model, although protein structures have been resolved from SFX using less than 10^4 diffraction images on occasion [18]. Although the MX170-HS had a slower frame rate (10 Hz), the higher dynamic range can make the MX170-HS a better choice for SFX experiments seeking to record high quality resolution data using higher flux of the FEL beam at atmospheric pressure. The previously published 1.9 Å A_{2A}AR SFX model (PDB: 5K2D) [24] was built using diffraction data from similarly sized crystals formed in similar crystallization conditions as the present study, collected for ~2 hours using 9.8 keV FEL beam and the CSPAD detector. Similarly, our model was built at 2.0 Å resolution using SFX data from ~2 hours of beamtime (Table 1). Despite the differences between the detectors and data acquisition rates used to record SFX data, our model and 5K2D are in high agreement as previously discussed. If we extrapolate our results with the MX170-HS to a 120 Hz repetition rate, it may be possible to collect a similar dataset in only 10 minutes of beamtime. This is suggestive of the potential of this methodology to deliver high resolution membrane protein crystal structures while minimizing SFX data collection time and sample consumption. Generally, the ideal detector for SFX data collection should have high dynamic range, low read noise, and high acquisition rate matching or exceeding the full pulse rate of the XFEL source. The newest generation of XFEL beamlines (LCLS-II/SHINE) are capable of repetition rates at or above 100kHz. For new detectors to be able to match the repetition rates of these new machines, the physical dimensions of the detectors and total amount of pixels could be diminished while increasing the pixel size [29]. Theoretically, a 1-megapixel array

(1,000 x1,000 pixels) could still achieve a 100kHz repetition rate [29]. Specifically, the JUNGFRAU 4M detector [30] is an example of a detector that combines high dynamic range with a higher repetition rate (120 Hz) and may allow future users to collect high-resolution diffraction data from crystals that were previously shown to provide weak, low-resolution diffraction at highly attenuated XFELs. The JUNGFRAU 4M will become the default detector for sample chamber 1 (SC1) at CXI instrument in mid-2020.

An additional benefit to our method is the better measurement of low-resolution diffraction spots from better intensity estimates due to the aforementioned detector characteristics. We have observed that the indexing rate from our experiment was 63.5% while the other A_{2A}AR models generated from SFX, 5K2D and 5NM4, showed indexing rates of 31.3% and 2.3%, respectively [5] (Table1). Despite the higher indexing rate, our overall $\langle I/\sigma(I) \rangle$ was lower than that of 5K2D (Table 1), possibly be due to background scattering from the helium path between the crystal and the beam stop [31]. Further, it has been shown that acquiring more images can improve signal to noise ratio of the dataset [32]. In our dataset we used less images (16,737) compared to 5K2D (72,753).

A central problem around SFX is the scarcity of XFEL facilities and the difficulty in obtaining experimental beamtime. Enabling the use of the full power of the XFEL source as demonstrated in this work along with a high dynamic range and high repetition rate detector should greatly increase the efficiency of SFX experiments for membrane protein microcrystals grown in delivered in LCP matrix. Additionally, simultaneous data collection in the primary vacuum sample chamber at CXI as well as in the secondary helium-filled chamber using the refocused beam should further increase the number of experiments conducted at the facility. The methods and hardware setup presented here

have led to the development of the Macromolecular Femtosecond Crystallography (MFX) instrument [33] at LCLS as well as the secondary Serial Sample Chamber [21, 22] at CXI to reuse the XFEL beam. Lastly, XFEL-SFX experiments had been regularly conducted in helium atmosphere at SACLA, further demonstrating the utility of performing XFEL-SFX experiments in helium environment [34-36].

Methods

Adenosine A_{2A}-BRIL receptor purification and crystallization

Receptor purification and crystallization followed previously published protocols [1]. Briefly, 1 liter-scale insect cell membranes were prepared as described, and solubilized in a buffer containing 50 mM HEPES at pH 7.5, 800 mM NaCl, 2 mM theophylline (Sigma), 1.0 mg/ml iodoacetamide (Sigma), EDTA-free cOmplete protease inhibitor cocktail (Roche), 1% (w/v) n-dodecyl-ß-D-maltopyranoside (DDM, Anatrace) and 0.2% (w/v) cholesteryl hemisuccinate (CHS, Sigma) for 3 hours at 4ºC. The insoluble material was removed by centrifugation at 250,000*g* for 45 minutes and the supernatant was incubated with TALON affinity chromatography resin (Takara-Clontech) overnight in the presence of 20 mM imidazole. The resin was washed using successive volumes of buffers containing 100 µM of ZM241385 (Tocris, prepared as 100 mM stock in dimethyl sulfoxide) with increasing concentrations of imidazole. A_{2A}AR was eluted in the elution buffer (50 mM HEPES pH 7.5, 800 mM NaCl, 10% glycerol, 100 µM of ZM241385, 0.01% (w/v) DDM, 0.002% (w/v) CHS, 300 mM imidazole) and subsequently concentrated to approximately 40 mg/mL using an Amicon centrifugation concentrator (100 kDa molecular weight cutoff; MilliPore).

The receptor was reconstituted in LCP by mixing with a lipid mixture consisting of 90% (w/w) monoolein and 10% (w/w) cholesterol at a ratio of 2 parts protein to 3 parts lipids by volume using a lipid syringe mixer [37]. The sample was then subject to crystallization in gas-tight Hamilton syringes as previously described [24, 25]. Each crystallization syringe contained approximately 5 µL of the LCP sample with 50 µL of the following precipitant solutions: 0.1 M sodium citrate pH 5.0, 26% or 28% PEG400, and either 30 mM, 50 mM, or 60 mM sodium thiocyanate. All syringes were sealed and incubated at 20 °C with crystal formation observed within 24 hours. All crystal samples were consumed within the allotted experiment time at LCLS.

XFEL-SFX diffraction data collection

A_{2A}AR samples were prepared for injection following previously published protocols [38].The final sample was loaded in the reservoir of an LCP injector [12], which was mounted in a helium enclosure at the CXI instrument. The unattenuated XFEL beam was refocused with 4 compound refractive lenses (CRLs) of 50 µm Radius of curvature [39] for a total focal length of 1.79 m. These lenses were placed 3 m downstream of CXI's 1 µm focus and 4.42 m upstream the sample. The beam size on the sample was estimated to be just below 3 µm due to the lens chromatic aberration and assuming a 30 eV bandwidth. The nominal FEL beam pulse energy exiting the undulator was around 2 mJ and estimated to be ~1 mJ at the focus. The SFX diffraction data were collected using a high dynamic range detector (Rayonix MH170-HS) at 10 Hz with a sample flow rate of 0.2 µL/min, under a helium path and normal atmospheric pressure.

Data processing and model building

The SFX data were first processed with *Cheetah* [40] to delineate patterns containing crystal diffraction, termed "hits", from the rest of the patterns using the following settings: peakFinder8, threshold of 50 detector units of intensity, min SNR 6, min peaks 15, min pixels/peak 2, local bg radius 4. 26,341 hits were found, with an average hit rate of 37.5%. *CrystFEL* (version 0.8.0+049c3eb4) was used for indexing and integration (integration radii 4,5,7) based on the peaks found by *Cheetah* [41, 42]. 16,737 patterns were successfully indexed using a combination of MOSFLM [43], DirAx [44], XDS [45], asdf [42], and XGANDALF [46]. The sample-to-detector distance along with detector geometry were optimized using *geoptimiser* [47] with lysozyme crystal diffraction patterns collected at the beginning of the experiment to generate a virtual powder pattern. Multiple indexing runs were performed using finer detector geometry corrections for each indexing run to arrive at the final stream of data. Reflections were scaled and merged using partialator with the "unity" model (i.e. no partiality modelling), a saturation cutoff of 10,000 detector intensity units, and 1 scaling/merging iteration. Using data up to a resolution of 2.0 Å, an initial model was generated by molecular replacement (MR) phasing using the 1.9 Å XFEL structure (PDB ID: 5K2D) modified to a poly-alanine model, as the search model in the Phaser-MR module (Phenix version 1.17 [48]) in order to reduce phase bias [49, 50]. Iterative cycles of model refinement using Phenix.refine with TLS refinement parameters in five TLS groups. Manual inspection and model modifications in Coot [51, 52] was subsequently performed. The ligand, lipid, and cholesterol molecules were manually modelled into electron densities using Coot, as

well. Data collection and refinement statistics are presented in Table 1. The protein structure images presented in the figures were generated using PyMol [53].

Acknowledgement. This work was supported by the National Institutes of Health (NIH) grants R35 GM127086 (V.C.), R21 DA042298 (W.L.), R01 GM124152 (W.L.), the National Science Foundation [54] BioXFEL Science and Technology Center 1231306 (W.L., U.W., V.C.), and the Maxwell computational resources operated at Deutsches Elektronen-Synchrotron (DESY), Hamburg, Germany. C.G. kindly thanks SLAC National Accelerator Laboratory and the Department of Energy for financial support through the Panofsky fellowship. Use of the Linac Coherent Light Source (LCLS), SLAC National Accelerator Laboratory, is supported by the U.S. Department of Energy, Office of Science, Office of Basic Energy Sciences under Contract No. DE-AC02-76SF00515.

References

1. Liu W, Chun E, Thompson AA, Chubukov P, Xu F, Katritch V, et al. Structural basis for allosteric regulation of GPCRs by sodium ions. Science. 2012;337(6091):232-6. doi: 10.1126/science.1219218. PubMed PMID: 22798613; PubMed Central PMCID: PMC3399762.

2. Fenalti G, Giguere PM, Katritch V, Huang XP, Thompson AA, Cherezov V, et al. Molecular control of delta-opioid receptor signalling. Nature. 2014;506(7487):191-6. doi: 10.1038/nature12944. PubMed PMID: 24413399; PubMed Central PMCID: PMC3931418.

3. Segala E, Guo D, Cheng RK, Bortolato A, Deflorian F, Dore AS, et al. Controlling the Dissociation of Ligands from the Adenosine A2A Receptor through Modulation of Salt Bridge Strength. J Med Chem. 2016;59(13):6470-9. doi: 10.1021/acs.jmedchem.6b00653. PubMed PMID: 27312113.

4. Rucktooa P, Cheng RKY, Segala E, Geng T, Errey JC, Brown GA, et al. Towards high throughput GPCR crystallography: In Meso soaking of Adenosine A2A Receptor crystals. Sci Rep. 2018;8(1):41. doi: 10.1038/s41598-017-18570-w. PubMed PMID: 29311713; PubMed Central PMCID: PMCPMC5758569.

5. Weinert T, Olieric N, Cheng R, Brunle S, James D, Ozerov D, et al. Serial millisecond crystallography for routine room-temperature structure determination at synchrotrons. Nat Commun. 2017;8(1):542. doi: 10.1038/s41467-017-00630-4. PubMed PMID: 28912485; PubMed Central PMCID: PMCPMC5599499.

6. Sliz P, Harrison SC, Rosenbaum G. How does radiation damage in protein crystals depend on X-ray dose? Structure. 2003;11(1):13-9. doi: 10.1016/s0969-2126(02)00910-3. PubMed PMID: 12517336.

7. Garman EF, Owen RL. Cryocooling and radiation damage in macromolecular crystallography. Acta Crystallogr D Biol Crystallogr. 2006;62(Pt 1):32-47. doi: 10.1107/S0907444905034207. PubMed PMID: 16369092.

8. Watenpaugh KD. Macromolecular Crystallography at Cryogenic Temperatures. Current Opinion in Structural Biology. 1991;1:1012-5. doi: 10.1016/0959-440X(91)90099-F.

9. Yamamoto M, Hirata K, Yamashita K, Hasegawa K, Ueno G, Ago H, et al. Protein microcrystallography using synchrotron radiation. IUCrJ. 2017;4(Pt 5):529-39. Epub 2017/10/11. doi: 10.1107/S2052252517008193. PubMed PMID: 28989710; PubMed Central PMCID: PMCPMC5619846.

10. Miller MS, Maheshwari S, Shi W, Gao Y, Chu N, Soares AS, et al. Getting the

Most Out of Your Crystals: Data Collection at the New High-Flux, Microfocus MX Beamlines at NSLS-II. Molecules. 2019;24(3). Epub 2019/02/02. doi: 10.3390/molecules24030496. PubMed PMID: 30704096; PubMed Central PMCID: PMCPMC6384729.

11. Martin-Garcia JM, Conrad CE, Nelson G, Stander N, Zatsepin NA, Zook J, et al. Serial millisecond crystallography of membrane and soluble protein microcrystals using synchrotron radiation. IUCrJ. 2017;4(Pt 4):439-54. doi: 10.1107/S205225251700570X. PubMed PMID: 28875031; PubMed Central PMCID: PMC5571807.

12. Weierstall U, James D, Wang C, White TA, Wang D, Liu W, et al. Lipidic cubic phase injector facilitates membrane protein serial femtosecond crystallography. Nat Commun. 2014;5:3309. doi: 10.1038/ncomms4309. PubMed PMID: 24525480; PubMed Central PMCID: PMC4061911.

13. Neutze R, Hajdu J. Femtosecond time resolution in x-ray diffraction experiments. Proceedings of the National Academy of Sciences of the United States of America. 1997;94(11):5651-5. doi: 10.1073/pnas.94.11.5651. PubMed PMID: 9159127; PubMed Central PMCID: PMC20833.

14. Stauch B, Cherezov V. Serial Femtosecond Crystallography of G Protein-Coupled Receptors. Annu Rev Biophys. 2018;47:377-97. doi: 10.1146/annurev-biophys-070317-033239. PubMed PMID: 29543504; PubMed Central PMCID: PMCPMC6290114.

15. Carini GA, Boutet S, Chollet M, Dragone A, Haller G, Hart PA, et al. Experience with the CSPAD during dedicated detector runs at LCLS. Journal of Physics: Conference Series. 2014;493:012011. doi: 10.1088/1742-6596/493/1/012011.

16. Blaj G, Caragiulo P, Carini G, Carron S, Dragone A, Freytag D, et al. X-ray detectors at the Linac Coherent Light Source. J Synchrotron Radiat. 2015;22(3):577-83. doi: 10.1107/S1600577515005317. PubMed PMID: 25931071; PubMed Central PMCID: PMCPMC4416673.

17. Martin-Garcia JM, Conrad CE, Coe J, Roy-Chowdhury S, Fromme P. Serial femtosecond crystallography: A revolution in structural biology. Archives of biochemistry and biophysics. 2016;602:32-47. doi: 10.1016/j.abb.2016.03.036. PubMed PMID: 27143509; PubMed Central PMCID: PMC4909539.

18. Coe JaR, A. Small Is Beautiful: Growth and Detection of Nanocrystals. In: Boutet S, Fromme, P., and Hunter, M.S., editor. X-ray Free Electron Lasers: A Revolution in Structural Biology: Springer Nature Switzerland AG; 2018. p. 59-86.

19. Stan CA, Milathianaki D, Laksmono H, Sierra RG, McQueen Trevor A, Messerschmidt M, et al. Liquid explosions induced by X-ray laser pulses. Nature Physics. 2016;12(10):966-71. Epub 23 May 2016. doi: 10.1038/nphys3779.

20. Fromme P. XFELs open a new era in structural chemical biology. Nature chemical biology. 2015;11(12):895-9. doi: 10.1038/nchembio.1968. PubMed PMID: 26575227; PubMed Central PMCID: PMC4839532.

21. Liang M, Williams GJ, Messerschmidt M, Seibert MM, Montanez PA, Hayes M, et al. The Coherent X-ray Imaging instrument at the Linac Coherent Light Source. J Synchrotron Radiat. 2015;22(3):514-9. doi: 10.1107/S160057751500449X. PubMed PMID: 25931062; PubMed Central PMCID: PMCPMC4416669.

22. Boutet S, Foucar L, Barends TR, Botha S, Doak RB, Koglin JE, et al. Characterization and use of the spent beam for serial operation of LCLS. J Synchrotron Radiat. 2015;22(3):634-43. doi: 10.1107/S1600577515004002. PubMed PMID: 25931079; PubMed Central PMCID: PMCPMC4416680.

23. Hunter MS, Yoon CH, DeMirci H, Sierra RG, Dao EH, Ahmadi R, et al. Selenium single-wavelength anomalous diffraction de novo phasing using an X-ray-free electron laser. Nat Commun. 2016;7:13388. doi: 10.1038/ncomms13388. PubMed PMID: 27811937; PubMed Central PMCID: PMCPMC5097167.

24. Batyuk A, Galli L, Ishchenko A, Han GW, Gati C, Popov PA, et al. Native phasing of x-ray free-electron laser data for a G protein-coupled receptor. Sci Adv. 2016;2(9):e1600292. doi: 10.1126/sciadv.1600292. PubMed PMID: 27679816; PubMed Central PMCID: PMCPMC5035125.

25. Liu W, Ishchenko A, Cherezov V. Preparation of microcrystals in lipidic cubic phase for serial femtosecond crystallography. Nature protocols. 2014;9(9):2123-34. doi: 10.1038/nprot.2014.141. PubMed PMID: 25122522; PubMed Central PMCID: PMC4209290.

26. Ballesteros JAW, H. Integrated Methods for the Construction of Three-dimensional Models and Computational Probing of Structure-function Relations in G Protein-coupled Receptors. Methods in Neurosciences. 1995;25:366-428. Epub 2 September 2007. doi: https://doi.org/10.1016/S1043-9471(05)80049-7.

27. Katritch V, Fenalti G, Abola EE, Roth BL, Cherezov V, Stevens RC. Allosteric sodium in class A GPCR signaling. Trends Biochem Sci. 2014;39(5):233-44. doi: 10.1016/j.tibs.2014.03.002. PubMed PMID: 24767681; PubMed Central PMCID: PMCPMC4106411.

28. Blaj G, Carini, G., Hart, P., Herrmann, S. Non-SLAC Detectors at LCLS. LCLS/SSRL Users' Meeting 2013 - LCLS Detectors Workshop. SLAC National Accelerator Laboratory2013.

29. Bergamaschi A, Mozzanica A, Schmitt B. XFEL detectors. Nature Reviews Physics. 2020;2(7):335-6. doi: 10.1038/s42254-020-0200-x.

30. Leonarski F, Redford S, Mozzanica A, Lopez-Cuenca C, Panepucci E, Nass K, et al. Fast and accurate data collection for macromolecular crystallography using the JUNGFRAU detector. Nat Methods. 2018;15(10):799-804. doi: 10.1038/s41592-018-0143-7. PubMed PMID: 30275593.

31. Perutz MF, Rogers GL. A Vacuum Tank for Use with a Single Crystal X-ray Goniometer. Journal of Scientific Instruments. 1946;23(9):217-. doi: 10.1088/0950-7671/23/9/408.

32. Glynn C, Rodriguez JA. Data-driven challenges and opportunities in crystallography. Emerging Topics in Life Sciences. 2019;3(4):423-32. doi: 10.1042/etls20180177.

33. Sierra RG, Batyuk A, Sun Z, Aquila A, Hunter MS, Lane TJ, et al. The Macromolecular Femtosecond Crystallography Instrument at the Linac Coherent Light Source. J Synchrotron Radiat. 2019;26(Pt 2):346-57. doi: 10.1107/S1600577519001577. PubMed PMID: 30855242; PubMed Central PMCID: PMCPMC6412173.

34. Tono K, Nango E, Sugahara M, Song C, Park J, Tanaka T, et al. Diverse application platform for hard X-ray diffraction in SACLA (DAPHNIS): application to serial protein crystallography using an X-ray free-electron laser. J Synchrotron Radiat. 2015;22(3):532-7. Epub 2015/05/02. doi: 10.1107/S1600577515004464. PubMed PMID: 25931065; PubMed Central PMCID: PMCPMC4817517.

35. Sugahara M, Nakane T, Masuda T, Suzuki M, Inoue S, Song C, et al. Hydroxyethyl cellulose matrix applied to serial crystallography. Sci Rep. 2017;7(1):703. Epub 2017/04/08. doi: 10.1038/s41598-017-00761-0. PubMed PMID: 28386083; PubMed Central PMCID: PMCPMC5429652.

36. Shimazu Y, Tono K, Tanaka T, Yamanaka Y, Nakane T, Mori C, et al. High-viscosity sample-injection device for serial femtosecond crystallography at atmospheric pressure. Journal of applied crystallography. 2019;52(Pt 6):1280-8. Epub 2019/12/05. doi: 10.1107/S1600576719012846. PubMed PMID: 31798359; PubMed Central PMCID: PMCPMC6878880.

37. Caffrey M, Cherezov V. Crystallizing membrane proteins using lipidic mesophases. Nature protocols. 2009;4(5):706-31. doi: 10.1038/nprot.2009.31. PubMed PMID: 19390528; PubMed Central PMCID: PMCPMC2732203.

38. Ishchenko A, Cherezov V, Liu W. Preparation and Delivery of Protein Microcrystals in Lipidic Cubic Phase for Serial Femtosecond Crystallography. LID - 10.3791/54463 [doi] LID - 54463. (1940-087X (Electronic)).

39. Chapman HN, Fromme P, Barty A, White TA, Kirian RA, Aquila A, et al.

Femtosecond X-ray protein nanocrystallography. Nature. 2011;470(7332):73-7. doi: 10.1038/nature09750.

40. Barty A, Kirian RA, Maia FR, Hantke M, Yoon CH, White TA, et al. Cheetah: software for high-throughput reduction and analysis of serial femtosecond X-ray diffraction data. Journal of applied crystallography. 2014;47(Pt 3):1118-31. doi: 10.1107/S1600576714007626. PubMed PMID: 24904246; PubMed Central PMCID: PMC4038800.

41. White TA. Processing serial crystallography data with CrystFEL: a step-by-step guide. Acta crystallographica Section D, Structural biology. 2019;75(Pt 2):219-33. doi: 10.1107/S205979831801238X. PubMed PMID: 30821710; PubMed Central PMCID: PMC6400257.

42. White TA, Mariani V, Brehm W, Yefanov O, Barty A, Beyerlein KR, et al. Recent developments in CrystFEL. Journal of applied crystallography. 2016;49(Pt 2):680-9. doi: 10.1107/S1600576716004751. PubMed PMID: 27047311; PubMed Central PMCID: PMC4815879.

43. Powell HR, Johnson O, Leslie AG. Autoindexing diffraction images with iMosflm. Acta Crystallogr D Biol Crystallogr. 2013;69(Pt 7):1195-203. doi: 10.1107/S0907444912048524. PubMed PMID: 23793145; PubMed Central PMCID: PMCPMC3689522.

44. Duisenberg A. Indexing in single-crystal diffractometry with an obstinate list of reflections. Journal of applied crystallography. 1992;25(2):92-6. doi: doi:10.1107/S0021889891010634.

45. Kabsch W. Xds. Acta Crystallogr D Biol Crystallogr. 2010;66(Pt 2):125-32. doi: 10.1107/S0907444909047337. PubMed PMID: 20124692; PubMed Central PMCID: PMCPMC2815665.

46. Gevorkov Y, Yefanov O, Barty A, White TA, Mariani V, Brehm W, et al. XGANDALF - extended gradient descent algorithm for lattice finding. Acta Crystallogr A Found Adv. 2019;75(Pt 5):694-704. doi: 10.1107/S2053273319010593. PubMed PMID: 31475914; PubMed Central PMCID: PMCPMC6718201.

47. Yefanov O, Mariani V, Gati C, White TA, Chapman HN, Barty A. Accurate determination of segmented X-ray detector geometry. Opt Express. 2015;23(22):28459-70. doi: 10.1364/OE.23.028459. PubMed PMID: 26561117; PubMed Central PMCID: PMCPMC4646514.

48. McCoy AJ, Grosse-Kunstleve RW, Adams PD, Winn MD, Storoni LC, Read RJ. Phaser crystallographic software. Journal of applied crystallography. 2007;40(Pt 4):658-74. doi: 10.1107/S0021889807021206. PubMed PMID: 19461840; PubMed Central

PMCID: PMCPMC2483472.

49. Adams PD, Afonine PV, Bunkoczi G, Chen VB, Davis IW, Echols N, et al. PHENIX: a comprehensive Python-based system for macromolecular structure solution. Acta Crystallogr D Biol Crystallogr. 2010;66(Pt 2):213-21. doi: 10.1107/S0907444909052925. PubMed PMID: 20124702; PubMed Central PMCID: PMC2815670.

50. Adams PD, Afonine PV, Bunkoczi G, Chen VB, Echols N, Headd JJ, et al. The Phenix software for automated determination of macromolecular structures. Methods. 2011;55(1):94-106. doi: 10.1016/j.ymeth.2011.07.005. PubMed PMID: 21821126; PubMed Central PMCID: PMC3193589.

51. Emsley P, Cowtan K. Coot: model-building tools for molecular graphics. Acta Crystallogr D Biol Crystallogr. 2004;60(Pt 12 Pt 1):2126-32. doi: 10.1107/S0907444904019158. PubMed PMID: 15572765.

52. Emsley P, Lohkamp B, Scott WG, Cowtan K. Features and development of Coot. Acta Crystallogr D Biol Crystallogr. 2010;66(Pt 4):486-501. doi: 10.1107/S0907444910007493. PubMed PMID: 20383002; PubMed Central PMCID: PMC2852313.

53. Schrodinger, LLC. The PyMOL Molecular Graphics System, Version 1.8. 2015.

54. Stansfeld PJ, Sansom MSP. Molecular simulation approaches to membrane proteins. Structure. 2011;19(11):1562-72. doi: 10.1016/j.str.2011.10.002.

Supplementary Figure 4.4

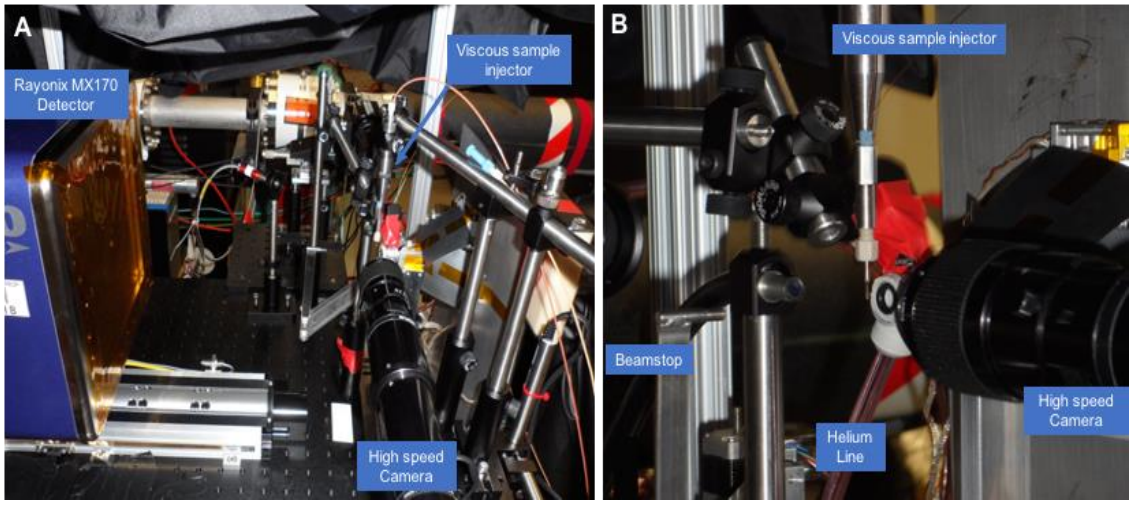

Supplementary Figure 4.4. Detailed instrument setup from Figure 1A inset region. A) Side profile view highlighting the location of the detector, viscous sample injector, and other instruments within the sample chamber. B) Another view of the viscous sample injector, beam stop, and helium line inside the sample chamber.

Supplementary Figure 4.5

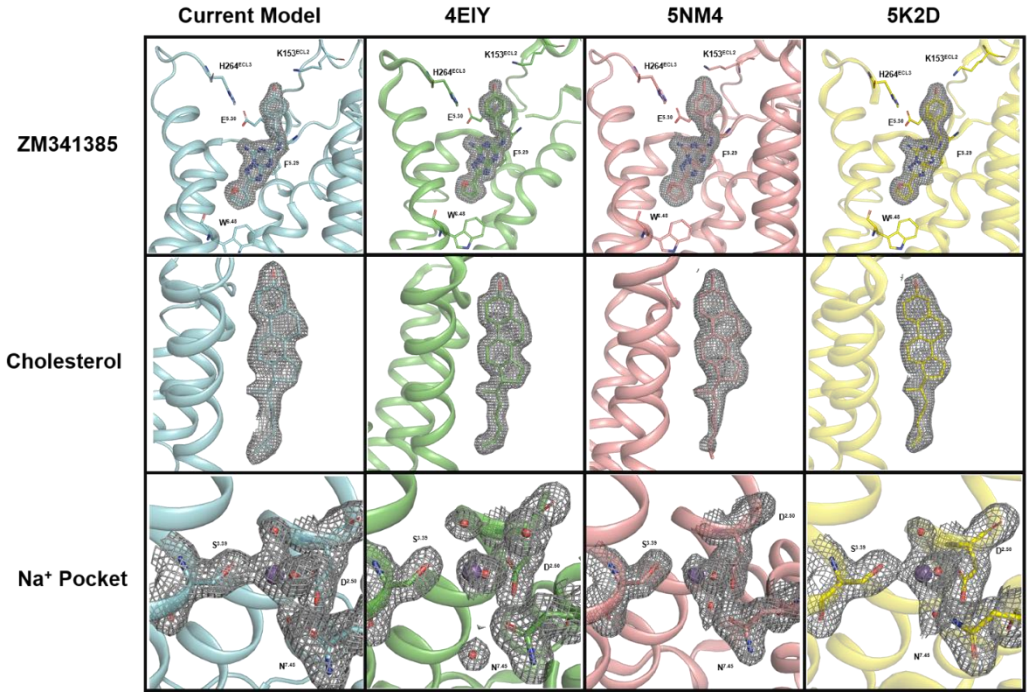

Supplementary Figure 4.5. Comparison of the ligand, cholesterol, and sodium pocket $2mF_o$-DF_c electron densities.

CHAPTER 5

CONCLUSIONS AND FUTURE DIRECTIONS

CCK_1R and Cholesterol

The simulations at the CCK receptors yielded exciting insights regarding the mechanism behind the cholesterol sensitivity of the CCK_1R. We found that cholesterol stuck to the CCK_1R at residue $F130^{3.41}$ stronger than any other receptor that we measured. Furthermore, the simulations showed that the CCK receptors bound cholesterol differentially both in the location and length of the interactions. This further supports the notion that the specific cholesterol interactions could be responsible for the sensitivity of the CCK_1R. In class-A GPCRs, mutations to position 3.41 have been shown to be important in the expression and stability of numerous engineered receptors for crystallization [1-3]. In the light of the previous data, it is not surprising that cholesterol interactions centered at F130 would have profound physiological effects. Moreover, previous studies support the hypothesis that interactions at TM3 could be responsible for the cholesterol sensitivity of the CCK_1R [4, 5].

The binding of the peptide hormone cholecystokinin (CCK) to the CCK_1R is known to cause satiation after the consumption of a meal [6, 7]. Knowing this, several pharmaceutical companies have developed CCK_1R agonists as appetite suppressants to aid in the weight loss of overweight patients [8, 9]. While the treatments generally did result in loss of weight, it was not greater than dieting alone, and because of concerns that more potent or longer duration full agonists might be associated with side effects and potential toxicity, this type of drug never reached clinical use. Since high-membrane cholesterol (something commonly found in obese patients) impedes the satiety effect of

the CCK_1R, it has been proposed that a positive allosteric modulator could be developed that would inhibit cholesterol interactions with the receptor and thus allow for enhanced signaling from the CCK_1R without the need for a potent agonist and the accompanying side effects. Our simulations were able to reveal a region centered on TM3 where cholesterol appears to bind the CCK_1R. A brief analysis of the surface contact potential of the CCK models revealed a clear cleft amenable to cholesterol binding at the CCK_1R (Fig. 5.1). However, to develop the proposed allosteric modulator, more detail of this binding cleft is needed. Fully atomistic computational approaches, such as molecular dynamics or docking, could provide clearer data regarding these receptor-cholesterol interactions. However, it should be noted that no high-resolution structures have been published for the CCK receptors and thus, even fully atomistic simulations arise from homology models of closely related receptors.

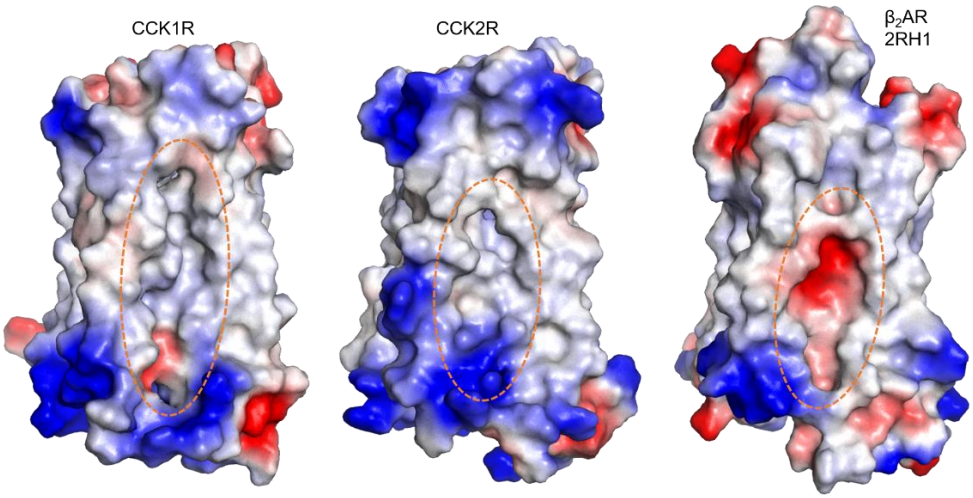

Figure 5. 1 Surface contact charge shown for the CCK receptors and the B2AR. Negative charges shown in red and positive charges shown in blue. A clear cleft on the CCK_1R is highlighted by the orange circle. The CCK_2R has a smaller cleft with opposite charge. The B2AR shows a largely negative cleft, potentially not amenable to cholesterol binding.

To this end, extensive rounds of receptor engineering have been performed in the pursuit of a stable, crystallization friendly construct of the CCK_1R. Through the incorporation of numerous truncations, mutations, and fusion proteins, the CCK_1R has been purified in a form that is monomeric and binds a small molecule antagonist (Fig. 5.2). Moreover, a pre-crystallization FRAP assay [10] has highlighted conditions that should be amenable to crystallization (Fig. 5.2). Theoretically, a high-resolution structure will help further elucidate the exact interactions between the CCK_1R and cholesterol and aid in the pursuit of the allosteric modulator.

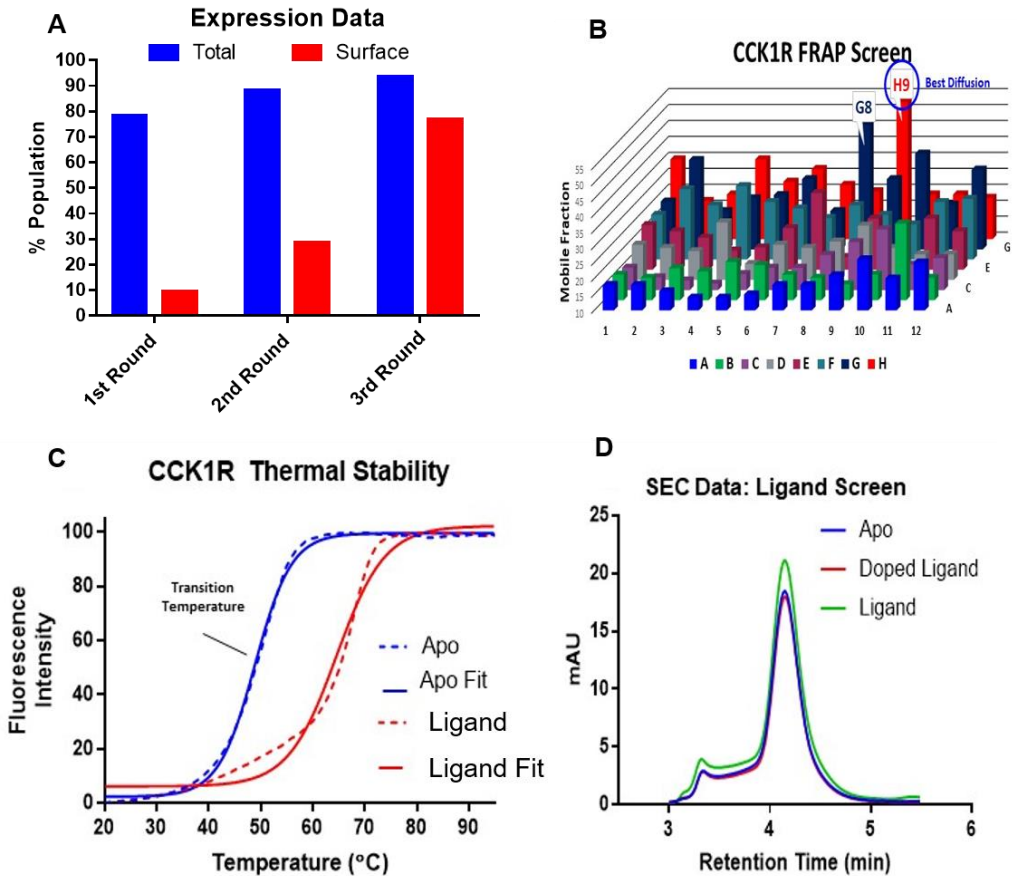

Figure 5.2 Towards a high-resolution CCK1R crystal structure A) Expression of the CCK_1R increased through numerous rounds of engineering. B) A FRAP assay showed multiple conditions that may be amenable to for the crystallization of the CCK_1R. C) A small molecule ligand stabilizes the receptor in a thermal denaturation assay, showing ligand binding ability of the construct. D) The construct purifies in a stable, monomeric form.

Additionally, more interesting questions concerning the dynamics of the receptor itself could be answered by more *in silico* research. For example, a fully atomistic simulation at the CCK_1R could show why the receptor binds ligand tighter as cholesterol is increased the membrane [5]. It is known the CCK receptors bind cholesterol differently [11]. Interestingly, unpublished data has led our collaborators to believe that the CCK_1R binds CCK in a similar fashion as the CCK_2R under a high cholesterol environment. Atomistic simulations could hypothetically yield more information into the different modes of ligand binding. Residues important for CCK binding could be compared from separate simulations with increasing membrane cholesterol content. Furthermore, detailed analysis of the conformational changes that the receptor exhibits in varying levels of membrane cholesterol could explain why the CCK_1R binds to an agonist stronger while exhibiting less downstream signaling under high cholesterol conditions [5]. It may be that cholesterol binding hinders the necessary outward swing of transmembrane helices necessary to facilitate G-protein binding.

A particularly interesting hypothesis is the notion that cholesterol could be inducing biased signaling pathways at the CCK_1R. In the canonical sense, stronger agonist binding would be expected to result in a stronger signal from the receptor. To date, the assays quantifying cholesterol's effect on the CCK_1R have only focused on Ca^{2+} efflux originating from the CCK_1R-Gq pathway. As highlighted in chapter 1, GPCRs can signal through numerous G-protein pathways. The CCK_1R has been shown to bind G_q, G_s, G_i, and G_o proteins to varying degrees, with the majority of downstream signaling originating from G_q binding. Interestingly investigations into the biased signaling (i.e. ligand preferentially signaling through one particular G-protein) of the CCK_1R showed

that mutations at the bottom of TM3 induced changes in the levels of downstream signaling arising from the different G-proteins. We believe that cholesterol binds the CCK_1R on TM3 slightly above these residues. Therefore, it is interesting to hypothesize that cholesterol binding may induce similar effects and result in a biased signaling cascade. This would, theoretically, reconcile the how the CCK_1R binds agonist stronger while limiting the signaling from the G_q pathway. The hypothesis could be tested using the same assays as described previously. However, fluorescent probes for other downstream molecules, such as cAMP or IP_3 in the place of Ca^{2+}, could quantify signals that arise from other G-proteins.

TM7 CRAC Sequence

One of the more exciting findings from our simulations was the discovery of a TM7 CRAC sequence that overlaps with the conserved NPxxY motif. After alignment, we discovered that this CRAC sequence is conserved across nearly 40% of class-A GPCRs. Unfortunately, CRAC sequences are ubiquitous on membrane proteins and are poor predictors of actual cholesterol binding. Realistically, it may be that this CRAC sequence has little physiological relevance for many receptors that contain it. Conversely, there is evidence in the literature that this CRAC sequence can be important for receptor function, such as at the type-1 cannabinoid receptor [12]. Moreover, our mutational analysis at the β_2AR showed that mutation of this CRAC sequence does change the receptors properties with respect to cholesterol in synthetic bilayers.

For cholesterol sensitive receptors, downstream signaling or ligand binding assays after the enhancing/depletion of membrane cholesterol could provide data that would validate the importance of this CRAC sequence. Mutations that remove the CRAC

sequence (or add the CRAC sequence to those receptors that don't naturally contain it) could show whether or not cholesterol binding at TM7 has any profound physiological effects.

General Directions

Our simulations were able to elucidate specific cholesterol binding pockets on GPCRs. While many studies have focused on the relationship between various receptors and cholesterol, there is still much to be learned. There are many receptors known to be sensitive to membrane cholesterol without specific information about where/how cholesterol interacts. Our simulation methods could be applied to numerous receptors and characterize these interactions.

Advances in X-ray Crystallography

Our experiments at the XFEL showed that data collection from an unattenuated X-ray beam can streamline data collection during SFX. We were able to generate an A_{2a}AR structure model from fewer images and less collection time than previously published models. A main problem around SFX is the scarcity of XFEL facilities and the difficulty in obtaining beamtime. Enabling the use of the full power of the XFEL source as demonstrated in this work along with a high dynamic range and high repetition rate detector should greatly increase the efficiency of SFX experiments. One clear limitation from our experiment was the low refresh rate (10 Hz) of the MX170-HS detector. However, if we extrapolate the rate of data collection to other detectors (120 Hz), a complete dataset could be collected in as little as 10 minutes. While current detectors, such as the JUNGFRAU 4M, offer high dynamic range and operate at 120 Hz, new generations of detectors will need to increase their refresh rate to match the 100 kHz

repetition rates of the newest generation of XFEL beamlines. To achieve such a high refresh rate, the physical dimensions of the detectors and the total number of pixels will need to be diminished while increasing the average pixel size. Theoretically, a 1-megapixel array (1,000 x1,000 pixels) could still achieve a 100kHz repetition rate [13]. The methods described here will aid researchers as they determine the structure of more GPCRs and other important proteins.

References

1. Heydenreich FM, Vuckovic Z, Matkovic M, Veprintsev DB. Stabilization of G protein-coupled receptors by point mutations. Frontiers in Pharmacology. 2015;6:82.

2. Rosenbaum DM, Cherezov V, Hanson MA, Rasmussen SGF, Thian FS, Kobilka TS, et al. GPCR Engineering Yields High-Resolution Structural Insights into β₂-Adrenergic Receptor Function. Science. 2007;318(5854):1266. doi: 10.1126/science.1150609.

3. Roth CB, Hanson MA, Stevens RC. Stabilization of the Human β2-Adrenergic Receptor TM4–TM3–TM5 Helix Interface by Mutagenesis of Glu1223.41, A Critical Residue in GPCR Structure. Journal of Molecular Biology. 2008;376(5):1305-19. doi: https://doi.org/10.1016/j.jmb.2007.12.028.

4. Desai AJ, Harikumar KG, Miller LJ. A Type 1 Cholecystokinin Receptor Mutant That Mimics the Dysfunction Observed for Wild Type Receptor in a High Cholesterol Environment. 2014;289(26):18314-26. doi: 10.1074/jbc.M114.570200.

5. Potter RM, Harikumar KG, Wu SV, Miller LJ. Differential sensitivity of types 1 and 2 cholecystokinin receptors to membrane cholesterol. 2012;53(1):137-48. doi: 10.1194/jlr.M020065.

6. Li Y, Owyang C. Endogenous cholecystokinin stimulates pancreatic enzyme secretion via vagal afferent pathway in rats. Gastroenterology. 1994;107(2):525-31. doi: https://doi.org/10.1016/0016-5085(94)90180-5.

7. Smith GP, Gibbs J. The Satiety Effect of Cholecystokinin Recent Progress and Current Problemsa. Annals of the New York Academy of Sciences. 1985;448(1):417-23. doi: 10.1111/j.1749-6632.1985.tb29936.x.

8. Aquino CJ, Armour DR, Berman JM, Birkemo LS, Carr RAE, Croom DK, et al. Discovery of 1,5-Benzodiazepines with Peripheral Cholecystokinin (CCK-A) Receptor Agonist Activity. 1. Optimization of the Agonist “Trigger”. Journal of Medicinal Chemistry. 1996;39(2):562-9. doi: 10.1021/jm950626d.

9. Desai AJ, Lam PCH, Orry A, Abagyan R, Christopoulos A, Sexton PM, et al. Molecular Mechanism of Action of Triazolobenzodiazepinone Agonists of the Type 1 Cholecystokinin Receptor. Possible Cooperativity across the Receptor Homodimeric Complex. Journal of Medicinal Chemistry. 2015;58(24):9562-77. doi: 10.1021/acs.jmedchem.5b01110.

10. Xu F, Liu W, Hanson MA, Stevens RC, Cherezov V. Development of an Automated High Throughput LCP-FRAP Assay to Guide Membrane Protein

Crystallization in Lipid Mesophases. Cryst Growth Des. 2011;11(4):1193-201. doi: 10.1021/cg101385e. PubMed PMID: 21660116.

11. Fourmy D, Escrieut C, Archer E, Galès C, Gigoux V, Maigret B, et al. Structure of Cholecystokinin Receptor Binding Sites and Mechanism of Activation/Inactivation by Agonists/Antagonists. Pharmacology & Toxicology. 2002;91(6):313-20. doi: 10.1034/j.1600-0773.2002.910608.x.

12. Oddi S, Dainese E, Fezza F, Lanuti M, Barcaroli D, De Laurenzi V, et al. Functional characterization of putative cholesterol binding sequence (CRAC) in human type-1 cannabinoid receptor. Journal of Neurochemistry. 2011;116(5):858-65. doi: 10.1111/j.1471-4159.2010.07041.x.

13. Bergamaschi A, Mozzanica A, Schmitt B. XFEL detectors. Nature Reviews Physics. 2020;2(7):335-6. doi: 10.1038/s42254-020-0200-x.

REFERENCES

1. Proceedings of the 2006 ACM/IEEE conference on Supercomputing2006; Tampa, Florida: Association for Computing Machinery.

2. Abraham MJ, Murtola T, Schulz R, Páll S, Smith JC, Hess B, et al. GROMACS: High performance molecular simulations through multi-level parallelism from laptops to supercomputers. SoftwareX. 2015;1-2:19-25. doi: https://doi.org/10.1016/j.softx.2015.06.001.

3. Adams PD, Afonine PV, Bunkoczi G, Chen VB, Davis IW, Echols N, et al. PHENIX: a comprehensive Python-based system for macromolecular structure solution. Acta Crystallogr D Biol Crystallogr. 2010;66(Pt 2):213-21. doi: 10.1107/S0907444909052925. PubMed PMID: 20124702; PubMed Central PMCID: PMC2815670.

4. Adams PD, Afonine PV, Bunkoczi G, Chen VB, Echols N, Headd JJ, et al. The Phenix software for automated determination of macromolecular structures. Methods. 2011;55(1):94-106. doi: 10.1016/j.ymeth.2011.07.005. PubMed PMID: 21821126; PubMed Central PMCID: PMC3193589.

5. Al-Sahouri Z, Lee M-Y, Li D, Liu W, Caffrey M. The Lipid Cubic Phase as a Medium for the Growth of Membrane Protein Microcrystals. In: Boutet S, Fromme P, Hunter MS, editors. X-ray Free Electron Lasers: A Revolution in Structural Biology. Cham: Springer International Publishing; 2018. p. 87-107.

6. Albert AD, Boesze-Battaglia K. The role of cholesterol in rod outer segment membranes. Progress in Lipid Research. 2005;44(2):99-124. doi: https://doi.org/10.1016/j.plipres.2005.02.001.

7. Alder BJ, Wainwright TE. Phase Transition for a Hard Sphere System. The Journal of Chemical Physics. 1957;27(5):1208-9. doi: 10.1063/1.1743957.

8. Alexander SPH CA, Davenport AP, Kelly E, Mathie A, Peters JA, Veale EL, Armstrong JF, Faccenda E, Harding SD, Pawson AJ, Sharman JL, Southan C, Davies JA; CGTP Collaborators. . The Concise Guide to PHARMACOLOGY 2019/20: G protein-coupled receptors. . Br J Pharmacology, 2019;176 (S1):S21-S141.

9. Alexandrov AI, Mileni M, Chien EYT, Hanson MA, Stevens RC. Microscale Fluorescent Thermal Stability Assay for Membrane Proteins. Structure. 2008;16(3):351-9. doi: https://doi.org/10.1016/j.str.2008.02.004.

10. Alonso MA, Millán J. The role of lipid rafts in signalling and membrane trafficking in T lymphocytes. Journal of Cell Science. 2001;114(22):3957.

11. Aquino CJ, Armour DR, Berman JM, Birkemo LS, Carr RAE, Croom DK, et al. Discovery of 1,5-Benzodiazepines with Peripheral Cholecystokinin (CCK-A) Receptor Agonist Activity. 1. Optimization of the Agonist "Trigger". Journal of Medicinal Chemistry. 1996;39(2):562-9. doi: 10.1021/jm950626d.

12. Ashkenazy H, Erez E, Martz E, Pupko T, Ben-Tal N. ConSurf 2010: calculating evolutionary conservation in sequence and structure of proteins and nucleic acids. Nucleic Acids Research. 2010;38(suppl_2):W529-W33. doi: 10.1093/nar/gkq399.

13. Baier CJ, Fantini J, Barrantes FJ. Disclosure of cholesterol recognition motifs in transmembrane domains of the human nicotinic acetylcholine receptor. Scientific Reports. 2011;1(1):69. doi: 10.1038/srep00069.

14. Ballesteros JA, Weinstein H. [19] Integrated methods for the construction of three-dimensional models and computational probing of structure-function relations in G protein-coupled receptors. In: Sealfon SC, editor. Methods in Neurosciences. 25: Academic Press; 1995. p. 366-428.

15. Ballesteros JA, Weinstein H. Integrated methods for the construction of three-dimensional models and computational probing of structure-function relations in G protein-coupled receptors. In: Sealfon SC, editor. Methods in Neurosciences. 25: Academic Press; 1995. p. 366-428.

16. Ballesteros JAW, H. Integrated Methods for the Construction of Three-dimensional Models and Computational Probing of Structure-function Relations in G Protein-coupled Receptors. Methods in Neurosciences. 1995;25:366-428. Epub 2 September 2007. doi: https://doi.org/10.1016/S1043-9471(05)80049-7.

17. Bari M, Battista N, Fezza F, Finazzi-Agrò A, Maccarrone M. Lipid Rafts Control Signaling of Type-1 Cannabinoid Receptors in Neuronal Cells: IMPLICATIONS FOR ANANDAMIDE-INDUCED APOPTOSIS. Journal of Biological Chemistry. 2005;280(13):12212-20.

18. Bari M, Paradisi A, Pasquariello N, Maccarrone M. Cholesterol-dependent modulation of type 1 cannabinoid receptors in nerve cells. Journal of Neuroscience Research. 2005;81(2):275-83. doi: 10.1002/jnr.20546.

19. Barnett-Norris J, Lynch D, Reggio PH. Lipids, lipid rafts and caveolae: Their importance for GPCR signaling and their centrality to the endocannabinoid system. Life Sciences. 2005;77(14):1625-39. doi: https://doi.org/10.1016/j.lfs.2005.05.040.

20. Baron R, Trzesniak D, de Vries AH, Elsener A, Marrink SJ, van Gunsteren WF. Comparison of Thermodynamic Properties of Coarse-Grained and Atomic-Level Simulation Models. ChemPhysChem. 2007;8(3):452-61. doi: 10.1002/cphc.200600658.

21. Barty A, Kirian RA, Maia FR, Hantke M, Yoon CH, White TA, et al. Cheetah: software for high-throughput reduction and analysis of serial femtosecond X-ray diffraction data. Journal of applied crystallography. 2014;47(Pt 3):1118-31. doi: 10.1107/S1600576714007626. PubMed PMID: 24904246; PubMed Central PMCID: PMC4038800.

22. Batyuk A, Galli L, Ishchenko A, Han GW, Gati C, Popov PA, et al. Native phasing of x-ray free-electron laser data for a G protein-coupled receptor. Sci Adv. 2016;2(9):e1600292. doi: 10.1126/sciadv.1600292. PubMed PMID: 27679816; PubMed Central PMCID: PMCPMC5035125.

23. Benned-Jensen T, Norn C Fau - Laurent S, Laurent S Fau - Madsen CM, Madsen Cm Fau - Larsen HM, Larsen Hm Fau - Arfelt KN, Arfelt Kn Fau - Wolf RM, et al. Molecular characterization of oxysterol binding to the Epstein-Barr virus-induced gene 2 (GPR183). (1083-351X (Electronic)).

24. Berman HM, Westbrook J, Feng Z, Gilliland G, Bhat TN, Weissig H, et al. The Protein Data Bank. Nucleic Acids Research. 2000;28(1):235-42. doi: 10.1093/nar/28.1.235.

25. Blaj G, Carini, G., Hart, P., Herrmann, S. Non-SLAC Detectors at LCLS. LCLS/SSRL Users' Meeting 2013 - LCLS Detectors Workshop. SLAC National Accelerator Laboratory2013.

26. Blaj G, Caragiulo P, Carini G, Carron S, Dragone A, Freytag D, et al. X-ray detectors at the Linac Coherent Light Source. J Synchrotron Radiat. 2015;22(3):577-83. doi: 10.1107/S1600577515005317. PubMed PMID: 25931071; PubMed Central PMCID: PMCPMC4416673.

27. Boutet S, Foucar L, Barends TR, Botha S, Doak RB, Koglin JE, et al. Characterization and use of the spent beam for serial operation of LCLS. J Synchrotron Radiat. 2015;22(3):634-43. doi: 10.1107/S1600577515004002. PubMed PMID: 25931079; PubMed Central PMCID: PMCPMC4416680.

28. Braun E, , Gilmer J, , Mayes HB, , et al. Best Practices for Foundations in Molecular Simulations Best Practices 2018;1(1). doi: 10.33011. PubMed PMID: Braun2018Best.

29. Brown MF. Modulation of rhodopsin function by properties of the membrane bilayer. (0009-3084 (Print)).

30. Bukiya AN, Dopico AM. Common structural features of cholesterol binding sites in crystallized soluble proteins. 2017;58(6):1044-54. doi: 10.1194/jlr.R073452.

31. Bussi G, Donadio D Fau - Parrinello M, Parrinello M. Canonical sampling through velocity rescaling. (0021-9606 (Print)).

32. Byrne EFX, Sircar R, Miller PS, Hedger G, Luchetti G, Nachtergaele S, et al. Structural basis of Smoothened regulation by its extracellular domains. (1476-4687 (Electronic)).

33. Caffrey M. Crystallizing Membrane Proteins for Structure Determination: Use of Lipidic Mesophases. Annual Review of Biophysics. 2009;38(1):29-51. doi: 10.1146/annurev.biophys.050708.133655.

34. Caffrey M. A comprehensive review of the lipid cubic phase or in meso method for crystallizing membrane and soluble proteins and complexes. Acta Crystallographica Section F. 2015;71(1):3-18. doi: doi:10.1107/S2053230X14026843.

35. Caffrey M, Cherezov V. Crystallizing membrane proteins using lipidic mesophases. Nat Protoc. 2009;4(5):706-31. doi: 10.1038/nprot.2009.31. PubMed PMID: 19390528; PubMed Central PMCID: PMCPMC2732203.

36. Calder PC, Yaqoob P. Lipid Rafts—Composition, Characterization, and Controversies. The Journal of Nutrition. 2007;137(3):545-7. doi: 10.1093/jn/137.3.545.

37. Cang X, Du Y, Mao Y, Wang Y, Yang H, Jiang H. Mapping the Functional Binding Sites of Cholesterol in β2-Adrenergic Receptor by Long-Time Molecular Dynamics Simulations. The Journal of Physical Chemistry B. 2013;117(4):1085-94. doi: 10.1021/jp3118192.

38. Carini GA, Boutet S, Chollet M, Dragone A, Haller G, Hart PA, et al. Experience with the CSPAD during dedicated detector runs at LCLS. Journal of Physics: Conference Series. 2014;493:012011. doi: 10.1088/1742-6596/493/1/012011.

39. Chapman HN, Caleman C, Timneanu N. Diffraction before destruction. Philosophical Transactions of the Royal Society B: Biological Sciences. 2014;369(1647):20130313. doi: 10.1098/rstb.2013.0313.

40. Chapman HN, Fromme P, Barty A, White TA, Kirian RA, Aquila A, et al. Femtosecond X-ray protein nanocrystallography. Nature. 2011;470(7332):73-7. doi: 10.1038/nature09750.

41. Chattopadhyay A, Rao BD, Jafurulla M. Solubilization of G protein-coupled receptors: a convenient strategy to explore lipid-receptor interaction. (1557-7988 (Electronic)).

42. Chen Z, Rand RP. The influence of cholesterol on phospholipid membrane curvature and bending elasticity. (0006-3495 (Print)).

43. Chen Z, Rand RP. The influence of cholesterol on phospholipid membrane curvature and bending elasticity. Biophys J. 1997;73(1):267-76. doi: 10.1016/S0006-3495(97)78067-6. PubMed PMID: 9199791.

44. Cherezov V, Clogston J, Misquitta Y, Abdel-Gawad W, Caffrey M. Membrane Protein Crystallization In Meso: Lipid Type-Tailoring of the Cubic Phase. Biophys J. 2002;83(6):3393-407. doi: https://doi.org/10.1016/S0006-3495(02)75339-3.

45. Cherezov V, Liu J, Griffith M, Hanson MA, Stevens RC. LCP-FRAP Assay for Pre-Screening Membrane Proteins for in Meso Crystallization. Cryst Growth Des. 2008;8(12):4307-15. doi: 10.1021/cg800778j. PubMed PMID: 19234616.

46. Cherezov V, Rosenbaum DM, Hanson MA, Rasmussen SGF, Thian FS, Kobilka TS, et al. High-Resolution Crystal Structure of an Engineered Human β₂-Adrenergic G Protein–Coupled Receptor. Science. 2007;318(5854):1258. doi: 10.1126/science.1150577.

47. Chun E, Thompson Aaron A, Liu W, Roth Christopher B, Griffith Mark T, Katritch V, et al. Fusion Partner Toolchest for the Stabilization and Crystallization of G Protein-Coupled Receptors. Structure. 2012;20(6):967-76. doi: https://doi.org/10.1016/j.str.2012.04.010.

48. Coe J, Ros A. Small Is Beautiful: Growth and Detection of Nanocrystals. In: Boutet S, Fromme P, Hunter MS, editors. X-ray Free Electron Lasers: A Revolution in Structural Biology. Cham: Springer International Publishing; 2018. p. 59-85.

49. Coe JaR, A. Small Is Beautiful: Growth and Detection of Nanocrystals. In: Boutet S, Fromme, P., and Hunter, M.S., editor. X-ray Free Electron Lasers: A Revolution in Structural Biology: Springer Nature Switzerland AG; 2018. p. 59-86.

50. Colozo AT, Park PSH, Sum CS, Pisterzi LF, Wells JW. Cholesterol as a determinant of cooperativity in the M2 muscarinic cholinergic receptor. Biochemical Pharmacology. 2007;74(2):236-55. doi: https://doi.org/10.1016/j.bcp.2007.04.009.

51. Conrad CE, Basu S, James D, Wang D, Schaffer A, Roy-Chowdhury S, et al. A novel inert crystal delivery medium for serial femtosecond crystallography. IUCrJ. 2015;2(4):421-30. doi: doi:10.1107/S2052252515009811.

52. Cooper RA. Influence of increased membrane cholesterol on membrane fluidity and cell function in human red blood cells. Journal of supramolecular structure. 1978;8(4):413-30. doi: 10.1002/jss.400080404. PubMed PMID: 723275.

53. Danielli JF, Davson H. A contribution to the theory of permeability of thin films. Journal of Cellular and Comparative Physiology. 1935;5(4):495-508. doi: 10.1002/jcp.1030050409.

54. de Jong DH, Baoukina S, Ingólfsson HI, Marrink SJ. Martini straight: Boosting performance using a shorter cutoff and GPUs. Computer Physics Communications. 2016;199:1 - 7. doi: http://dx.doi.org/10.1016/j.cpc.2015.09.014.

55. de Jong DH, Singh G, Bennett WFD, Arnarez C, Wassenaar TA, Schäfer LV, et al. Improved Parameters for the Martini Coarse-Grained Protein Force Field. Journal of Chemical Theory and Computation. 2013;9(1):687-97. doi: 10.1021/ct300646g.

56. de Vries M, Herrmann A, Veit M. A cholesterol consensus motif is required for efficient intracellular transport and raft association of a group 2 HA from influenza virus. (1470-8728 (Electronic)).

57. Desai AJ, Harikumar KG, Miller LJ. A Type 1 Cholecystokinin Receptor Mutant That Mimics the Dysfunction Observed for Wild Type Receptor in a High Cholesterol Environment. 2014;289(26):18314-26. doi: 10.1074/jbc.M114.570200.

58. Desai AJ, Lam PCH, Orry A, Abagyan R, Christopoulos A, Sexton PM, et al. Molecular Mechanism of Action of Triazolobenzodiazepinone Agonists of the Type 1 Cholecystokinin Receptor. Possible Cooperativity across the Receptor Homodimeric Complex. Journal of Medicinal Chemistry. 2015;58(24):9562-77. doi: 10.1021/acs.jmedchem.5b01110.

59. Eastman P, Swails J, Chodera JD, McGibbon RT, Zhao Y, Beauchamp KA, et al. OpenMM 7: Rapid development of high performance algorithms for molecular dynamics. PLOS Computational Biology. 2017;13(7):e1005659. doi: 10.1371/journal.pcbi.1005659.

60. Echelmeier A, Sonker M, Ros A. Microfluidic sample delivery for serial crystallography using XFELs. Analytical and Bioanalytical Chemistry. 2019;411(25):6535-47. doi: 10.1007/s00216-019-01977-x.

61. Emma P, Akre R, Arthur J, Bionta R, Bostedt C, Bozek J, et al. First lasing and operation of an ångstrom-wavelength free-electron laser. Nature Photonics. 2010;4(9):641-7. doi: 10.1038/nphoton.2010.176.

62. Emsley P, Cowtan K. Coot: model-building tools for molecular graphics. Acta Crystallogr D Biol Crystallogr. 2004;60(Pt 12 Pt 1):2126-32. doi: 10.1107/S0907444904019158. PubMed PMID: 15572765.

63. Emsley P, Lohkamp B, Scott WG, Cowtan K. Features and development of Coot. Acta Crystallogr D Biol Crystallogr. 2010;66(Pt 4):486-501. doi: 10.1107/S0907444910007493. PubMed PMID: 20383002; PubMed Central PMCID: PMC2852313.

64. Epand RM. Cholesterol and the interaction of proteins with membrane domains. (0163-7827 (Print)).

65. Eramian D, Eswar N, Shen M-Y, Sali A. How well can the accuracy of comparative protein structure models be predicted? Protein Science. 2008;17(11):1881-93. doi: 10.1110/ps.036061.108.

66. Eroglu Ç, Brügger B, Wieland F, Sinning I. Glutamate-binding affinity of Drosophila metabotropic glutamate receptor is modulated by association with lipid rafts. Proceedings of the National Academy of Sciences. 2003;100(18):10219. doi: 10.1073/pnas.1737042100.

67. Fantini J, Barrantes F. How cholesterol interacts with membrane proteins: an exploration of cholesterol-binding sites including CRAC, CARC, and tilted domains. Frontiers in Physiology. 2013;4:31.

68. Fatakia SN, Sarkar P, Chattopadhyay A. A collage of cholesterol interaction motifs in the serotonin(1A) receptor: An evolutionary implication for differential cholesterol interaction. (1873-2941 (Electronic)).

69. Fenalti G, Giguere PM, Katritch V, Huang XP, Thompson AA, Cherezov V, et al. Molecular control of delta-opioid receptor signalling. Nature. 2014;506(7487):191-6. doi: 10.1038/nature12944. PubMed PMID: 24413399; PubMed Central PMCID: PMC3931418.

70. Fiser A, Do RKG, Šali A. Modeling of loops in protein structures. Protein Science. 2000;9(9):1753-73. doi: 10.1110/ps.9.9.1753.

71. Fourmy D, Escrieut C, Archer E, Galès C, Gigoux V, Maigret B, et al. Structure of Cholecystokinin Receptor Binding Sites and Mechanism of Activation/Inactivation by Agonists/Antagonists. Pharmacology & Toxicology. 2002;91(6):313-20. doi: 10.1034/j.1600-0773.2002.910608.x.

72. Fredriksson R, Lagerström MC, Lundin L-G, Schiöth HB. The G-Protein-Coupled Receptors in the Human Genome Form Five Main Families. Phylogenetic Analysis, Paralogon Groups, and Fingerprints. 2003;63(6):1256-72. doi: 10.1124/mol.63.6.1256 %J Molecular Pharmacology.

73. Fromme P. XFELs open a new era in structural chemical biology. Nature chemical biology. 2015;11(12):895-9. doi: 10.1038/nchembio.1968. PubMed PMID: 26575227; PubMed Central PMCID: PMC4839532.

74. Fromme R, Ishchenko A, Metz M, Chowdhury SR, Basu S, Boutet S, et al. Serial femtosecond crystallography of soluble proteins in lipidic cubic phase. IUCrJ. 2015;2(5):545-51. doi: doi:10.1107/S2052252515013160.

75. García-Nafría J, Lee Y, Bai X, Carpenter B, Tate CG. Cryo-EM structure of the adenosine A2A receptor coupled to an engineered heterotrimeric G protein. eLife. 2018;7:e35946. doi: 10.7554/eLife.35946.

76. García-Nafría J, Tate CG. Cryo-EM structures of GPCRs coupled to Gs, Gi and Go. Molecular and Cellular Endocrinology. 2019;488:1-13. doi: https://doi.org/10.1016/j.mce.2019.02.006.

77. Garman EF, Owen RL. Cryocooling and radiation damage in macromolecular crystallography. Acta Crystallographica Section D. 2006;62(1):32-47. doi: doi:10.1107/S0907444905034207.

78. Genheden S, Essex JW, Lee AG. G protein coupled receptor interactions with cholesterol deep in the membrane. Biochimica et Biophysica Acta (BBA) - Biomembranes. 2017;1859(2):268-81. doi: https://doi.org/10.1016/j.bbamem.2016.12.001.

79. Gimpl G. Interaction of G protein coupled receptors and cholesterol. Chemistry and Physics of Lipids. 2016;199:61-73. doi: https://doi.org/10.1016/j.chemphyslip.2016.04.006.

80. Gimpl G, Burger K, Fahrenholz F. Cholesterol as Modulator of Receptor Function. Biochemistry. 1997;36(36):10959-74. doi: 10.1021/bi963138w.

81. Gimpl G, Wiegand V, Burger K, Fahrenholz F. Chapter 4 Cholesterol and steroid hormones: modulators of oxytocin receptor function. Progress in Brain Research. 139: Elsevier; 2002. p. 43-55.

82. Goddard AD, Watts A. Regulation of G protein-coupled receptors by palmitoylation and cholesterol. BMC Biol. 2012;10:27-. doi: 10.1186/1741-7007-10-27. PubMed PMID: 22429402.

83. Goluszko P, Nowicki B. Membrane Cholesterol: a Crucial Molecule Affecting Interactions of Microbial Pathogens with Mammalian Cells. Infection and Immunity. 2005;73(12):7791. doi: 10.1128/IAI.73.12.7791-7796.2005.

84. González-Maeso J, Meana JJ. Heterotrimeric g proteins: insights into the neurobiology of mood disorders. Curr Neuropharmacol. 2006;4(2):127-38. doi: 10.2174/157015906776359586. PubMed PMID: 18615130.

85. Gorter E, Grendel F. ON BIMOLECULAR LAYERS OF LIPOIDS ON THE CHROMOCYTES OF THE BLOOD. Journal of Experimental Medicine. 1925;41(4):439-43. doi: 10.1084/jem.41.4.439.

86. Guixà-González R, Albasanz JL, Rodriguez-Espigares I, Pastor M, Sanz F, Martí-Solano M, et al. Membrane cholesterol access into a G-protein-coupled receptor. Nature Communications. 2017;8(1):14505. doi: 10.1038/ncomms14505.

87. Guixà-González R, Albasanz JL, Rodriguez-Espigares IA-O, Pastor M, Sanz F, Martí-Solano M, et al. Membrane cholesterol access into a G-protein-coupled receptor. (2041-1723 (Electronic)).

88. Gurevich VV, Gurevich EV. GPCR Signaling Regulation: The Role of GRKs and Arrestins. Frontiers in Pharmacology. 2019;10:125.

89. Hanson MA, Cherezov V, Griffith MT, Roth CB, Jaakola V-P, Chien EYT, et al. A specific cholesterol binding site is established by the 2.8 A structure of the human beta2-adrenergic receptor. Structure (London, England : 1993). 2008;16(6):897-905. doi: 10.1016/j.str.2008.05.001. PubMed PMID: 18547522.

90. Hauptman HA. History of X-ray crystallography. Chemometrics and Intelligent Laboratory Systems. 1991;10(1):13-8. doi: https://doi.org/10.1016/0169-7439(91)80029-P.

91. Hauser AS, Attwood MM, Rask-Andersen M, Schiöth HB, Gloriam DE. Trends in GPCR drug discovery: new agents, targets and indications. Nature Reviews Drug Discovery. 2017;16(12):829-42. doi: 10.1038/nrd.2017.178.

92. Hauser AS, Chavali S, Masuho I, Jahn LJ, Martemyanov KA, Gloriam DE, et al. Pharmacogenomics of GPCR Drug Targets. Cell. 2018;172(1-2):41-54.e19. Epub 2017/12/14. doi: 10.1016/j.cell.2017.11.033. PubMed PMID: 29249361.

93. Hedger G, Sansom MSP. Lipid interaction sites on channels, transporters and receptors: Recent insights from molecular dynamics simulations. Biochimica et Biophysica Acta (BBA) - Biomembranes. 2016;1858(10):2390 - 400. doi: 10.1016/j.bbamem.2016.02.037.

94. Hess B. P-LINCS: A Parallel Linear Constraint Solver for Molecular Simulation. Journal of Chemical Theory and Computation. 2008;4(1):116-22. doi: 10.1021/ct700200b.

95. Heydenreich FM, Vuckovic Z, Matkovic M, Veprintsev DB. Stabilization of G protein-coupled receptors by point mutations. Frontiers in Pharmacology. 2015;6:82.

96. Hsu P-C, Bruininks BMH, Jefferies D, Cesar Telles de Souza P, Lee J, Patel DS, et al. CHARMM-GUI Martini Maker for modeling and simulation of complex bacterial membranes with lipopolysaccharides. J Comput Chem. 2017;38(27):2354-63. doi: 10.1002/jcc.24895.

97. Hua T, Vemuri K, Nikas SP, Laprairie RB, Wu Y, Qu L, et al. Crystal structures of agonist-bound human cannabinoid receptor CB1. Nature. 2017;547(7664):468-71. doi: 10.1038/nature23272.

98. Huang P, Xu W, Yoon S-I, Chen C, Chong PL-G, Liu-Chen L-Y. Cholesterol reduction by methyl-β-cyclodextrin attenuates the delta opioid receptor-mediated signaling in neuronal cells but enhances it in non-neuronal cells. Biochemical Pharmacology. 2007;73(4):534-49. doi: https://doi.org/10.1016/j.bcp.2006.10.032.

99. Humphrey W, Dalke A, Schulten K. VMD: Visual molecular dynamics. Journal of Molecular Graphics. 1996;14(1):33-8. doi: https://doi.org/10.1016/0263-7855(96)00018-5.

100. Hunter JD. Matplotlib: A 2D Graphics Environment. Computing in Science Engineering. 2007;9(3):90-5. doi: 10.1109/MCSE.2007.55.

101. Hunter MS, Yoon CH, DeMirci H, Sierra RG, Dao EH, Ahmadi R, et al. Selenium single-wavelength anomalous diffraction de novo phasing using an X-ray-free electron laser. Nat Commun. 2016;7:13388. doi: 10.1038/ncomms13388. PubMed PMID: 27811937; PubMed Central PMCID: PMCPMC5097167.

102. Ingólfsson HI, Lopez CA, Uusitalo JJ, de Jong DH, Gopal SM, Periole X, et al. The power of coarse graining in biomolecular simulations. WIREs Computational Molecular Science. 2014;4(3):225-48. doi: 10.1002/wcms.1169.

103. Insel PA, Sriram K, Gorr MW, Wiley SZ, Michkov A, Salmerón C, et al. GPCRomics: An Approach to Discover GPCR Drug Targets. Trends in Pharmacological Sciences. 2019;40(6):378-87. doi: 10.1016/j.tips.2019.04.001.

104. Ishchenko A, Cherezov V, Liu W. Preparation and Delivery of Protein Microcrystals in Lipidic Cubic Phase for Serial Femtosecond Crystallography. LID - 10.3791/54463 [doi] LID - 54463. (1940-087X (Electronic)).

105. Istvan ES, Deisenhofer J. Structural mechanism for statin inhibition of HMG-CoA reductase. (0036-8075 (Print)).

106. Jafurulla M, Aditya Kumar G, Rao BD, Chattopadhyay A. A Critical Analysis of Molecular Mechanisms Underlying Membrane Cholesterol Sensitivity of GPCRs. In: Rosenhouse-Dantsker A, Bukiya AN, editors. Cholesterol Modulation of Protein Function: Sterol Specificity and Indirect Mechanisms. Cham: Springer International Publishing; 2019. p. 21-52.

107. Jafurulla M, Tiwari S, Chattopadhyay A. Identification of cholesterol recognition amino acid consensus (CRAC) motif in G-protein coupled receptors. Biochemical and

Biophysical Research Communications. 2011;404(1):569-73. doi: https://doi.org/10.1016/j.bbrc.2010.12.031.

108. Jo S, Kim T, Iyer VG, Im W. CHARMM-GUI: A web-based graphical user interface for CHARMM. Journal of Computational Chemistry. 2008;29(11):1859-65. doi: 10.1002/jcc.20945.

109. Johansson LC, Wöhri AB, Katona G, Engström S, Neutze R. Membrane protein crystallization from lipidic phases. Curr Opin Struct Biol. 2009;19(4):372-8. doi: https://doi.org/10.1016/j.sbi.2009.05.006.

110. Joosten RP, Long F, Murshudov GN, Perrakis A. The PDB_REDO server for macromolecular structure model optimization. IUCrJ. 2014;1(Pt 4):213-20. doi: 10.1107/S2052252514009324. PubMed PMID: 25075342; PubMed Central PMCID: PMCPMC4107921.

111. Katritch V, Fenalti G, Abola EE, Roth BL, Cherezov V, Stevens RC. Allosteric sodium in class A GPCR signaling. Trends Biochem Sci. 2014;39(5):233-44. doi: 10.1016/j.tibs.2014.03.002. PubMed PMID: 24767681; PubMed Central PMCID: PMCPMC4106411.

112. Kendrew JC, Bodo G, Dintzis HM, Parrish RG, Wyckoff H, Phillips DC. A Three-Dimensional Model of the Myoglobin Molecule Obtained by X-Ray Analysis. Nature. 1958;181(4610):662-6. doi: 10.1038/181662a0.

113. Khelashvili G, Grossfield A, Feller SE, Pitman MC, Weinstein H. Structural and dynamic effects of cholesterol at preferred sites of interaction with rhodopsin identified from microsecond length molecular dynamics simulations. Proteins. 2009;76(2):403-17. doi: 10.1002/prot.22355. PubMed PMID: 19173312.

114. Kirilovsky J, Schramm M. Delipidation of a beta-adrenergic receptor preparation and reconstitution by specific lipids. Journal of Biological Chemistry. 1983;258(11):6841-9.

115. Kolf-Clauw M, Chevy F Fau - Wolf C, Wolf C Fau - Siliart B, Siliart B Fau - Citadelle D, Citadelle D Fau - Roux C, Roux C. Inhibition of 7-dehydrocholesterol reductase by the teratogen AY9944: a rat model for Smith-Lemli-Opitz syndrome. (0040-3709 (Print)).

116. Lagane B, Gaibelet G, Meilhoc E, Masson J-M, Cézanne L, Lopez A. Role of Sterols in Modulating the Human μ-Opioid Receptor Function in Saccharomyces cerevisiae. Journal of Biological Chemistry. 2000;275(43):33197-200.

117. Lee AG. Interfacial Binding Sites for Cholesterol on G Protein-Coupled Receptors. Biophys J. 2019;116(9):1586-97. doi: https://doi.org/10.1016/j.bpj.2019.03.025.

118. Lee J, Cheng X, Swails JM, Yeom MS, Eastman PK, Lemkul JA, et al. CHARMM-GUI Input Generator for NAMD, GROMACS, AMBER, OpenMM, and CHARMM/OpenMM Simulations Using the CHARMM36 Additive Force Field. Journal of Chemical Theory and Computation. 2016;12(1):405-13. doi: 10.1021/acs.jctc.5b00935.

119. Lee JY, Lyman E. Predictions for Cholesterol Interaction Sites on the A\textsubscript2A Adenosine Receptor. Journal of the American Chemical Society. 2012;134(40):16512--5. doi: 10.1021/ja307532d.

120. Leonarski F, Redford S, Mozzanica A, Lopez-Cuenca C, Panepucci E, Nass K, et al. Fast and accurate data collection for macromolecular crystallography using the JUNGFRAU detector. Nature Methods. 2018;15(10):799-804. doi: 10.1038/s41592-018-0143-7.

121. Levitt ES, Clark Mj Fau - Jenkins PM, Jenkins Pm Fau - Martens JR, Martens Jr Fau - Traynor JR, Traynor JR. Differential effect of membrane cholesterol removal on mu- and delta-opioid receptors: a parallel comparison of acute and chronic signaling to adenylyl cyclase. (0021-9258 (Print)).

122. Li H, Papadopoulos V. Peripheral-type benzodiazepine receptor function in cholesterol transport. Identification of a putative cholesterol recognition/interaction amino acid sequence and consensus pattern. (0013-7227 (Print)).

123. Li Y, Owyang C. Endogenous cholecystokinin stimulates pancreatic enzyme secretion via vagal afferent pathway in rats. Gastroenterology. 1994;107(2):525-31. doi: https://doi.org/10.1016/0016-5085(94)90180-5.

124. Liang M, Williams GJ, Messerschmidt M, Seibert MM, Montanez PA, Hayes M, et al. The Coherent X-ray Imaging instrument at the Linac Coherent Light Source. J Synchrotron Radiat. 2015;22(3):514-9. doi: 10.1107/S160057751500449X. PubMed PMID: 25931062; PubMed Central PMCID: PMCPMC4416669.

125. Liu W, Cherezov V. Crystallization of Membrane Proteins in Lipidic Mesophases. JoVE. 2011;(49):e2501. doi: doi:10.3791/2501.

126. Liu W, Chun E, Thompson AA, Chubukov P, Xu F, Katritch V, et al. Structural basis for allosteric regulation of GPCRs by sodium ions. Science. 2012;337(6091):232-6. doi: 10.1126/science.1219218. PubMed PMID: 22798613; PubMed Central PMCID: PMC3399762.

127. Liu W, Hanson MA, Stevens RC, Cherezov V. LCP-Tm: an assay to measure and understand stability of membrane proteins in a membrane environment. Biophys J. 2010;98(8):1539-48. doi: 10.1016/j.bpj.2009.12.4296. PubMed PMID: 20409473.

128. Liu W, Ishchenko A, Cherezov V. Preparation of microcrystals in lipidic cubic phase for serial femtosecond crystallography. Nature Protocols. 2014;9(9):2123-34. doi: 10.1038/nprot.2014.141.

129. Liu W, Wacker D, Gati C, Han GW, James D, Wang D, et al. Serial Femtosecond Crystallography of G Protein–Coupled Receptors. Science. 2013;342(6165):1521. doi: 10.1126/science.1244142.

130. Luchetti G, Sircar R, Kong JH, Nachtergaele S, Sagner A, Byrne EF, et al. Cholesterol activates the G-protein coupled receptor Smoothened to promote Hedgehog signaling. eLife. 2016;5:e20304. doi: 10.7554/eLife.20304. PubMed PMID: 27705744.

131. Luchetti G, Sircar R, Kong JH, Nachtergaele S, Sagner A, Byrne EFX, et al. Cholesterol activates the G-protein coupled receptor Smoothened to promote Hedgehog signaling. eLife. 2016;5:e20304. doi: 10.7554/eLife.20304.

132. Macchi P. Cryo-Crystallography: Diffraction at Low Temperature and More. In: Rissanen K, editor. Advanced X-Ray Crystallography. Berlin, Heidelberg: Springer Berlin Heidelberg; 2012. p. 33-67.

133. Mahoney JP, Sunahara RK. Mechanistic insights into GPCR-G protein interactions. Curr Opin Struct Biol. 2016;41:247-54. Epub 2016/11/18. doi: 10.1016/j.sbi.2016.11.005. PubMed PMID: 27871057.

134. Manglik A, Kobilka BK, Steyaert J. Nanobodies to Study G Protein-Coupled Receptor Structure and Function. Annu Rev Pharmacol Toxicol. 2017;57:19-37. Epub 2016/12/07. doi: 10.1146/annurev-pharmtox-010716-104710. PubMed PMID: 27959623.

135. Marrink SJ, Risselada HJ, Yefimov S, Tieleman DP, de Vries AH. The MARTINI Force Field: Coarse Grained Model for Biomolecular Simulations. The Journal of Physical Chemistry B. 2007;111(27):7812-24. doi: 10.1021/jp071097f.

136. Marrink SJ, Risselada Hj Fau - Yefimov S, Yefimov S Fau - Tieleman DP, Tieleman Dp Fau - de Vries AH, de Vries AH. The MARTINI force field: coarse grained model for biomolecular simulations. (1520-6106 (Print)).

137. Marrink SJ, Tieleman DP. Perspective on the Martini model. (1460-4744 (Electronic)).

138. Martin-Garcia JM, Conrad CE, Coe J, Roy-Chowdhury S, Fromme P. Serial femtosecond crystallography: A revolution in structural biology. Archives of

biochemistry and biophysics. 2016;602:32-47. doi: 10.1016/j.abb.2016.03.036. PubMed PMID: 27143509; PubMed Central PMCID: PMC4909539.

139. Martin-Garcia JM, Conrad CE, Nelson G, Stander N, Zatsepin NA, Zook J, et al. Serial millisecond crystallography of membrane and soluble protein microcrystals using synchrotron radiation. IUCrJ. 2017;4(Pt 4):439-54. doi: 10.1107/S205225251700570X. PubMed PMID: 28875031; PubMed Central PMCID: PMC5571807.

140. McCammon JA, Gelin BR, Karplus M. Dynamics of folded proteins. Nature. 1977;267(5612):585-90. doi: 10.1038/267585a0.

141. McGraw C, Yang L, Levental I, Lyman E, Robinson AS. Membrane cholesterol depletion reduces downstream signaling activity of the adenosine A\textsubscript2A receptor. Biochimica et Biophysica Acta (BBA) - Biomembranes. 2019;1861(4):760 - 7. doi: 10.1016/j.bbamem.2019.01.001.

142. Meyer BH, Segura J-M, Martinez KL, Hovius R, George N, Johnsson K, et al. FRET imaging reveals that functional neurokinin-1 receptors are monomeric and reside in membrane microdomains of live cells. Proceedings of the National Academy of Sciences. 2006;103(7):2138. doi: 10.1073/pnas.0507686103.

143. Miller LJ, Desai AJ. Metabolic Actions of the Type 1 Cholecystokinin Receptor: Its Potential as a Therapeutic Target. Trends in Endocrinology & Metabolism. 2016;27(9):609-19. doi: 10.1016/j.tem.2016.04.002.

144. Miller LJ, Holicky EL, Ulrich CD, Wieben ED. Abnormal processing of the human cholecystokinin receptor gene in association with gallstones and obesity. Gastroenterology. 1995;109(4):1375-80. doi: 10.1016/0016-5085(95)90601-0.

145. Mirzadegan T, Benkö G, Filipek S, Palczewski K. Sequence Analyses of G-Protein-Coupled Receptors: Similarities to Rhodopsin. Biochemistry. 2003;42(10):2759-67. doi: 10.1021/bi027224+.

146. Mitchell DC, Straume M, Miller JL, Litman BJ. Modulation of metarhodopsin formation by cholesterol-induced ordering of bilayer lipids. Biochemistry. 1990;29(39):9143-9. doi: 10.1021/bi00491a007.

147. Mitchell DC, Straume M Fau - Miller JL, Miller Jl Fau - Litman BJ, Litman BJ. Modulation of metarhodopsin formation by cholesterol-induced ordering of bilayer lipids. (0006-2960 (Print)).

148. Mitchell E, Kuhn P, Garman E. Demystifying the synchrotron trip: a first time user's guide. Structure. 1999;7(5):R111-R21. doi: 10.1016/S0969-2126(99)80063-X.

149. Mizuno GR, Chapman CJ, Chipault JR, Pfeiffer DR. Lipid composition and (Na+ + K+)-ATPase activity in rat lens during triparanol-induced cataract formation. Biochimica et Biophysica Acta (BBA) - Biomembranes. 1981;644(1):1-12. doi: https://doi.org/10.1016/0005-2736(81)90052-3.

150. Monastyrskaya K, Hostettler A, Buergi S, Draeger A. The NK1 Receptor Localizes to the Plasma Membrane Microdomains, and Its Activation Is Dependent on Lipid Raft Integrity. Journal of Biological Chemistry. 2005;280(8):7135-46.

151. Monticelli L, Kandasamy SK, Periole X, Larson RG, Tieleman DP, Marrink S-J. The MARTINI Coarse-Grained Force Field: Extension to Proteins. Journal of Chemical Theory and Computation. 2008;4(5):819-34. doi: 10.1021/ct700324x.

152. Monticelli L, Kandasamy SK, Periole X, Larson RG, Tieleman DP, Marrink SJ. The MARTINI Coarse-Grained Force Field: Extension to Proteins. (1549-9618 (Print)).

153. Neale C, Herce HD, Pomès R, García AE. Can Specific Protein-Lipid Interactions Stabilize an Active State of the Beta 2 Adrenergic Receptor? Biophys J. 2015;109(8):1652 - 62. doi: 10.1016/j.bpj.2015.08.028.

154. Neutze R, Hajdu J. Femtosecond time resolution in x-ray diffraction experiments. Proceedings of the National Academy of Sciences of the United States of America. 1997;94(11):5651-5. doi: 10.1073/pnas.94.11.5651. PubMed PMID: 9159127; PubMed Central PMCID: PMC20833.

155. Nezil FA, Bloom M. Combined influence of cholesterol and synthetic amphiphillic peptides upon bilayer thickness in model membranes. (0006-3495 (Print)).

156. Nguyen DH, Taub D. CXCR4 Function Requires Membrane Cholesterol: Implications for HIV Infection. The Journal of Immunology. 2002;168(8):4121. doi: 10.4049/jimmunol.168.8.4121.

157. Nguyen DH, Taub D. Cholesterol is essential for macrophage inflammatory protein 1β binding and conformational integrity of CC chemokine receptor 5. Blood. 2002;99(12):4298-306. doi: 10.1182/blood-2001-11-0087.

158. Nguyen DH, Taub DD. Inhibition of chemokine receptor function by membrane cholesterol oxidation. Experimental Cell Research. 2003;291(1):36-45. doi: https://doi.org/10.1016/S0014-4827(03)00345-8.

159. Nicolson GL. The Fluid—Mosaic Model of Membrane Structure: Still relevant to understanding the structure, function and dynamics of biological membranes after more than 40years. Biochimica et Biophysica Acta (BBA) - Biomembranes. 2014;1838(6):1451-66. doi: https://doi.org/10.1016/j.bbamem.2013.10.019.

160. Niu SL, Mitchell Dc Fau - Litman BJ, Litman BJ. Manipulation of cholesterol levels in rod disk membranes by methyl-beta-cyclodextrin: effects on receptor activation. (0021-9258 (Print)).

161. O'Malley MA, Helgeson ME, Wagner NJ, Robinson AS. The Morphology and Composition of Cholesterol-Rich Micellar Nanostructures Determine Transmembrane Protein (GPCR) Activity. Biophys J. 2011;100(2):L11-L3. doi: 10.1016/j.bpj.2010.12.3698.

162. Oates J, Faust B, Attrill H, Harding P, Orwick M, Watts A. The role of cholesterol on the activity and stability of neurotensin receptor 1. Biochimica et Biophysica Acta (BBA) - Biomembranes. 2012;1818(9):2228-33. doi: https://doi.org/10.1016/j.bbamem.2012.04.010.

163. Oddi S, Dainese E, Fezza F, Lanuti M, Barcaroli D, De Laurenzi V, et al. Functional characterization of putative cholesterol binding sequence (CRAC) in human type-1 cannabinoid receptor. Journal of Neurochemistry. 2011;116(5):858-65. doi: 10.1111/j.1471-4159.2010.07041.x.

164. Okashah N, Wan Q, Ghosh S, Sandhu M, Inoue A, Vaidehi N, et al. Variable G protein determinants of GPCR coupling selectivity. Proceedings of the National Academy of Sciences. 2019;116(24):12054. doi: 10.1073/pnas.1905993116.

165. Oldham WM, Hamm HE. Heterotrimeric G protein activation by G-protein-coupled receptors. Nature Reviews Molecular Cell Biology. 2008;9(1):60-71. doi: 10.1038/nrm2299.

166. Paila YD, Chattopadhyay A. The function of G-protein coupled receptors and membrane cholesterol: specific or general interaction? Glycoconjugate Journal. 2008;26(6):711. doi: 10.1007/s10719-008-9218-5.

167. Paila YD, Jindal E, Goswami SK, Chattopadhyay A. Cholesterol depletion enhances adrenergic signaling in cardiac myocytes. Biochimica et Biophysica Acta (BBA) - Biomembranes. 2011;1808(1):461-5. doi: https://doi.org/10.1016/j.bbamem.2010.09.006.

168. Paila YD, Pucadyil Tj Fau - Chattopadhyay A, Chattopadhyay A. The cholesterol-complexing agent digitonin modulates ligand binding of the bovine hippocampal serotonin 1A receptor. (0968-7688 (Print)).

169. Pal S, Chakraborty H, Bandari S, Yahioglu G, Suhling K, Chattopadhyay A. Molecular rheology of neuronal membranes explored using a molecular rotor: Implications for receptor function. Chemistry and physics of lipids. 2016;196:69-75. doi: 10.1016/j.chemphyslip.2016.02.004. PubMed PMID: 26879380.

170. Palczewski K, Kumasaka T, Hori T, Behnke CA, Motoshima H, Fox BA, et al. Crystal Structure of Rhodopsin: A G Protein-Coupled Receptor. Science. 2000;289(5480):739. doi: 10.1126/science.289.5480.739.

171. Palmer M. Cholesterol and the activity of bacterial toxins. (0378-1097 (Print)).

172. Pándy-Szekeres G, Munk C, Tsonkov TM, Mordalski S, Harpsøe K, Hauser AS, et al. GPCRdb in 2018: adding GPCR structure models and ligands. Nucleic Acids Research. 2017;46(D1):D440-D6. doi: 10.1093/nar/gkx1109.

173. Pang L, Graziano M, Wang S. Membrane Cholesterol Modulates Galanin−GalR2 Interaction. Biochemistry. 1999;38(37):12003-11. doi: 10.1021/bi990227a.

174. Parrinello M, Rahman A. Polymorphic transitions in single crystals: A new molecular dynamics method. Journal of Applied Physics. 1981;52(12):7182-90. doi: 10.1063/1.328693.

175. Periole X, Cavalli M, Marrink S-J, Ceruso MA. Combining an Elastic Network With a Coarse-Grained Molecular Force Field: Structure, Dynamics, and Intermolecular Recognition. Journal of Chemical Theory and Computation. 2009;5(9):2531-43. doi: 10.1021/ct9002114.

176. Pettersen EF, Goddard TD, Huang CC, Couch GS, Greenblatt DM, Meng EC, et al. UCSF Chimera—A visualization system for exploratory research and analysis. Journal of Computational Chemistry. 2004;25(13):1605-12. doi: 10.1002/jcc.20084.

177. Phillips JC, Braun R, Wang W, Gumbart J, Tajkhorshid E, Villa E, et al. Scalable molecular dynamics with NAMD. Journal of Computational Chemistry. 2005;26(16):1781-802. doi: 10.1002/jcc.20289.

178. Pike LJ. Rafts defined: a report on the Keystone symposium on lipid rafts and cell function. Journal of Lipid Research. 2006;47(7):1597-8.

179. Potter RM, Harikumar KG, Wu SV, Miller LJ. Differential sensitivity of types 1 and 2 cholecystokinin receptors to membrane cholesterol. 2012;53(1):137-48. doi: 10.1194/jlr.M020065.

180. Prasanna X, Chattopadhyay A, Sengupta D. Cholesterol modulates the dimer interface of the β_2-adrenergic receptor via cholesterol occupancy sites. (1542-0086 (Electronic)).

181. Prasanna X, Chattopadhyay A, Sengupta D. Cholesterol modulates the dimer interface of the β_2-adrenergic receptor via cholesterol occupancy sites. Biophys J. 2014;106(6):1290-300. doi: 10.1016/j.bpj.2014.02.002. PubMed PMID: 24655504.

182. Pucadyil TJ, Chattopadhyay A. Cholesterol modulates ligand binding and G-protein coupling to serotonin1A receptors from bovine hippocampus. Biochimica et Biophysica Acta (BBA) - Biomembranes. 2004;1663(1):188-200. doi: https://doi.org/10.1016/j.bbamem.2004.03.010.

183. Pucadyil TJ, Chattopadhyay A. Cholesterol modulates the antagonist-binding function of hippocampal serotonin1A receptors. Biochimica et Biophysica Acta (BBA) - Biomembranes. 2005;1714(1):35-42. doi: https://doi.org/10.1016/j.bbamem.2005.06.005.

184. Pydi SP, Jafurulla M, Wai L, Bhullar RP, Chelikani P, Chattopadhyay A. Cholesterol modulates bitter taste receptor function. (0006-3002 (Print)).

185. Pydi SP, Jafurulla M, Wai L, Bhullar RP, Chelikani P, Chattopadhyay A. Cholesterol modulates bitter taste receptor function. Biochimica et Biophysica Acta (BBA) - Biomembranes. 2016;1858(9):2081-7. doi: https://doi.org/10.1016/j.bbamem.2016.06.005.

186. Qi Y, Ingólfsson HI, Cheng X, Lee J, Marrink SJ, Im W. CHARMM-GUI Martini Maker for Coarse-Grained Simulations with the Martini Force Field. Journal of Chemical Theory and Computation. 2015;11(9):4486-94. doi: 10.1021/acs.jctc.5b00513.

187. R. J. Gowers ML, J. Barnoud, T. J. E. Reddy, M. N. Melo, S. L. Seyler, D. L. Dotson, J. Domanski, S. Buchoux, I. M. Kenney, and O. Beckstein. . MDAnalysis: A Python package for the rapid analysis of molecular dynamics simulations. . Proceedings of the 15th Python in Science Conference,. 2016:98/105. doi: 10.25080/majora-629e541a-00e.

188. Raffy S, Teissié J. Control of lipid membrane stability by cholesterol content. Biophys J. 1999;76(4):2072-80. doi: 10.1016/S0006-3495(99)77363-7. PubMed PMID: 10096902.

189. Ragnarsson L, Andersson Å, Thomas WG, Lewis RJ. Mutations in the NPxxY motif stabilize pharmacologically distinct conformational states of the α_{1B}- and β₂-adrenoceptors. Science Signaling. 2019;12(572):eaas9485. doi: 10.1126/scisignal.aas9485.

190. Ribas C, Penela P, Murga C, Salcedo A, García-Hoz C, Jurado-Pueyo M, et al. The G protein-coupled receptor kinase (GRK) interactome: Role of GRKs in GPCR regulation and signaling. Biochimica et Biophysica Acta (BBA) - Biomembranes. 2007;1768(4):913-22. doi: https://doi.org/10.1016/j.bbamem.2006.09.019.

191. Robertson JD. The ultrastructure of cell membranes and their derivatives. Biochem Soc Symp. 1959;16:3-43. PubMed PMID: 13651159.

192. Rosenbaum DM, Cherezov V, Hanson MA, Rasmussen SGF, Thian FS, Kobilka

TS, et al. GPCR Engineering Yields High-Resolution Structural Insights into β₂-Adrenergic Receptor Function. Science. 2007;318(5854):1266. doi: 10.1126/science.1150609.

193. Rossmann MG, Blow DM. The detection of sub-units within the crystallographic asymmetric unit. Acta Crystallographica. 1962;15(1):24-31. doi: doi:10.1107/S0365110X62000067.

194. Roth CB, Hanson MA, Stevens RC. Stabilization of the Human β2-Adrenergic Receptor TM4–TM3–TM5 Helix Interface by Mutagenesis of Glu1223.41, A Critical Residue in GPCR Structure. Journal of Molecular Biology. 2008;376(5):1305-19. doi: https://doi.org/10.1016/j.jmb.2007.12.028.

195. Rouviere E, Arnarez C, Yang L, Lyman E. Identification of Two New Cholesterol Interaction Sites on the A\textsubscript2A Adenosine Receptor. Biophys J. 2017;113(11):2415 - 24. doi: 10.1016/j.bpj.2017.09.027.

196. Rucktooa P, Cheng RKY, Segala E, Geng T, Errey JC, Brown GA, et al. Towards high throughput GPCR crystallography: In Meso soaking of Adenosine A2A Receptor crystals. Sci Rep. 2018;8(1):41. doi: 10.1038/s41598-017-18570-w. PubMed PMID: 29311713; PubMed Central PMCID: PMCPMC5758569.

197. Sali A, Blundell TL. Comparative protein modelling by satisfaction of spatial restraints. (0022-2836 (Print)).

198. Šali A, Blundell TL. Comparative Protein Modelling by Satisfaction of Spatial Restraints. Journal of Molecular Biology. 1993;234(3):779-815. doi: https://doi.org/10.1006/jmbi.1993.1626.

199. Sampson NS, Vrielink A. Cholesterol oxidases: a study of nature's approach to protein design. (0001-4842 (Print)).

200. Sarkar P, Chattopadhyay A. Cholesterol interaction motifs in G protein-coupled receptors: Slippery hot spots? WIREs Systems Biology and Medicine. 2020;12(4):e1481. doi: 10.1002/wsbm.1481.

201. Schlichting I. Serial femtosecond crystallography: the first five years. IUCrJ. 2015;2(2):246-55. doi: doi:10.1107/S205225251402702X.

202. Segala E, Guo D, Cheng RK, Bortolato A, Deflorian F, Dore AS, et al. Controlling the Dissociation of Ligands from the Adenosine A2A Receptor through Modulation of Salt Bridge Strength. J Med Chem. 2016;59(13):6470-9. doi: 10.1021/acs.jmedchem.6b00653. PubMed PMID: 27312113.

203. Sengupta D, Chattopadhyay A. Identification of Cholesterol Binding Sites in the Serotonin1A Receptor. The Journal of Physical Chemistry B. 2012;116(43):12991-6. doi: 10.1021/jp309888u.

204. Sengupta D, Chattopadhyay A. Identification of Cholesterol Binding Sites in the Serotonin\textsubscript1A Receptor. The Journal of Physical Chemistry B. 2012;116(43):12991--6. doi: 10.1021/jp309888u.

205. Sengupta D, Chattopadhyay A. Molecular dynamics simulations of GPCR–cholesterol interaction: An emerging paradigm. Biochimica et Biophysica Acta (BBA) - Biomembranes. 2015;1848(9):1775 - 82. doi: 10.1016/j.bbamem.2015.03.018.

206. Sensi C, Daniele S, Parravicini C, Zappelli E, Russo V, Trincavelli ML, et al. Oxysterols act as promiscuous ligands of class-A GPCRs: in silico molecular modeling and in vitro validation. (1873-3913 (Electronic)).

207. Sezgin E, Levental I, Mayor S, Eggeling C. The mystery of membrane organization: composition, regulation and roles of lipid rafts. Nature Reviews Molecular Cell Biology. 2017;18(6):361-74. doi: 10.1038/nrm.2017.16.

208. Shih AY, Arkhipov A, Freddolino PL, Schulten K. Coarse Grained Protein−Lipid Model with Application to Lipoprotein Particles. The Journal of Physical Chemistry B. 2006;110(8):3674-84. doi: 10.1021/jp0550816.

209. Sierra RG, Batyuk A, Sun Z, Aquila A, Hunter MS, Lane TJ, et al. The Macromolecular Femtosecond Crystallography Instrument at the Linac Coherent Light Source. J Synchrotron Radiat. 2019;26(Pt 2):346-57. doi: 10.1107/S1600577519001577. PubMed PMID: 30855242; PubMed Central PMCID: PMCPMC6412173.

210. Simon MI, Strathmann MP, Gautam N. Diversity of G proteins in signal transduction. Science. 1991;252(5007):802. doi: 10.1126/science.1902986.

211. Simons K, Ehehalt R. Cholesterol, lipid rafts, and disease. (0021-9738 (Print)).

212. Singer SJ, Nicolson GL. The Fluid Mosaic Model of the Structure of Cell Membranes. Science. 1972;175(4023):720. doi: 10.1126/science.175.4023.720.

213. Sjögren B, Hamblin MW, Svenningsson P. Cholesterol depletion reduces serotonin binding and signaling via human 5-HT7(a) receptors. European Journal of Pharmacology. 2006;552(1):1-10. doi: https://doi.org/10.1016/j.ejphar.2006.08.069.

214. Sliz P, Harrison SC, Rosenbaum G. How does Radiation Damage in Protein Crystals Depend on X-Ray Dose? Structure. 2003;11(1):13-9. doi: https://doi.org/10.1016/S0969-2126(02)00910-3.

215. Smith GP, Gibbs J. The Satiety Effect of Cholecystokinin Recent Progress and Current Problemsa. Annals of the New York Academy of Sciences. 1985;448(1):417-23. doi: 10.1111/j.1749-6632.1985.tb29936.x.

216. Smith JS, Rajagopal S. The β-Arrestins: Multifunctional Regulators of G Protein-coupled Receptors. Journal of Biological Chemistry. 2016;291(17):8969-77.

217. Smyth MS, Martin JH. x ray crystallography. Mol Pathol. 2000;53(1):8-14. doi: 10.1136/mp.53.1.8. PubMed PMID: 10884915.

218. Soubias O, Gawrisch K. The role of the lipid matrix for structure and function of the GPCR rhodopsin. Biochim Biophys Acta. 2012;1818(2):234-40. Epub 2011/09/05. doi: 10.1016/j.bbamem.2011.08.034. PubMed PMID: 21924236.

219. Stan CA, Milathianaki D, Laksmono H, Sierra RG, McQueen Trevor A, Messerschmidt M, et al. Liquid explosions induced by X-ray laser pulses. Nature Physics. 2016;12(10):966-71. Epub 23 May 2016. doi: 10.1038/nphys3779.

220. Stansfeld PJ, Sansom MSP. Molecular simulation approaches to membrane proteins. Structure. 2011;19(11):1562-72. doi: 10.1016/j.str.2011.10.002.

221. Stauch B, Cherezov V. Serial Femtosecond Crystallography of G Protein-Coupled Receptors. Annual review of biophysics. 2018;47:377-97. Epub 2018/03/15. doi: 10.1146/annurev-biophys-070317-033239. PubMed PMID: 29543504.

222. Suno R, Kimura KT, Nakane T, Yamashita K, Wang J, Fujiwara T, et al. Crystal Structures of Human Orexin 2 Receptor Bound to the Subtype-Selective Antagonist EMPA. Structure. 2018;26(1):7-19.e5. doi: 10.1016/j.str.2017.11.005.

223. Taylor GL. Introduction to phasing. Acta Crystallogr D Biol Crystallogr. 2010;66(Pt 4):325-38. Epub 2010/03/24. doi: 10.1107/S0907444910006694. PubMed PMID: 20382985.

224. Thompson AA, Liu JJ, Chun E, Wacker D, Wu H, Cherezov V, et al. GPCR stabilization using the bicelle-like architecture of mixed sterol-detergent micelles. Methods. 2011;55(4):310-7. doi: https://doi.org/10.1016/j.ymeth.2011.10.011.

225. Tsai C-J, Marino J, Adaixo R, Pamula F, Muehle J, Maeda S, et al. Cryo-EM structure of the rhodopsin-Gαi-βγ complex reveals binding of the rhodopsin C-terminal tail to the gβ subunit. eLife. 2019;8:e46041. doi: 10.7554/eLife.46041.

226. Van Der Spoel D, Lindahl E, Hess B, Groenhof G, Mark AE, Berendsen HJC. GROMACS: Fast, flexible, and free. Journal of Computational Chemistry. 2005;26(16):1701-18. doi: 10.1002/jcc.20291.

227. van der Walt S, Colbert, S. C., and Varoquaux, G. The NumPy Array: A Structure for Efficient Numerical Computation. Computing in Science Engineering. 2011;13(2):22-30. doi: 10.1109/MCSE.2011.37.

228. Villar VAM, Cuevas S, Zheng X, Jose PA. Chapter 1 - Localization and signaling of GPCRs in lipid rafts. In: K. Shukla A, editor. Methods in Cell Biology. 132: Academic Press; 2016. p. 3-23.

229. Virtanen P, Gommers R, Oliphant TE, Haberland M, Reddy T, Cournapeau D, et al. SciPy 1.0: fundamental algorithms for scientific computing in Python. Nature Methods. 2020;17(3):261-72. doi: 10.1038/s41592-019-0686-2.

230. Wang B-C. Resolution of phase ambiguity in macromolecular crystallography. Methods in Enzymology. 115: Academic Press; 1985. p. 90-112.

231. Watenpaugh KD. Macromolecular Crystallography at Cryogenic Temperatures. Curr Opin Struct Biol. 1991;1:1012-5. doi: 10.1016/0959-440X(91)90099-F.

232. Waterhouse AM, Procter JB, Martin DMA, Clamp M, Barton GJ. Jalview Version 2—a multiple sequence alignment editor and analysis workbench. Bioinformatics. 2009;25(9):1189-91. doi: 10.1093/bioinformatics/btp033.

233. Webb B, Sali A. Comparative Protein Structure Modeling Using MODELLER. (1934-340X (Electronic)).

234. Webb B, Sali A. Comparative Protein Structure Modeling Using MODELLER. Current Protocols in Bioinformatics. 2016;54(1):5.6.1-5.6.37. doi: 10.1002/cpbi.3.

235. Webb RJ, East JM, Sharma RP, Lee AG. Hydrophobic Mismatch and the Incorporation of Peptides into Lipid Bilayers: A Possible Mechanism for Retention in the Golgi. Biochemistry. 1998;37(2):673-9. doi: 10.1021/bi972441+.

236. Weierstall U, James D, Wang C, White TA, Wang D, Liu W, et al. Lipidic cubic phase injector facilitates membrane protein serial femtosecond crystallography. Nat Commun. 2014;5:3309. doi: 10.1038/ncomms4309. PubMed PMID: 24525480; PubMed Central PMCID: PMC4061911.

237. Weierstall U, James D, Wang C, White TA, Wang D, Liu W, et al. Lipidic cubic phase injector facilitates membrane protein serial femtosecond crystallography. Nature Communications. 2014;5(1):3309. doi: 10.1038/ncomms4309.

238. Weinert T, Olieric N, Cheng R, Brunle S, James D, Ozerov D, et al. Serial millisecond crystallography for routine room-temperature structure determination at synchrotrons. Nat Commun. 2017;8(1):542. doi: 10.1038/s41467-017-00630-4. PubMed PMID: 28912485; PubMed Central PMCID: PMCPMC5599499.

239. Weis WI, Kobilka BK. The Molecular Basis of G Protein-Coupled Receptor Activation. Annu Rev Biochem. 2018;87:897-919. doi: 10.1146/annurev-biochem-060614-033910. PubMed PMID: 29925258.

240. White TA. Processing serial crystallography data with CrystFEL: a step-by-step guide. Acta crystallographica Section D, Structural biology. 2019;75(Pt 2):219-33. doi: 10.1107/S205979831801238X. PubMed PMID: 30821710; PubMed Central PMCID: PMC6400257.

241. White TA, Mariani V, Brehm W, Yefanov O, Barty A, Beyerlein KR, et al. Recent developments in CrystFEL. Journal of applied crystallography. 2016;49(Pt 2):680-9. doi: 10.1107/S1600576716004751. PubMed PMID: 27047311; PubMed Central PMCID: PMC4815879.

242. Xu F, Liu W, Hanson MA, Stevens RC, Cherezov V. Development of an Automated High Throughput LCP-FRAP Assay to Guide Membrane Protein Crystallization in Lipid Mesophases. Cryst Growth Des. 2011;11(4):1193-201. doi: 10.1021/cg101385e. PubMed PMID: 21660116.

243. Xu W, Yoon S-I, Huang P, Wang Y, Chen C, Chong PL-G, et al. Localization of the κ Opioid Receptor in Lipid Rafts. Journal of Pharmacology and Experimental Therapeutics. 2006;317(3):1295. doi: 10.1124/jpet.105.099507.

244. Ye L, Neale C, Sljoka A, Lyda B, Pichugin D, Tsuchimura N, et al. Mechanistic insights into allosteric regulation of the A\textsubscript2A adenosine G protein-coupled receptor by physiological cations. Nature Communications. 2018;9(1):1372. doi: 10.1038/s41467-018-03314-9.

245. Yefanov O, Mariani V, Gati C, White TA, Chapman HN, Barty A. Accurate determination of segmented X-ray detector geometry. Opt Express. 2015;23(22):28459-70. doi: 10.1364/OE.23.028459. PubMed PMID: 26561117; PubMed Central PMCID: PMCPMC4646514.

246. Yin J, Babaoglu K, Brautigam CA, Clark L, Shao Z, Scheuermann TH, et al. Structure and ligand-binding mechanism of the human OX1 and OX2 orexin receptors. Nature Structural & Molecular Biology. 2016;23(4):293-9. doi: 10.1038/nsmb.3183.

247. Yin J, Mobarec JC, Kolb P, Rosenbaum DM. Crystal structure of the human OX2 orexin receptor bound to the insomnia drug suvorexant. Nature. 2015;519(7542):247-50. doi: 10.1038/nature14035.

248. Yu J, Fischman DA, Steck TL. Selective solubilization of proteins and phospholipids from red blood cell membranes by nonionic detergents. Journal of Supramolecular Structure. 1973;1(3):233-48. doi: 10.1002/jss.400010308.

249. Zhang J, Zhang K, Gao Z-G, Paoletta S, Zhang D, Han GW, et al. Agonist-bound structure of the human P2Y12 receptor. Nature. 2014;509(7498):119-22. doi: 10.1038/nature13288.

250. Zholents AA. Method of an enhanced self-amplified spontaneous emission for x-ray free electron lasers. Physical Review Special Topics - Accelerators and Beams. 2005;8(4):040701. doi: 10.1103/PhysRevSTAB.8.040701.

251. Zidovetzki R, Levitan I. Use of cyclodextrins to manipulate plasma membrane cholesterol content: Evidence, misconceptions and control strategies. Biochimica et Biophysica Acta (BBA) - Biomembranes. 2007;1768(6):1311-24. doi: https://doi.org/10.1016/j.bbamem.2007.03.026.